Combinatorial Development of novel Catalysts for Soot Oxidation

Dissertation

Zur Erlangung des Grades
des Doktors der Ingenieurwissenschaften
der Naturwissenschaftlich-Technischen Fakultät III
Chemie, Pharmazie, Bio- und Werkstoffwissenschaften
der Universität des Saarlandes

von

Nelson Ewane Olong

Saarbrücken
2007

This work had been achieved during the time from February 2004 to September 2007 at the Universtät des Saarlandes in Saarbrücken, in the group of Prof. Dr. Wilhelm F. Maier. I have worked with a great number of people whose contribution to the reasearch and the making of the thesis deserve special mention. It is a pleasure to convey gratitude to them all in my humble acknowledgement.

I would like to express the deepest appreciation to my supervisor, Prof. Dr. Wilhelm F. Maier for his advice and guidance throughout this work. Above all, he provided me unflinching encouragement and support in various ways. His truly scientist intuition has made him as a constant oasis of ideas and passsions in science, which exceptionally inspire and enrich my growth as a researcher. I am indebted to him more than he knows.

I would like to thank Prof. Dr. Rolf Hemplemann for accepting to review this work

Many thanks go to Prof. Klaus Stöwe for his valuable advice and support throughout the XRD experiment and using his precious time to read part of this work. My special thanks go to Dipl. Ing. Rudolf Richter, for the technical advice and the help he offered for the development of the library-spray equipment. To Mrs Heike Höltzen, thank you for your assistance in product analysis. Furthermore, I would like to thank Mrs. Roswitha Nagel and Mr. Christof Thome for helping with the BET measurements.

I am very grateful to Dr. Jörg Jochel and Dipl. Ing. Kristina Pokorna for the stimulating discussion and the good interaction we had throughout this work. I convey special acknowledgement to Robert Bosch GmbH for the financial support.

Thanks to Dipl. Ing. Schmauch in the group of Prof. Dr. Birringer Rainer at the Universität des Saarlandes for the TEM and EDX measurements.

It is a pleasure to pay tribute to all my colleagues for giving me such a pleasant time while working together with them. To Dr. Gerald Frenzer, i say thank you for letting me use your reactor. I gratefully thank Dipl. Chem. Alexander Kolb for accepting to read this work.

Finally, my parents deserve special mention for their unconditional support and prayers. Words fail me to express my appreciation for their life-long love.

Diesel soot is one of the major environmental pollutants especially in the developed world where the number of cars running on diesel engine is tremendously on the raise. While engine modification was enough to allow diesel cars pass the previous legislation such as Euro 3, it is clear that such modifications are not enough to allow the certification of future diesel cars. The automobile industries are now concentrating their efforts in developing after-treatment systems. The most promising approach in eradicating diesel soot from diesel exhaust emission is the application of particulate filters that trap the soot from the exhaust. Though the particulate filter have offered a break-through in trapping diesel soot, it comes at a price because the trapped soot increases the filter back pressure which concomitantly leads to an increase in fuel consumption. A clever way of preventing filter plugging is to apply oxidation catalyst on the filter system that will allow the regeneration of the filter at temperatures attainable in the exhaust. Our objective was to search for noble metal free diesel soot oxidation catalyst by established technologies of combinatorial heterogeneous catalysis. All in all about 1400 materials were tested for soot oxidation in 16 libraries in a high-throughput fashion.

Dieselruß ist einer der Hauptumweltschadstoffe, besonders in ökonomisch weit entwickelten Ländern, da dort die Zahl der Automobile mit Dieselmotor in den letzten Jahren ungemein zunimmt. Zwar waren Motorenveränderungen ausreichend um vorherige Verordnungen wie Euro 3 zu erfüllen, allerdings ist vorhersehbar, dass solche Veränderungen nicht ausreichend sein werden, um Zulassungen zukünftiger Dieselautos zu erlauben. Die Autoindustrie konzentriert ihre Anstrengungen nun auf die Entwicklung von Nachbehandlungssystemen. Der vielversprechendste Ansatz zur Entfernung von Dieselruß aus Dieselabgasen ist die Verwendung von Partikelfiltern zum Einfangen von Ruß aus Abgasen. Obwohl die Partikelfilter einen Durchbruch in Dieselrußentfernung mit sich brachten, musste dies mit einem Preis bezahlt werden, da der aufgefangene Ruß zur Erhöhung des Filterrückdruckes führt und als begleitender Nebeneffekt zu einem erhöhten Treibstoffverbrauch nachsichzieht. Ein raffinierter Weg um Filterverstopfung zu verhindern ist die Anwendung von Oxidationskatalysatoren im Filtersystem, die es erlauben werden den Filter zu regenerieren, bei im Abgas erreichbaren Temperaturen. Unser Ziel war die Suche nach edelmetallfreien Dieselruß-Oxidationskatalysatoren mit etablierten Methoden der kombinatorischen heterogenen Katalyse. Insgesamt wurden 1400 Materialien in 16 Bibliotheken auf die Oxidation von Ruß mittels Hochdurchsatz-experimenten untersucht.

1 Introduction

1.1 General

Due to their higher efficiency the sales of cars running on diesel fuel has been increasing significantly since the mid 90's [1]. In western Europe, the percentage of diesel passenger cars increased from 14 % in 1990 to 32 % in 2000 and further to 46 % in 2004 [2]. Although beneficial through a reduction of petrol consumption through the higher fuel efficiency, it contributes to another environmental problem, the diesel soot and nitrogen oxides. Diesel soot is hazardous to human health due to its potential mutagenic and carcinogenic activity. Because of the small size of its particles, it can penetrate into the lungs [3]. Government legislations for permissible diesel exhaust emission levels are being tightened because this emission is being linked to a number of respiratory problems. The parliament of the European Union has issued stricter emission standards for diesel engines of heavy duty commercial vehicles. According to the Euro 4 standard, which became effective in October 2005, emissions of particulate matter (PM) from diesel trucks have to be reduced by 80 % compared to Euro 3. Several different technical solutions to reduce exhaust gas emissions have been suggested. One of the leading technologies involves the use of particulate traps [4]. The wall-flow diesel particulate filter (DPF) attains filtration efficiencies over 90 % (for solid matter) under normal operating conditions [5]. Though particulate traps show high filtration efficiency, there is a need for filter regeneration to prevent filter plugging and back pressure increase. The development of a filter with catalyst coverage that combines retention and oxidation of the emitted particulate matter has drawn wide attention [6, 7]. Most of the oxidation catalysts used in the international markets are noble metal based (Pt, Pd), which are expensive and due to a low abundance vulnerable to further price increases upon increasing demand. Therefore the search for catalysts free of or low in noble metals is of global importance.

Nitrogen oxides (NO_x) in the exhaust of diesel cars are of critical concern because these byproducts are toxic environmental pollutants that lead to acid rain and the depletion of the stratospheric ozone layer [8]. A variety of methods have been developed to alleviate NO_x emission such as selective catalytic reduction (SCR), selective non catalytic reduction (SNCR), direct catalytic decomposition of NO_x and others [9, 10]. Simultaneous removal of soot and NO_x in a single suitable catalyzed trap has received serious attention in resent years

[11]. As in most heterogeneous catalysis projects, the search of noble metal free diesel soot oxidation catalysts is dominated by the conventional one at-a-time approach which is expensive and time consuming. The synthesis and testing of the thousands of potential candidate catalysts would require an enormous amount of time and effort. Alternatively, a high-throughput synthesis and screening method would allow the synthesis and screening of a large number of materials within a reasonable period [12]. An overview of the state-of-the-art in the development of catalysts for soot oxidation and NO_x reduction is given in this chapter. Also the operating conditions, requirements and limitations of the exhaust treatment devices for diesel engines as well as the advancement of combinatorial heterogeneous catalysis will be briefly introduced.

1.2 Diesel Engine Emissions

Diesel engines emission composition varies considerably depending on the fuel, lubricating oil, engine type, and driving conditions [13, 14, 15]. Diesel emissions are a mixture of gases, vapours, liquid aerosols and substances made of particles. A typical diesel engine exhaust gas consist of carbon (soot), CO, CO_2, NO, NO_2, N_2O, NH_3, SO_2, aliphatic hydrocarbons, polynuclear aromatic hydrocarbons, organic acids, and halogenated organic compounds. The composition of the diesel particulate matter depends on where and how they are collected. In the tailpipe, where the temperature is high, most of the volatile materials are in the gas phase. As the exhaust gas cools down and is diluted by the ambient air, nucleation, condensation, and adsorption transform the volatile materials to solid and liquid particulate matter [16]. Particulate matter (PM) and NO_x are considered to be the main pollutants of the diesel engine. Therefore, a lot of effort is being put on the reduction of PM and NO_x. Particulate matter is defined by the US Environmental Protection Agency (EPA) as all compounds collected on a preconditioned filter in dilute diesel exhaust gases at a maximum temperature of 52 °C. Carbon monoxide and hydrocarbons are easily oxidized to CO_2 by diesel oxidation catalyst. The SO_x concentration of the exhaust gas is directly proportional to the sulphur content of the fuel, therefore appropriate measures during the distillation process will deminish its presence. Shown in Figure 1.1 is the structure of primary soot and associated compounds.

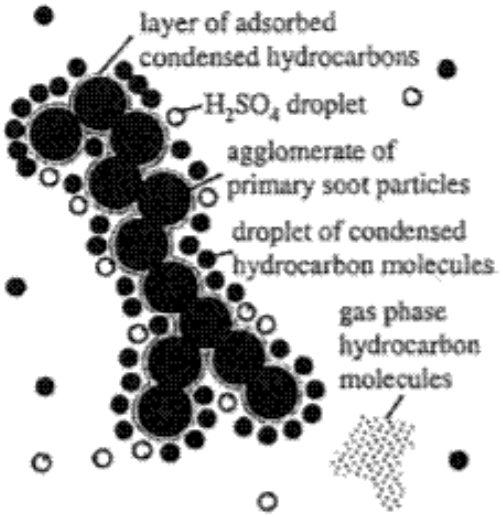

Figure1.1 Schematic structure of a chainlike aggregate of primary soot and associated compounds.

1.2.1 Diesel Engine Emissions legislature

Diesel emission of PM and NO_x is currently discussed with regards to human health and the environment. The EU commission and the Environmental Protection Agency in the United States are highlighting fine particulate as one of the current priorities for environmental hygiene in Europe and the United States respectively. The international community has acknowledged this problem and imposed limits on diesel emission. Progressively, the emission standards are becoming more and more stringent. European legislation on exhaust emissions has made major progress since its initiation in 1992. Euro Standards adopted for the reduction of diesel exhaust gas pollutants is summaries in Table 1.1, which is divided among passenger cars, light duty trucks and heavy duty trucks.

According to Euro 5 legislation planned to be implemented by mid 2008, only passenger cars and heavy duty diesel trucks with PM emissions under 0.005 g/km and 0.02 g/kWh respectively will be certified for driving in the EU. These values indicate a reduction of 96% compared to Euro 1. The emission testing is performed over the ECE 15 + EUDC / NEDC chassis dynamometer procedure. The new European Driving Cycle (NEDC) that came into effect in 2000 (Euro) used to test the emissions of passenger cars and light duty vehicles (LDV), is composed of three repetition of Urban Driving Cycle (ECE) that simulates city driving followed by an Extra Urban Driving Cycle (EUDC) simulating highway driving conditions.

Diesel cars, [g/km]					
Tier	Date	CO	HC+NOx	NOx	PM
Euro 1	1992.07	2.72	0.97	-	0.14
Euro 2, DI	1996.01[a]	1.0	0.9	-	0.10
Euro 2, IDI	1996.01	1.0	0.7	-	0.08
Euro 3	2000.01	0.64	0.56	0.50	0.05
Euro 4	2005.01	0.50	0.30	0.25	0.025
Euro 5	Mid-2008	0.50	0.25	0.20	0.005

Light duty trucks, [g/km]						
Class	Tier	Date	CO	HC+NOx	NOx	PM
Class I <1305kg	Euro 1	1994.10	2.72	0.97	-	0.14
	Euro 2, IDI	1998.01	1.0	0.70	-	0.08
	Euro 2 ID	1998	1.0	0.90	-	0.10
	Euro 3	2000.01	0.64	0.56	0.50	0.05
	Euro 4	2005.01	0.50	0.30	0.25	0.025
	Euro 5	Mid-2008	0.50	0.25	0.20	0.005
Class II 1305-1760kg	Euro 1	1994.10	5.17	1.40	-	0.19
	Euro 2, IDI	1998.01	1.25	1.0	-	0.12
	Euro 2 ID	1998	1.25	1.30	-	0.14
	Euro 3	2001.01	0.80	0.72	0.65	0.07
	Euro 4	2006.01	0.63	0.39	0.33	0.04
	Euro 5	Mid-2008	0.63	0.32	0.26	0.005
Class III >1760kg	Euro 1	1994.10	6.90	1.70	-	0.25
	Euro 2, IDI	1998.01	1.5	1.20	-	0.17
	Euro 2 ID	1998	1.5	1.60	-	0.20
	Euro 3	2001.01	0.95	0.86	0.78	0.10
	Euro 4	2006.01	0.74	0.46	0.39	0.06
	Euro 5	Mid-2008	0.74	0.38	0.31	0.005

Heavy duty diesel trucks, [g/kWh]					
Tier	Date	CO	HC	NOx	PM
Euro 1	1992, <85kW	4.5	1.1	8.0	0.612
	1992, >85kW	4.5	1.1	8.0	0.36
Euro 2	1996.10	4.0	1.1	7.0	0.25
	1998.10	4.0	1.1	7.0	0.15
Euro 3	2000.10	2.1	0.66	5.0	0.10
Euro 4	2005.10	1.5	0.46	3.5	0.02
Euro 5	2008.10	1.5	0.46	2.0	0.02

Table 1.1 A summary of the European emission standards for diesel passenger cars and light-duty and heavy duty trucks and their implementation dates.

The US Environmental Protection agency has imposed a tiered system for emissions reduction through 2010. Under the tiered 2 regulations which were finalized in 1999 and to be phased-in between 2004 and 2009, the same emission standards apply to all vehicle weight categories when tested on the Federal Test Procedure 75 driving cycle and emissions are measured in g/mile (FTP) [17]. The tiered 2 emissions standards are structured into 8 permanent and 3 temporary certification levels of different stringency called certification bins and an average fleet standard for NO_x emissions. Vehicle manufacturers have a choice to certify particular vehicles to any of the available bins. The tier bin 5 standard planned to be phased-in by 2007 requires light duty diesel vehicles to meet the corporate average 120.000 miles NO_x standard of 0.07 g/mi and 0.01 g/mi particulate matter standard. There is growing call to standardize the test cycles worldwide.

1.2.2 Diesel emission treatment technologies

Diesel engines generate fewer greenhouse gas emissions but emit larger amounts of PM and NO_x compared to their gasoline counterparts. During the combustion of diesel fuel, fuel is injected into pre-compressed air forming droplets surrounded by oxygen deficiency, which results in incomplete combustion and thus leads to solid soot formation. Since the introduction of Euro 4 in January 2005 by the European legislation, diesel engine technologies such as cool exhaust gas recirculation (Cooled EGR), multi injection-ignition, and using high pressure fuel pumps can no longer lead to emission levels that will allow the certification of diesel vehicles in the EU zone. Thus a convenient way of treating diesel off-

gases is needed. The catalytic after treatment techniques that aims at the combustion of pre-formed PM in the exhaust stream rather than avoiding the formation of PM is the most promising technology. Wall flow ceramic monoliths are the most common type of diesel filter substrate. The channels of the filter are open and plugged at opposite ends thereby forcing the exhaust gases through the porous filter walls. Large soot particles which cannot flow through the pores are collected on the filter walls. The wall flow particulate filter has a high surface area per unit volume, a high collection efficiency (over 95 %), and a tolerable backpressure in the exhaust. The two most popular ceramic compositions of filters are Cordierite and Silicon Carbide. Cordierite filters are manufactured via an extrusion process as a 'whole piece' (monolith). By contrast, many Silicon Carbide filters are typically extruded in smaller segments and cemented together to form the appropriate filter [18]. The diesel oxidation catalyst is an effective device to control CO, HC, poly-aromatic hydrocarbon (PAH), hydrocarbon derivatives, such as aldehydes, and a large part of constituents of the soluble organic fraction (SOF) of diesel particulate. Though the particulate conversion efficiency is much less than the filtration efficiency of a wall-flow filter, it is sometimes enough for many current engines to pass the existing emission standards. The catalyst coated on the filter or added to the fuel decreases the combustion temperature of the soot down to temperatures attainable in a diesel exhaust (300 °C). At low load though, low particulate conversion efficiency is attained due to the fact that the exhaust gas temperature is not sufficient to activate the catalyst.

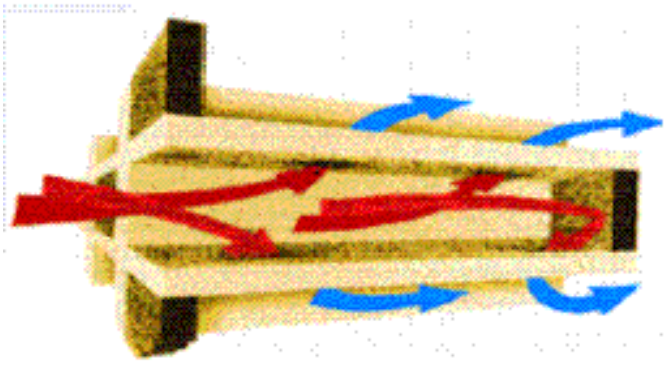

Figure 1.2 Wall flow diesel particulate filter illustrating how the exhaust gas can pass through the filter walls. Particulate matter becomes trapped in the walls.

1.2.3 Oxidation catalyst

The pursuit of a technique for diesel soot control has prompted a plethora of research into the application of catalysts to lower ignition temperatures and so promote combustion [19-29]. Most oxidation catalysts are coated on a Ceramic honeycomb structure or monolith held in a metal can in the exhaust stream. The catalyst is impregnated into a highly porous washcoat about 20-40 μm thick that is applied to the passageway walls. The filter both act as a means of collecting the soot particles and a substrate for catalyst. The attained catalyst-soot contact is poor compared to fuel borne catalysts. However this system reduces extra cost of using a separate system for catalyst blending and storage. Most of the oxidation catalysts used in the international markets are noble metals based, which are expensive and due to a low abundance vulnerable to further price increases upon increasing demand [30]. Moreover precious metals catalyze the formation of sulphate and sulphuric acid. EU, USA and Japan have decided to reduce the sulphur content of diesel fuel. Low sulphur will prevent the deactivation of the catalyst by poisoning from sulphur oxides.

Many kinds of catalysts have been studied for soot combustion applications, including single and mixed transition metals oxides, low melting point compounds, and perovskite and spinnel type oxides. Tikhomirov et al. used a TGA-DTA/DSC device to study the oxidation of soot by MnO_x-CeO_2 mixed oxides. $Mn_{25}Ce_{75}$ was found to oxidize soot significantly between 250 °C-450 °C [31]. A comparison of the effect on soot oxidation by different nanostructured spined-type oxides was given by Fino and co-workers [11]. They found that $CoCr_2O_4$ was the most active among the considered catalyst oxidizing soot between 300-450 °C. Using a Magnetic Suspension balance, Vinalli et al. observed that Ru supported on Na-Y zeolite could oxidize 10 % of soot at 375 °C with and without NO presence in the gas stream. The Pt/NaY became almost inactive in the absence of NO in the gas stream [32]. A representative summary of soot oxidation catalysts found in the literature is given in Table1.2. Unfortunately several testing methods have been used by different researchers which make comparison of results difficult. The most commonly used catalytic testing method is a semi-batch packed bed micro-reactor through which the effluent gases simulating the diesel exhaust gases are fed. The reactor is heated gradually, while the effluent gases are analyzed for carbon conversion to determine the combustion. Also there are several studies using thermogravimetric analysis to determine the temperature of soot ignition. Thermogramimetry (TG) is a technique for measuring the change in weight of a sample as a function of temperature whilst the sample is subjected to a controlled temperature programme. The reported catalytic activities are

dependent on the contact between the soot and the catalyst, feed composition and the model soot used. Neeft et. al. studied the influence of the catalyst-soot contact on the catalytic activity [33,34]. Mixing the catalyst with a mechanical mill, the so called tight contact was found to oxidize soot at a temperature 200 °C lower than the catalyst mixed with the soot with a spatula (loose contact). Since diesel soot composition varies considerably depending on the fuel, lubricating oil, engine type, and driving conditions, most research groups use model soot (Printex-U), a commercially available carbon black which is said to posses almost identical properties as real diesel soot [15].

Catalytic Phase	Oxidation T [°C]	Contact	Test method	Feed gas	Cat/soot ratio	Ref
$Mn_{25}Ce_{75}$	300-400	Loose	TGA-DSC	O_2+NO	20:1	31
Co/CeO_2	T_{ign}= 300	Loose	TPO	O_2+NO	20:1	35
$CoCr_2O_4$	300-450	Tight	TPR	O_2+NO	9:1	11
$Cs\text{-}FeV/Al_20_3$	T_{ign} = 322	Tight	TPO	Air	20:1	20
$CeO_2\text{-}PrCrO_3$	390	Tight	TPO		9:1	36
Co,K/MgO	300-450	Tight	TPO	O_2	20:1	19
$La_{0.8}Cr_{0.8}$ $\text{-}Li_{0.2}O_3$	320-450	Tight	TPC	Air	4:1	7
$K\text{-}Cu_xFe_2O_4$	T_{ign} = 285	Tight	TGA	O_2	9:1	37
K_2FeO_2	T_{ign} = 302	Tight	TGA	O_2	4:1	38
$K_2Mn_2O_6$	T_{ign} = 289	Tight	TGA	O_2	4:1	
Pt/MO_x	321-550		Bench	Simulated Exhaust	10:1	21
$CoPbO_x$	385		Bench	Simulated Exhaust	10:1	6
$K\text{-}La_2O_3$	350-400	Tight	TGA	O_2		39
$Cs_2SO_4V_2O_5$	400-500	Tight	TPO	Simulated Exhaust	20:1	40
Mo/Al_2O_3	453	Loose	DSC TPO	O_2	2:1	27

Table 1.2 Summary of the important diesel soot oxidation catalysts reported.

The NO_x-aided continuously generating trap (CRT) was commercialized by Johnson Matthey for trucks and buses. It comprises an oxidation catalyst (Pt) followed by a wall-flow monolith [41]. The system does not require additional heat. The precious metal oxidation catalyst placed in the first chamber, upstream of the DPF converts the CO and hydrocarbons present to CO_2 and NO to NO_2. The collected soot on the DPF in the second chamber is oxidized by the NO_2 which is a much better oxidant than oxygen. An average temperature of 260 °C, a NO_x / PM ratio of at least 25 and an ultra low sulphur fuel (50ppm) are required for proper regeneration. This system converts 90 % of the CO and hydrocarbons present to CO_2, 20-50

% of NO to NO_2 and 90 % of particulate matter. Most of the NO_2 is reduced back to NO during soot oxidation, therefore the total amount of NO_x reduction is low (about 5 %). By adding catalysts to the filter in addition to having the upstream oxidation catalysts, it is possible to reoxidise the NO to NO_2 and so improve the overall efficiency of soot removal. This so-called Catalysed Continuously Regenerating Trap (CCRT) are being used on selected heavy-duty diesel applications where the duty cycle does not always provide sufficient temperature for proper functioning of the CRT [42] While this system functions well in Europe where ultra low sulphur diesel fuel is widespread, the system may fail in countries with high sulphur fuel. Its dependency on NO_x may render this system inadequate if the required NO_x-to-soot ratio is not met in future engines.

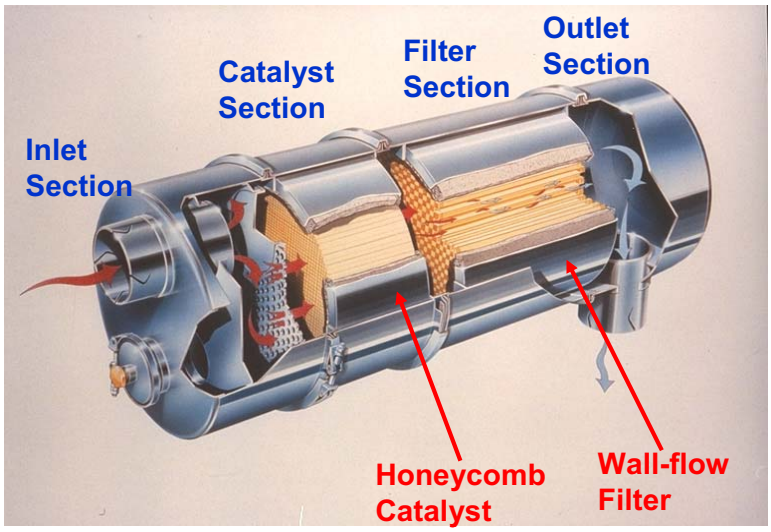

Figure 1.2 Continuous regenerating particulate filter.

Toyota Motor Corporation was the first to introduce a washcoated filter system in series production. This system works on a simultaneous reduction of nitrogen oxides and oxidation of particulate matter [43]. The Toyota system (D-Cat) integrates a flow through NO_x Storage Reduction Filter (NSR), a wall flow Diesel Particulate NO_x Reduction (DPNR) filter and an oxidation catalyst coated wall flow filter in the same casing. The NSR as well as DPNR are coated with NO_x storage material $BaCO_3$ and oxidation catalyst Pt, while the last filter in the assembly is coated with Pt for HC combustion. Its effective operation relies on the engine management system being able to vary the fuel-air ratio in the exhaust gases. This variation has been made possible by a fifth injection nozzle placed up stream of the casing. Periodically, fuel is injected downstream of the exhaust manifold to create the rich condition

in the NSR and DPNR units which allows the release and reduction of the NO_x stored. Because of the high Pt-content, the system requires low sulphur fuel. The D-Cat system, an example shown in Figure1.3, dramatically reduces particulate matter and nitrogen oxides below Euro IV levels.

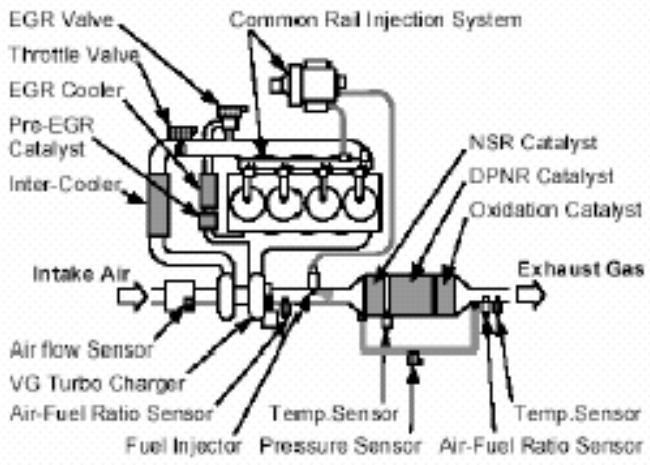

Figure1.3 Illustration of the D-CAT system developed by Toyota to provide very low NO_x and PM emissions [43].

Toorisaka and coworkers have developed a DPF system impregnated with Platinum for Hino Motors [44]. The system consists of a diesel oxidation catalyst filter (DOC) impregnated with platinum and catalyzed diesel particulate filter in a compact arrangement. Unlike in the Toyota D-Cat system where soot and NO_x are treated in single unit, the Hino Motors system combust only soot. The soot accumulation on the filter is monitored by a differential pressure sensor which triggers fuel injection at critical moments to increase the temperature of the exhaust gases, thereby causing the combustion of soot on the DPF. The exhaust gas temperature is further increased on the DOC filter by burning the unburned hydrocarbons of the post injected fuel. The authors claim that the system is capable to limit PM emission below 0.02 g/KWh.

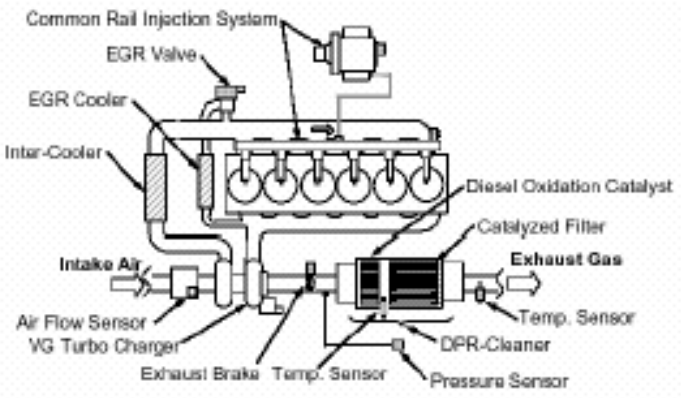

Figure 1.4 Particulate emission control system [44].

Alternatively, the quality of induced self-supporting regeneration of a particle filter can be improved with a built-in metal catalyst. The catalyst is incorporated during the soot-formation process. These catalytic fuel additives (fuel borne catalysts) which are blended into the fuel (typically 10-100ppm) interfere with the structure of the soot leading to better catalyst-soot contact which may be crucial for solid-solid reactions. In 2000, Peugeot-Citroen introduced a serial production of Peugeot 607 HDI (High pressure direct Injection) luxury sedan with a particulate filter (SiC) fitted as a standard equipment. In Peugeot's system, a cerium based additive contained in a separate tank (5-litre) is automatically blended to the fuel tank. The collected soot particles on the DPF contain the oxidation catalyst which lowers the combustion temperature of the soot. Post-injection in the expansion phase causes post combustion in the cylinder resulting in a temperature increase of 200 °C to 250 °C. Further increase of the exhaust gas temperature (>100 °C) is achieved by the combustion of the unburned hydrocarbons arising from the post injection by the oxidation catalyst placed upstream of the filter. The oxidation catalyst is more important during least favourable driving circumstances where the increase of the exhaust gas temperature up to 450 °C is difficult. The disadvantages of the given system are that the additive tank has to be replenished after every 80,000 km and it causes extra ash accumulation on the diesel particulate filter. Ash accumulation makes complete soot oxidation at each regeneration phase impossible. The cleaning of the additive ash from the filter after every 80,000 km is necessary [45]. The high equipment cost (storage tank, precision dosing pump etc) makes this system attractive only to the luxury car market [4]. On the other hand compared with the precious metal catalytic filter systems, this system allows the use of fuel with sulphur levels up to 350 ppm. The performance of the PSA Peugeot-Citroen system allows particulate emissions well below the Euro 4 (2005) limits even after a high mileage [46].

1.2.4 Catalytic Soot Oxidation Mechanism

The scientific understanding of the mechanism of soot oxidation is still the subject of intensive research although the combustion of carbon is an ancient practice. Numerous mechanistic studies of carbon combustion have already been performed and most researchers use the accumulated literature as the starting point for understanding the mechanism of soot combustion. However, soot combustion is in fact more complex due to the complex structure of the soot containing absorbed hydrocarbons and impurities, which originate from fuel and lubricating oil [47,48]. The mechanistic nature of the oxidation of soot particulate may involve either activation of carbon atoms within the particulate or the catalyst acting as a source of activated oxygen which can be regenerated. Two oxidation mechanisms are proposed to occur in the catalyzed carbon oxidation: a redox mechanism and a spill-over mechanism. According to van Setten [4], Amariglio and Duval were the first to suggest that only metals which can oscillate between two oxidation states can catalyze the oxidation of graphite sheets. Setzer et al. found that the oxides of metals which readily change valency are superior catalysts. Cu, Fe, and Co were found to be more active than Ni and Zn [49]. Redox mechanism requires physical contact between the catalyst and graphite. Neeft et al. found that the oxides of Co_3O_4, V_2O_5, Fe_2O_3, La_2O_3, MnO_2, and NiO exhibit high to moderate activities in tight contact but hardly any activity in loose contact [28]. Miro et al. reported that for tight contact, Co,K/MgO catalysts burned soot at a lower temperature [19, 50-51]. The fact that tight contact gave more efficient catalysis was attributed to increase contact points between the catalysts particle and soot particulate. However, some catalysts can oxidise graphite without being in contact. Baumgarten et al. observed increased rate of coke oxidation while there was no direct contact between the catalyst and coke [52]. The catalyst catalyzes the formation of a mobile compound (Oads) which migrates to the coke where it reacts to form CO_2 and/or CO. This mechanism is known as the spillover mechanism. The NOx-aided gas-phase coke oxidation mechanism proposed by Cooper and Thoss [53], is also a sort of spillover mechanism whereby NO is oxidized to NO_2 and the noncatalytic soot oxidation is achieved by NO_2.

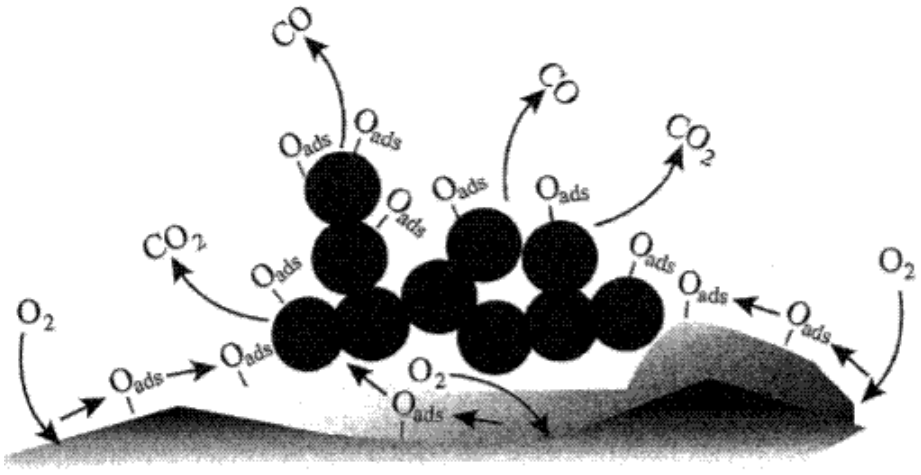

Figure 1.5 Illustration of spillover soot-oxidation mechanism on a catalyst surface.

Using physical mixtures of carbon black and several transition metal oxides treated in labelled O_2, Mul et al. showed that both spillover and redox mechanism can occur simultaneously. The activity of the Cr_2O_3 catalyst towards carbon black oxidation was said to be due to its redox property and its ability to activate gas phase oxygen and subsequent transfer of the activated species to carbon black. The dominating mechanism depends on the degree of physical contact between the catalyst and soot [54]. Previous studies have examined three types of physical contact between catalyst and soot particulate: (i) "loose contact" where mixing of soot and catalyst was performed just with a spatula; (ii) "tight contact" involving mixing with a mechanical mill; and (iii) "in situ contact" where diesel soot particulate was filtered from an exhaust stream on to a bed of catalyst particulates. The in situ contact data were found to be very similar to the loose contact results [28].

1.2.5 NO_x Abatement

Diesel engines have higher A/F ratios which changes drastically depending on the load. Diesel exhaust always contains an excess of oxygen which is advantageous for the oxidation of HCs and CO but it makes NOx control extremely difficult. The reducing CO is present in low concentrations and NO has to compete with oxygen to react with hydrocarbons making catalytic reduction of NOx hard to achieve. NOx abatement techniques under development are based on two different approaches. The first is the continuous catalytic reduction of NOx with either the unburned hydrocarbon from fuel or with ammonia or urea injected in the diesel exhaust. Noble metals, zeolites, and metal oxides have been used as catalysts for SCR. Most

catalysts have a narrow temperature window and low conversion of NO_x at lower temperature [10, 55]. Hirata, et al, provides a comprehensive review of a modern SCR system as developed by Nissan Diesel for Japan [56]. They use a DOC in front of the system to generate NO_2, which with equimolar quantities of NO, reacts most efficiently with ammonia at low temperatures. Addition of DOC increased the NO_x removal efficiency at 200 °C from 40 % to 70 %. Further, a zeolite SCR catalyst was chosen over the traditional vanadia-based catalyst because of better performance and smaller size [45]. SCR operation in very cold climates can cause problems, as the standard urea solution freezes at about -10 °C. Ammonium formate with the same ammonia content as urea freezes at -20 to -30 °C [57]. An alternative is to heat the tank using engine cooling water and heating elements for the lines [56]. The second approach of NO_x abatement involve NO_x storage during lean condition and reduction during short duration, carefully controlled, fuel rich conditions (NSR) pioneered by Toyota for mobile applications [58]. The catalyst used for the NSR process comprises a noble metal component that can catalyze oxidation and reduction reactions (Pt) and a storage component (Alkali or alkali earth metals) [59] The current trend in diesel exhaust abatement involves combining several diesel emissions control systems into a single unit to minimize space requirements. Oxidation catalyst, PM filtration and ammonia SCR for NO_x control on heavy-duty diesels have been ingeniously combined in a single compact container [60, 61]. A more ambitious approach is to use a single suitable catalyzed trap for the simultaneous removal of soot and NO_x from diesel emissions. This approach is under intensive investigation [23, 29, 62-64]. The catalytic system having such corporate property may offer considerable advantages in terms of both investment cost and pressure drop reduction.

1.2.6 Diesel Exhaust Gas Purification Patents

Most of the patented catalysts for the diesel exhaust gas purification consist of at least one element of the noble metal group as the catalytic component [65-71]. Different metal support oxides (Al_2O_3, SiO_2, TiO_2) and zeolites (Y-zeolite, ZSM5) are said to act in the catalyst as support materials for the noble metals. In order to enable the noble metals to be deposited in as highly a dispersed manner as possible on the support, preference is given to support materials with high specific surface area. Zhang disclosed a coated diesel exhaust particulate filter formed by wash coating a catalyst comprising alkali catalytic metal oxide (Li_2PtO_3) uniformly dispersed on an alkali metal aluminate ($LiAlO_2$) onto a ceramic monolithic support material [72]. A process of manufacture of a catalyst coating for a diesel exhaust particulate filter containing platinum group metal and a silver vanadate is disclosed by Hartwig [73].

Dang et al. outlines catalytic preparation, particulate filter coating and PM filter test. A ceramic monolith was dipped in 500 ml of an aqueous solution containing 15 g/l of magnesium (magnesium nitrate). The filter element was dried at 125 °C (2h) and then calcined at 550 °C (2h). After cooling, the filter element was dipped in a 500 ml aqueous solution containing platinum salt at a 10 g/l loading. Following impregnation, the coated filter element was dried at 125 °C for 2h and calcined at 550 °C (3h). The platinum loading on a by weight basis was 1.8 g/l. The regeneration of the exhaust filter of the invention takes place at temperatures around 400 °C [74].

Noble metal free catalysts have also been used to substantially reduce the diesel soot ignition temperature [75-76]. Common to these patents is the use of alkali or alkali earth metals to oxidize soot. Unfortunately, these catalysts are volatile resulting in impractical short life times. Also transition metals and their mixtures have been reported as active materials for soot oxidation [77, 78]. Domesle et al. disclosed the use of silver vanadate coated on a cordierite monolithic filter to reduce the ignition temperature of diesel soot collected on the filter [79].

1.3 Combinatorial Chemistry

Heterogeneous catalysis remains the workhorse for many industrial synthesis and treatment processes for environmental emissions. Therefore, an enormous interest exists in the development of new, and the optimization of currently implemented heterogeneously catalyzed processes. The often used empirical catalytic research approach is very labour-intensive and uneconomical, since the potential for optimization is limited by the small body of knowledge available from pervious work [80]. With increasing demand for economical and efficient materials, nowadays new strategies for heterogeneous catalysts research are developing. The pharmaceutical industry faced with the paradox to decrease research expenditure while bringing to the market-place more drugs entities per unit time opted for combinatorial chemistry as the new paradigm of doing business. The success of combinatorial technology in the pharmaceutical chemistry and industry in the early 90s encouraged material scientists to apply the technology to their field. Combinatorial synthesis and sophisticated screening technologies are now being applied to the discovery of more efficient catalysts and materials. Combinatorial catalysis is a methodology or set of tools where large diversities of solid-state materials libraries are prepared, processed, and tested for activity and selectivity in

a high-throughput fashion [81]. This methodology was first introduced by Hanak in 1970 to search for new semiconductors, superconductors, and magnetic materials, he named his approached as “Multiple Sample Concept” (MSC) [82]. This method does not only facilitate the discovery and optimization of new and/or superior compounds with new and/or enhanced material properties but it also enhances the recognition of trends and patterns of structure-activity relations from which new catalytic materials can be designed more efficiently. With methods of combinatorial chemical synthesis evolving together with rapid analysis and high-throughput screening, high-capacity information processing and data management becomes an essential component of this methodology since the data and information generated are vast. In the subsequent chapter, combinatorial material synthesis, high throughput screening, high-throughput hardware and software, and data management will be discussed.

1.3.1 Combinatorial synthesis of inorganic material libraries

Combinatorial methods are established tools for the development of new lead structures in the areas of organic, biochemical, and pharmaceutical chemistry [83, 84]. High throughput techniques used in the preparation of solid-state libraries of catalytic materials can be grouped into thin film deposition based methods and solution-based methods. Schultz and co-workers were the first to modify technologies used to make integrated circuit chips to prepare materials libraries with spatial resolution [85]. The material libraries were obtained by depositing the compounds as thin films through radio frequency (RF) sputtering in conjunction with physical masks. Weinberg et al. combined masking and physical vapour deposition to generate material libraries [86, 87]. Other thin-film deposition methods, such as thermal [88, 89] and chemical-vapour deposition [90, 91], molecular beam epitaxy [92, 93], and pulsed-laser deposition [94, 95] have been used to produce materials libraries. These techniques are typically used to explore three- or four- component compositions (as well as the substrate nature) and usually the composition of the deposited material depends linearly on its position in the array slate. The advantage of the thin film techniques is controlled access to nearly all elemental combinations of the periodic system. However, the implementation of thin film techniques to heterogeneous catalysis is a significantly more challenging problem than in other areas of materials science. The amount of solid catalyst film is in the range from very few milligrams to 100 micrograms. The scale up of newly discovered materials may pose serious problems because of the chemical and physical differences between thin films and bulk catalysts.

Solution-based preparations reproduce the conventional procedures used at the laboratory scale by means of automated robotic systems that deal with dosing of multiple liquids and solids, heating and stirring, libraries of liquid solutions and/or gels with a wide range of viscosities, filtration and washing of suspensions and resins, controlled solvent evaporation etc. Senkan et al. applied a co-impregnation method to synthesize a library of 66 catalysts [96]. Porous alumina pellets were immersed into the aqueous solutions of catalyst precursors at different concentrations, prepared by an accurate liquid delivery system. In this case the carrier primarily determines the surface area and mechanical properties of the final catalyst. In contrast to thin films, the pellet dimensions allow for easy scale up of newly discovered catalysts for commercial applications. The coprecipitation and precipitation methods were introduced by Schüth and coworkers to synthesize catalysts libraries for CO oxidation [97]. H. An et al. reported a polymerizable-complex method (PCM) of powder processing combined with inkjet deposition for the combinatorial syntheses of complex oxide catalyst systems [98]. In PCM, metal ions are dissolved in solution with a chelating agent (citric acid) and ethylene glycol. This liquid mix method enables the mixture of metal ions on a molecular level. In 1998, Maier and co-workers disclosed a multireactor autoclave that allows 37 hydrothermal syntheses to be run in parallel [99]. The said reactor was used to prepare mixtures of titanium-containing silicate. Further, hydrothermal synthesis of zeolites libraries using a 100 fold multiautoclave was published by D. E. Akporiaye et al [100]. Also, sol-gel techniques have been successfully miniaturized and used for the preparation of libraries of catalytic materials [101-102]. Unlike hydrothermal synthesis, the sol-gel synthesis method requires lower processing temperatures. The automated systems used for the solution based library synthesis can generate solid catalysts, amounts ranging from 25 to 1000 mg. In summary, various techniques are applied for the systematic and automatic synthesis of large combinatorial libraries of catalytic materials.

1.3.2 High-throughput equipment

In an efficient high-throughput process you should “analyze in a day what you make in a day” [103]. High-throughput analysis is often the most important technology for the success of combinatorial catalysis. A multiphase strategy is often considered in high-throughput catalyst development. A first-stage screen may only test for one or two critical properties which are easily and quickly measured on a microscale. At this stage 100s-1000s samples may be synthesized and screened per day. The primary screening may be followed by a second screen

to optimize the properties of the discovered catalyst hereby a lower number of catalysts but under realistic reaction conditions are tested per day. Other differences between primary and secondary screening include: the amount of each material processed and the accuracy or reliability of the experimental results. In fact, the reliability of the screening often decreases with increasing library size due to the vast differences between the synthesis and catalytic testing conditions with those applied at a large scale. Therefore the best materials from primary screening have to be validated at a standard laboratory scale where such parameters as mass balance are more accurately determined. A number of complementary techniques have been developed to screen and/or test libraries of solid-state materials for catalytic activities. Although each specific application must be evaluated to identify the most suitable screening tool, optical and mass spectrometry have been the most commonly used methods because of their broad applicability and relative speed compared to chromatography.

High-throughput equipment used for the primary screening of catalysts libraries can be divided into sequential and parallel techniques. The parallel mode of operation is less time consuming compared to the sequential. The time lag between testing different catalyst spots may become considerable for a large library. Furthermore, if the whole catalyst library is maintained at high reaction temperatures and heat induced catalyst deactivation phenomena occur, then under sequential operation the catalyst spots are not tested under identical conditions. Resonance–enhanced multiphoton ionization (REMPI) with microelectrode detection has been reported by Senkam [104]. This technique combines the speed of optical methods and the selectivity of mass spectrometry which allows the high-speed screening of catalysts libraries for activity and selectivity. The approach is based on the in-situ ionization of reaction products by UV lasers, followed by the detection of the photonions or electrons by spatially addressable micro electrodes placed in the vicinity of the laser beam. The REMPI process can be used repeatedly to detect different products using different laser frequencies, thereby allowing the determination of selectivity. The disadvantage of this technique is that the REMPI features of many molecules are not known which needs to be determined before the application of this technique to catalyst screening. Other techniques, such as IR-thermography [105, 106], Laser induced fluorescence imaging (LIFI) [107], photothermal deflection (PTD) [108], Fourier transform infrared (FTIR) [109, 110], gas sensors [111], and colour indicator methods [112, 113] have been used for the parallel screening of catalyst libraries.

Mass spectrometry is a mature and widely used detection technology and can readily be applied to analyze complex gas mixtures. This technology has been successfully adapted to screen catalyst libraries. In 1999, Maier and coworkers disclosed a system capable of detecting selectivity differences of heterogeneous catalysts on libraries by spatially resolved mass spectrometry. They employed a commercially available gas analyzer and a synthesis robot, whereby the pipetting unit of the robot was exchanged for the capillary bundle consisting of an outer steel, two inner steel, and the MS capillaries. The authors reported the same selectivity for the reaction of propene with air (500 °C) at the higher mass range as those identified under conventional reaction conditions [114]. Other groups have equally reported the used of MS to analyze heterogeneous libraries products [115, 116]. Further sequencial methods include gaschromatography [117] and auto-loading high resolution modulated thermogravimetry analyser (TGA). McGinn and coworkers applied a commercial auto-loading TGA to sequencially screen alkali metal doped oxides for diesel soot combustion [118]. The difference between this system and a normal TGA analyzer is that the said system does not require manual loading and off loading of the sample from the TGA furnace.

Parallelized catalyst screening techniques which are close to conventional catalysis research, the so called stage two screening are mostly accomplished with parallel and miniature conventional catalytic reactors such as fixed bed reactors [119-120] or continuous stirred tank reactors [121, 122]. To guarantee the correct reactor operation and reliability of the catalytic test results in such a design, the following issues are important: ultra-fast methods for the quantitative analysis of reaction products, such as micro GC and GC-MS; control of reaction temperature and pressure in each channel and capability of working under industrially realistic condition; representative sampling operation, minimizing the cross-talk between channels; modular reactor design, allowing easy loading and unloading of catalysts; possibilities of carrying out in situ catalysts pre-treatment or activation [123]. Yamada et al. developed a powder dispenser and a reaction controller which simply parallelized conventional methods for conventional materials [111, 124]. A five fold L-type fixed bed flow-type reactor made of quartz was employed while the products were analyzed with a gas sensor system. The setup was used to screen CO oxidation and selective oxidation of propane catalysts.

1.3.3 Emissivity Corrected Infrared Thermogravimetry (EC-IRT)

Infrared thermography detects the infrared radiation emitted by all objects. IR radiation is actively emitted from all objects and no external light source is required for imaging. Even gases emit IR radiation. The IR image of an object is composed of emitted and reflected radiation, the relative ratio is different for each source. The different colours on these images visualize different photon intensities of detected IR radiation. From these photon intensities blackbody temperatures can be calculated by Planck`s law. These blackbody temperatures can be converted to the actual surface temperature of the body only if no reflection occurs or becomes insignificant and its emissivity is known. Though originally developed for military applications and surveillance, its present-day applications include: aircraft and electronics industry, medicine, engineering, quality control, environmental protection, building inspection, law enforcement, and science. Infrared thermography is also gaining applicability in the high-throughput screening of catalyst libraries because this method which measures heat production on the surface of catalysts bed is a truly parallel method whose screening time is independent of the number of samples on the library.

The applicability of IR thermography in heterogeneous catalysis was first demonstrated in 1987 by Pawlicki et al. where oscillations in a catalytic reaction of hydrogen with oxygen across a 4 cm^2 catalyst wafer could by monitored. Because of the exothermic nature of this reaction, the temperature variations were as large as 70 °C [125]. Sermon and co-workers also applied this technology for the analysis of temperature profiles of exothermic reaction on platinum catalysts supported on silicon oxide [126]. Infrared thermography with its poor resolution is difficult to be applied to measure small temperature differences on a catalyst library. The image of an object is composed of emitted and reflected radiation. Reflectivity and emissivity are material specific properties and may change from sample to sample. Local differences in emissivity and reflectivity on a library surface and its individual catalysts spots do appear as different photon intensities, which can be misinterpreted as different temperatures, although true surface temperatures are identical. To be able to image the temperatures changes in real time during a catalytic experiment, suitable calibration data, which account for these emissivity and reflectivity differences have to be recorded prior to the experiment.

To deal with these potential difficulties, Maier and co-workers introduced the technique of emissivity –corrected IR thermogrphy [101]. Prior to a measurement, the library emissivity is

determined at six different temperatures in a range of +/-5 K around the desired reaction temperature under inert gas flow to correct the emissivity differences across the library plate and calibrate the detector pixels sensitivity. After this calibration, temperatures changes can be determined from measured emission changes for both low and high emitting materials accurately. Shortly after calibration, before the start of the actual measurement, the reactor temperature is brought to the reaction temperature and an additional infrared image of the library is recorded which will be subtracted as background image from all other following IR images. A major problem of IR thermography is that signal intensity is related to total heat produced. The method is also sensitive to parallel and sequential reactions such as total combustion, the heat of which indiscriminately adds to the signal intensity. The method therefore has to be used with care in selective reactions and cannot be used to quantify the reaction products.

1.3.4 Combinatorial Experimental design strategies

High-throughput techniques have accelerated our ability to generate large numbers of experiments. In high-throughput experimentations, the kinds of problems, the desired outcomes, and the appropriate strategies are significantly different from those associated with conventional experimentation. HTE in heterogeneous catalysis relies on the iterative preparation and testing of large libraries of solids. Even with combinatorial methods, the entire chemical space can never be explored comprehensively because of its nearly infinite nature. An important issue in combinatorial catalysis is how to design the experiments in order to explore and optimize the high solution space while minimizing the number of trials to achieve a solution. To overcome this bottleneck, high-throughput experimentation has to be combined with intelligent optimization strategies in order to effectively search for new materials in the infinite parameter spaces of compositions based on the periodic table. The process starts with the design of an initial set of catalysts, which can be done either randomly, or following certain rules, or be based on the experience and intuition of the library designer.

The techniques used in the experimental design can be distinguished in three groups: (1) statistical procedures like factorial designs, (2) deterministic optimization procedures such as simplex, holographic search [127] or split and pool [128], and (3) stochastic procedures such as annealing or genetic algorithms (GAs). Stochastic procedures are procedures well-suited for the optimisation of multi-dimensional problems, with GAs being specially useful for application in the field of combinatorial catalysis since this method uses a population of

points to conduct the search, the objective is to find an approximate global maximum, and can tolerate noisy experimental data [129, 130]. The group of Baerns applied an evolutionary strategy to optimize catalysts for the oxidative dehydrogenation of propane [129]. Elements of the periodic table were a priori selected according to heuristic knowledge to form the parameter space which limits the search. After evaluation of randomly selected quarternary formulations in a catalytic flow system, the catalysts were ranked with respect to the target criterion. The next generation was designed following principles of biological evolution and thus an altered catalyst population was generated. After generation 4, the algorithm converged towards a zone at 15 % conversion and 55 % selectivity to propene over the V, Mg, Mo and Ga catalysts. Maier and Co-workers also applied an evolutionary strategy in conjunction with kriging technique to discover CO oxidation catalyst [131]. Furthermore, this technique was applied by Grubert et al. to search for new catalysts materials for the water-gas shift reaction (WGSR). Because the group intentionally included elements known to be active for the water-gas shift reaction in their search-space, they found well-known catalyst compositions for the WGSR as well as new catalyst compositions [132]. Evolutionary strategies and stochastic design are the most useful for the discovery of new leads. Saalfrank et al. applied the directed evolution method to search for noble metal free catalysts for the oxidation of CO with air at room temperature [102]. Their search strategy was based on the concept of evolution, involving variation and selection, whereby variation was obtained by doping and composition spread, while selection was based on the catalytic activity which was determined through heat of reaction. The authors repeated the doping and composition spread procedure until no further improvement of the catalytic activity was possible. Using the said approach, the catalyst $Al_1Mn_{6.7}Co_{92.3}$ was identified for CO oxidation at room temperature.

Corma and co-workers developed a new approach for experimental design that involves the combination of an artificial neural network (data-mining technique) with high-dimensional optimisation algorithms (generic algorithm), in such a way that the knowledge extracted from the previous experiment can be applied in the design of the new subset of catalysts to be experimentally screened in the next optimisation step. The group used this approach for the integration of an ANN prediction model with GA in the optimisation of epoxidation catalysts [122]. Initially a series of candidates for the new generation (virtual generation) is designed by GA operators and stochastic pre-screening was then carried to design the new generation (real generation) to be experimentally tested. The pre-screening process is carried out in two steps: first, the performance of the candidates is predicted by ANN and second, stochastic

selection of the catalysts takes into account their predicted catalytic performance. Subsequently, this new real generation is experimentally evaluated and the optimisation cycle is repeated until no further convergence criterion is satisfied. Two types of Ti-silicate mesoporous catalysts (Ti-MCM-41 and Ti-MCM-48) with enhanced epoxidation activity and selectivity were identified.

Computational screening has also been deployed as an alternative to experimental screening. Barteau et al. applied computational screening to study ethylene epoxidation catalysts, predicting a Cu/Ag alloy catalyst that is more selective than Ag to ethylene oxide [133]. Though computational methods may make important contributions to combinatorial chemistry, some difficulties needs to be recognized: it may be easy to create new materials with well-defined structures on a computer screen but the laboratory synthesis of these materials are seldom straight forward, some catalytic centres can exhibit dynamic behaviour during the reaction, rendering molecular simulations significantly more difficult to implement and connect to experiments.

1.3.5 Sol-gel methods

Sol-gel methods represent and attractive an easy to tailor alternative to conventional synthesis methods, such as impregnation, precipitation, ceramic firing or ion exchange on supported oxides. Historically, the sol-gel method has employed the use of metal alkoxide precursors that readily undergo catalyzed hydrolysis and condensation to form a sol of metal oxide particles with nanoscale dimensions (1-100 nm). The sol-gel process allows the preparation of metal oxides in the liquid phase at room temperature. This enables the preparation of mixed oxides under kinetically controlled reaction conditions. One of the most important features of the sol-gel process is the three-dimensional development of the metal-oxygen-metal bonds. Several important properties of the materials can be controlled by the sol-gel preparation method, such as: (i) control of well defined pore size distribution, (ii) high surface area, (iii) high purity of the components, (iv) homogeneous elemental distribution, and readily controlled composition [134, 135]. Approaches for sol-gel monolith synthesis include methods like gelation of colloidal powders, hydrolysis and polycondensation of alkoxides or nitrate precursors followed by either supercritical drying of gel, or by aging and drying under ambient conditions [136]. Through separation of the mechanism of the sol-gel process into multi steps (hydrolysis, acid- or base-catalysed polycondensation for gelation, aging, drying,

and condensation), each step can be controlled by directed parameter variation to affect the final microstructure in such a way that catalytic properties are improved. For example, when the pore liquid is removed as gas phase from the interconnected solid gel network under hypercritical conditions, the network does not collapse resulting in large volume gel with low density (aerogel). Conversely, the removal of pore liquid at or near ambient pressure by thermal evaporation leads to dry gel with large surface area (> 400 m^2/g) and very small average pore radius (<10 nm) [136]. Under basic conditions, polycondensation continues preferentially not at the terminal end of the freshly forming polyoxides chain but at central positions leading to small particle formation. Basic catalysed hydrolysis is not suited for the formation of mixed oxides because it results in precipitation and inhomogeneous sols depending on the differences in the metal centers' electronegativity [137]. Secondly many metals form insoluble hydroxides under basic conditions which prevents condensation. As shown in Figure 1.6 (a), the hydroxide ion is the attacking reagent under basic gelation, which attacks directly at the metal ion to accelerate both hydrolysis and polycondensation. The accelerated hydrolysis and condensation of the more electropositive ions results to immediate oxide domain formation and thus undesired phase separation [138].

Due to its capability to form truly mixed oxides, the acid catalyst sol-gel process is more attractive to the combinatorial synthesis of mixed metal oxides. In contrast to conventional synthesis procedures, the common operations of additional heating, filtration, adjustment of pH and other procedures are not required for gelation in sol-gel processing, which suits the use of pipetting robots. When mixed oxides are used as catalysts, the homogeneity of the composition is a crucial factor in controlling the surface reactivity. The mechanism of the acid catalyzed sol-gel process is given in Figure 1.6 (b, c) based on tetraethoxysilan (TEOS). Under acidic and water condition, the alkoxide group is initially protonated reversibly. The electron density is withdrawn from silicon, making it more electrophilic. The protonated alkoxide is then attacked by a water molecule from the rear and acquires a partial positive charge. The positive charge of the protonated alkoxide is correspondingly reduced, making alcohol a better leaving group. The transition state decays by displacement of alcohol accompanied by inversion of the silicon tetrahedron [137]. Under acidic conditions, linear polycondensate are preferentially formed. The linear chain formation continues until the whole reaction volume is filled with linear oxides chains. Cross-linking starts upon growth at inner chain positions and accelerates with the diffusional limitation of continuing terminal chain growth.

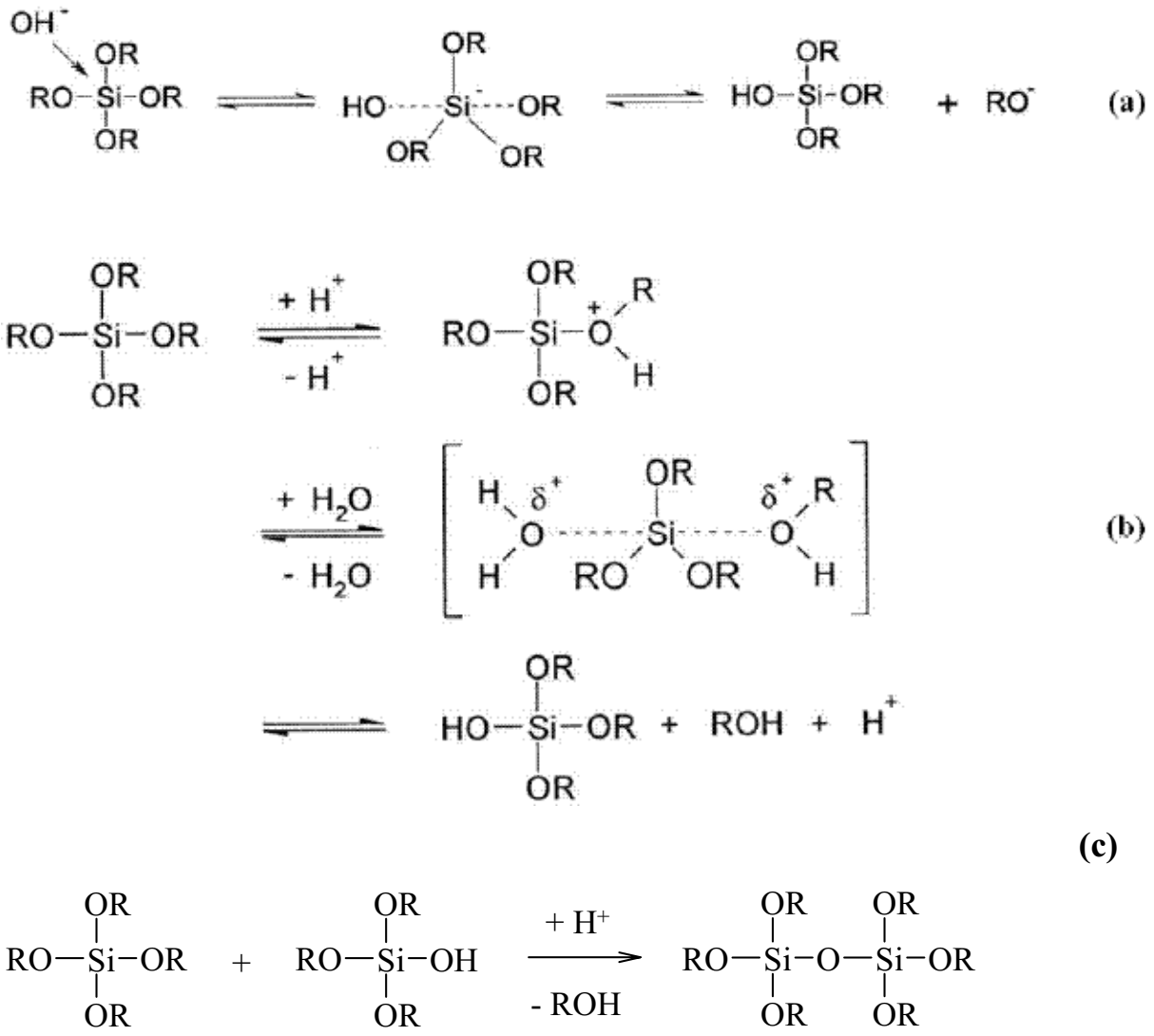

Figure 1.6 General hydrolysis reaction under (a) basic and (b) acidic conditions during sol-gel process, (c) Acid catalysed condensation.

In preparing homogeneous multicomponent gels, comparable rates of hydrolysis and condensation are required during the reaction. Furthermore the electronegativity of the central atoms will affect the chance for the formation of the desired mixed oxides. Chelating agents as well as prehydrolysis has been used to compensate for the differences in reactivity of the precursors. Mendez-Vivar and coworkers have shown that the stability of the sol depends on the chelating agent used during the preparation of Si-Ti-Zr oxide [139]. The authors claim that the use of monomeric Ti and Zr precursors stabilized with chelating agents, and pre-hydrolyzed Si sol is appropriate to control the reactivity of the components. The pore size structure of the solid was affect by the chelating agent. The sol-gel process is an effective

route to prepare active materials with high specific surface areas and homogeneity, as well as tailored properties. This method provides a means for uniformly distributing different constituents at the atomic scale. Due to its ability to proceed under mild conditions, this method is readily adapted to commercial synthesis robots.

1.4 High-throughput development of diesel soot catalysts

Despite the growing demand for efficient diesel soot combustion catalysts, the search for better catalysts is still dominated by the conventional catalyst search methods. Until now, to the best of my knowledge, just one research group (the group of McGinn) has introduced combinatorial and high-through methodology in the search of efficient diesel soot oxidation catalysts [140]. This group applied the polymerizable-complex method (PCM) to synthesize complex oxide catalyst systems. In PCM, metal ions are dissolved in solution with a chelating agent (citric acid) and a polyhydroxyl alcohol (ethylene glycol). The metal ions are chelated by the citric acid and are evenly distributed throughout the solution. Upon heating, the solvent evaporates, and the ethylene glycol undergoes polyesterification. By heating to higher temperatures, the resin is decomposed and the oxide powder is formed. A drop-on-demand printer was applied to dispense the stock solution into stainless steel sample holders. A library consisting of 15 elements was generated using 300 µl precursor solutions. After deposition, each library was processed to develop the final oxide powders. On each sample holder, a soot suspension in methanol at a concentration of 1.5 weight % was dispensed manually with a pipette. The soot solution was allowed to dry on the powders at 90 °C for 10 min. Both serial characterisation using auto-loading TGA and parallel characterisation using infrared thermography were applied. The exothermic oxidation of soot was used as a diagnostic test to examine the behaviour of the catalysts libraries using an infrared-camera.

The authors heated a copper-potassium library with 15 members to temperatures between 340 °C and 400 °C in increments of 5 °C while allowing the system to equilibrate for 5 minutes at each temperature in order to minimise the exhaustion of the soot before characterisation at higher temperatures. The authors claim that the Cu_xK_{1-x}-O system was active for the catalytic oxidation of soot in this temperature region but that the temperature increase was small (1.5-2 °C) which was close to temperature increase observed when no reaction was occurring. They stressed the need of a more sensitive system to unambiguously detect these signals which was not available for their study. Also in the study, the smooth uniform surface required by IR-

thermography could not be achieved by manually pipetting the soot on the catalysts, which reduced the accuracy of the results. Furthermore, their IR camera was unable to distinguish temperature increases over the sample from the radiant effects of the walls. Their conclusion was that though the IR-thermography approach to screen soot oxidation catalyst was seemingly fast, the obtained results were too ambiguous. The authors did not address the reproducibility of their results.

Using the same synthesis approach combined with an automated serial screening method, the same authors screened a large number of alkali-doped oxides. The soot suspension was dispersed on the catalyst powder with a pipette. After drying, the catalyst-soot mixtures were characterised serially in an auto-loading high resolution modulated thermogravimetric analyzer (TGA). Using this approach, they identified $CuFe_2O_4$, $CuMn_2O_4$, $CoFe_2O_4$ and $CoMn_2O_4$ as potential soot oxidation catalysts. The activities of the said catalysts were increased by adding alkali metal dopants. The advantage of the automated TGA system compared to commonly used TGA is that the system can run unattended. In comparison with the IR thermography technique, the TGA method leads to more reliable results. However, the automated TGA approach is relatively slow and therefore more suited for secondary screening.

1.5 Selective oxidation of alcohols by molecular oxygen

The major objective of this study was to develop soot oxidation catalysts, however potential soot oxidation catalysts may also possess strong activities for the selective oxidation of alcohols by molecular oxygen, therefore catalysts found to be active for soot combustion were also screened for this reaction. The selective oxidation of olefins and alcohols to the corresponding epoxides, aldehydes and ketones is of great importance in the fine chemical and pharmaceutical industries. Most often, these catalytic processes are still performed with strong inorganic oxidants and organic solvents which lead to a great deal of environmental undesirable waste. It is highly desirable to replace the conventional processes by an environmentally benign procedure. Clearly, there is great demand for solid materials that can catalyze the oxidation of organic substrates by molecular oxygen or H_2O_2. Most successful examples of selective oxidation of organic substrates by molecular oxygen are focused on homogeneous catalysts [141-144]. A number of catalysts with high activity and selectivity for the oxidation of olefins and alcohols using H_2O_2 under mild condition have been reported

[145-146]. Though H_2O_2 is atom efficient and the only by-product is water, compared to molecular oxygen, its relatively high cost may hinder its application.

Wang and co-workers described that single site Co(II) catalysts present in faujasite zeolite or in MCM-41 are active in the aerobic epoxidation of styrene [147]. Kantam et al. reported the molecular oxygen epoxidation of different styrene by Co-SiO_2 catalyst in the presence of dimethyl furan [148]. The oxidation was carried out in air in a 100 mL three necked round-bottom flask equipped with a magnetic stirrer and reflux condenser. Styrene, dimethyl furan and the catalyst were added in the reactor and heated to the desired temperature. The reaction was started by bubbling of air into the liquid and after completion of the reaction, the catalyst was filtered off, and the liquid organic products analyzed by a gas chromatograph. The authors achieved a styrene conversion of 72 % with epoxide selectivity of 77 %. Meng and coworkers have shown that $Cu_2(OH)PO_4$ and $Cu_4O(PO_4)_2$ are capable to oxidise styrene, cyclohexene, benzyl alcohol and cyclohexanol with molecular oxygen [149]. The reactions were performed without the addition of a solvent. Both catalyst exhibited high catalytic activity by molecular oxygen, giving styrene conversion of 30.2 and 27.7 % respectively. Styrene epoxide and benzaldehyde were the only products from both catalysts. The catalyst showed cyclohexene conversion of 46.7 % and 45.6 % and cyclohexenone selectivity of 65.7 and 68.6 % respectively.

Weinberg and co-workers have developed a combinatorial approach to the discovery and optimisation of catalysts for selective aerobic alcohol oxidation [150]. The authors claim that the high-throughput robotic synthesis and screening of polyoxometalate and supported-metal libraries have enabled the discovery of highly selective catalysts for the oxidation of various diverse alcohols substrates. Ninety-six-well high-throughput high-pressure batch reactors were used for the oxidation of 2-butyl-5-hydroxymethyl-imidazole to 2-butyl-5-formyl imidazole, an important pharmaceutical intermediate. Yamaguchi and co-workers have reported that Ru/Al_2O_3 can act as an efficient heterogeneous catalyst for the oxidation of alcohol with 1 atm of molecular oxygen or air without additives [151, 152].

1.6 Research Objective and Scope

Presently most continuous regenerating systems are based on catalysts, which consist of noble metals (Pt, Pd) or their mixtures with different base metals. These systems are not just

expensive but also difficult to apply in regions with high fuel sulphur content. Introduction of a diesel oxidation catalyst technology free of noble metal or with low noble metal content gives additional advantages with respect to cost reduction and system stability. Although significant research has been accomplished internationally to develop noble metal free diesel oxidation catalyst, the results are not satisfactory mainly due to increasing stringent emission legislature. The objective of this research was to develop a high throughput technology, which allows the efficient search of new catalysts formulations to lower diesel soot oxidation temperature. For this purpose a two step approach was developed, one in-charge of the primary screening of the possible catalysts and the other in-charge of the validation of possible catalyst leads. Printex U an industrial flame soot produced by high temperature pyrolysis was used as model soot for the primary screening. Studies from the Mouljin group have shown that Printex U approximates diesel soot for laboratory experimental purposes [28]. The combinatorial synthesis of mixed metal oxides was employed for the development of low temperature soot oxidation catalysts. The automated sol-gel synthesis method, which has established its potential for the synthesis of large solid state material libraries, was applied for the library synthesis.

Emissivity corrected infrared thermogravimetry is established as a true parallel screening technique for gas phase heterogeneous reactions. The task here was to extend the applicability of this technology in the screening of soot oxidation catalysts. Bearing in mind that high-throughput techniques are prone to errors, a reliable secondary screening technique was imperative. Here a thermogavimetry analyser as well as a semi plug flow reactor has been used to confirm the materials discovered by high-throughput experiments. The development of a single catalyst unit capable of oxidizing soot as well as reducing the NO content will safe both cost and space in diesel exhaust system. An extensive search in the specialized publication and patent literature shows a lack in reliable multi-purpose soot oxidation and NO_x reduction catalysts. A further objective of this work was to develop such multi purpose catalyst. Because of the complex nature of such a system, it is not possible to used high-throughput screening technique therefore a conventional unit was used to access such catalysts.

The catalyst discovered should be investigated for their potential to catalyze selective oxidation reactions, such as selective oxidation of alcohols to their corresponding aldehydes and ketones by molecular oxygen.

2 Results and Discussion

2.1.1 Combinatorial syntheses

The aim of this work was to develop new catalysts for low temperature soot oxidation using the combinatorial approach of material discovery. The chemical space is nearly infinite and cannot be searched in a systematic way even with high-throughput experimentation (HTE). As such, the primary objective was to develop a search strategy that will ensure a greater probability of obtaining hits for this reaction. The search strategy used in this work is presented in Figure 2.1. Initially the chemical elements, the preparation method, as well as the test method were defined. Two strategies can be considered by the choice of elements used in a combinatorial discovery: (i) the choice of elements from the periodic table could be based on prior information on the activity of the element on a particular reaction, or (ii) elements are chosen with no precedence to the catalytic reaction [153]. In the first approach, relevant and/ or potentially relevant factors are thought to be known so that libraries can be designed in a well defined frame. Library design would concentrate on a composition and parameter space around systems which are known to work and which are varied in a systematic and efficient way.

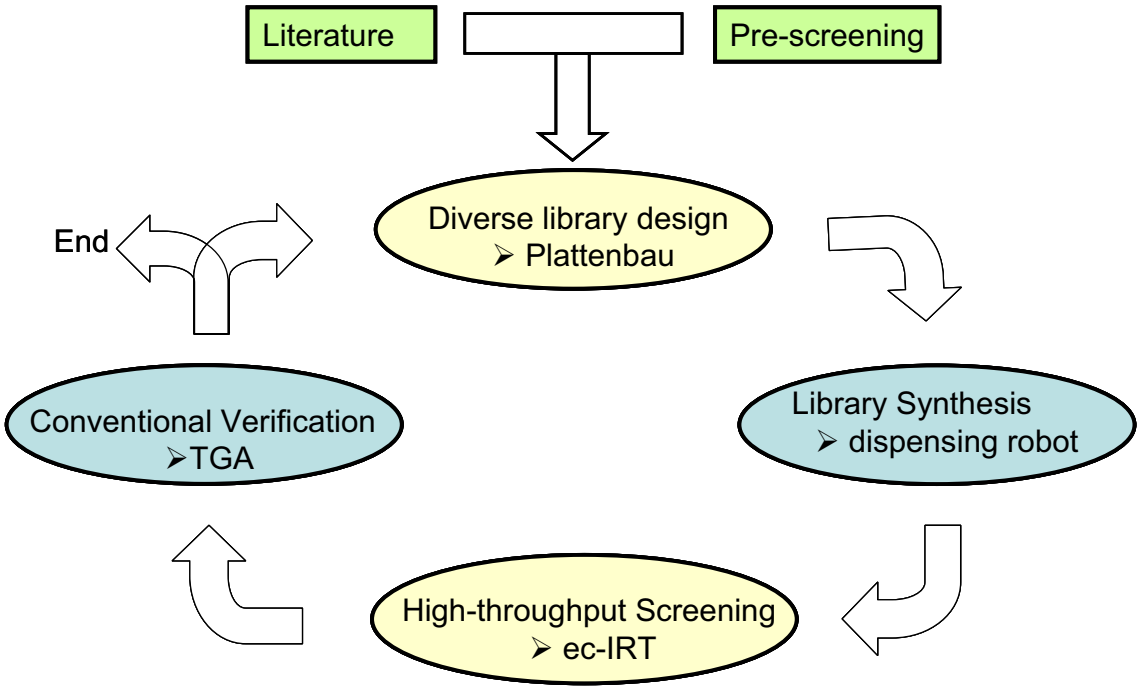

Figure 2.1 High-throughput experimentation design cycle

The disadvantage of this approach is that the discovery of new materials is limited. The probability of new discovery is higher with the second approach. A combination of the two strategies was applied in this work.

The starting library consisted of catalysts synthesized by different co-workers in our group to test for their activities on different oxidation reactions. Unfortunately this start library did not lead to any hit. Therefore another start library was consider whereby the based elements Co, Mn, and Ce known to catalyze soot oxidation were doped with different elements of the periodic table. The elements used to dope the base elements are given in Table 2.1 below. The purpose of this doping here was to achieve a highly diversified starting library thereby increasing the chance for the discovery of novel soot oxidation catalyst. After each optimisation cycle, the results from the high-throughput and the conventional experiments were used for the planning of the next libraries.

Li												B					
Na	Mg											Al	Si				
K	Ca	Sc	Ti	V	Cr	Mn	Fe	Co	Ni	Cu	Zn	Ga	Ge		Se		
Rb	Sr	Y	Zr	Nb	Mo		Ru	Rh		Ag	Cd	In	Sn	Sb	Te		
Cs			Hf	Ta	W				Pt				Pb	Bi			

La	Ce	Pr	Nd		Sm	Eu	Gd	Tb	Dy	Ho	Er	Tm	Yb	Lu

Table 2.1 Used periodic elements in the present study

The central elements with the expected atomic % given in subscripts as expected from the composition of the starting sol are used to denote the samples. For example La_3Co_{97} is a mixed metal oxide composed of 3 mol % La-oxide and 97 mol % Co-oxide, respectively. The oxidation states of the mixed oxides, which rely on the reaction conditions, were not determined. Therefore the oxygen content which is dependent on the oxidation states of the elements remains unspecified.

2.1.2 Library Synthesis

The sol-gel method whose validity to synthesize catalyst materials has been proven in the group of Maier, was deployed for the syntheses of the mixed metal oxides considered in this work. The motivation for the sol-gel processing as mentioned in the introduction is its ability to allow the preparation of metal oxides in the liquid phase at room temperature and atmospheric pressure. This property of the sol-gel method allows the easy coupling of the sol-gel synthesis to a synthesis robot, thereby increasing the speed at which materials are synthesized. The recipes tolerant to precursor variation have been developed. The software "Plattenbau" was used for the planning of the catalysts library synthesis [154]. This software available in Maier's group significantly accelerates the design of catalysts library. The software calculates based on a parameterized recipe, the volume of the different solutions of the starting materials as required for the preparation of the individual samples. The optimized pipetting list generated is then transferred to the synthesis robot of type Lissy (Zinsser Analytic). This robot is equipped with two tips used to transfer reagents solution from the reagent rack to the reaction mixture rack. The robot workbench is used to define the layout of racks and substrate on the deck of the robot. The stock solutions positioned in 10 or 20 ml vials placed in the wells of a metal plate are transferred by the tip into 2 ml HPLC-vials positioned in racks of 50 vials. The metal nitrate, alkoxide or chloride precursors used were initially dissolved in methanol or isopropanol solution. After the pipetting process of an entire rack was completed, the entire rack was stirred by an orbital shaker for homogenisation. The obtained samples from gelation were calcined using appropriate heating rates and constant temperature programmes. The calcinations step enabled the burning of the organic constituent in the sample.

2.1.3 Thin film libraries

The catalyst powders obtained after calcinations were crashed with a glass rod in the vial and manually transferred into the 206 hexagonally positioned wells in the library plate. It is essential to maintain a constant filling height of the catalysts in the wells in order to achieve a uniform soot film after coating. The catalyst library was later decorated with a smooth soot film using a commercial air brush and dried. An example of such a decorated library is show in Figure 2.2 below. The advantage of this method is the short time (5 min) required to achieve such a decorated library. On the other hand, it is difficult to achieve the same soot

thickness on each catalyst spot which renders the reproducibility of the results obtained from such libraries difficult.

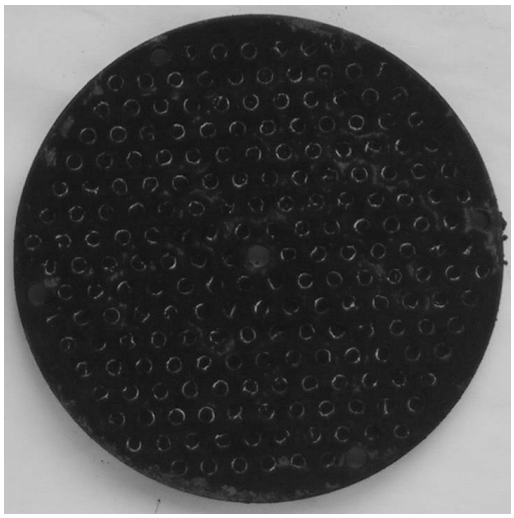

Figure 2.2 An example of a soot coated library.

2.1.4 High-throughput Screening

Emissivity-corrected IR-thermography (ec-IRT) was used for the parallel screening of potential soot oxidation catalysts. Ec-IRT allows the detection of heats of reaction of a particular reaction on the catalysts surface, which can be interpreted as catalytic activity. The oxidation of soot with oxygen is an exothermic reaction leading to the release of heat. The released heat increases the surface temperature of the catalyst in the library slate. The increased temperature is directly linked to the catalytic activity. The IR-image of an object is composed of emitted and reflected radiation. Reflectivity and emissivity are material specific properties and may change from sample to sample. Local differences in emissivity and reflectivity on a library surface and its individual catalysts spots do appear as different photon intensities, which can be misinterpreted as different temperatures, although the true temperature are identical. In order to be able to quantify temperature changes from measured emission changes on combinatorial libraries with diverse materials, emisivity correction is imperative. Figure 2.3 shows a picture of the used reactor closed with a sapphire glass and the IR-camera employed to investigate the catalytic activity of 206 catalysts in a library. A full description of the IR-thermographic measurement technique is given under the experimental section (3.4).

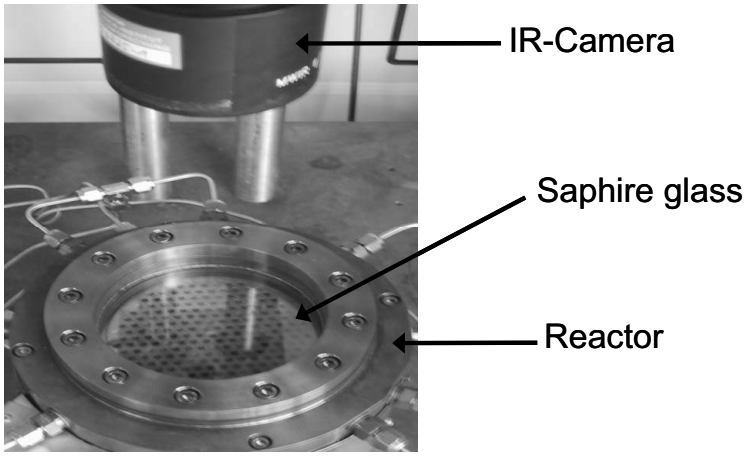

Figure 2.3 IR-thermography reactor with sapphire glass and Camera

The high-throughput screening process was completely automated, controlled by the "TestRig" software [154]. Before each high-throughput screening, the user simply defines the screening conditions and sequence in the IR-Testrig software as shown in Table 2.2 below. The screening protocol can be divided into the preconditioning stage, the temperature calibration stage, background IR-imaging before reaction stage, reaction IR-imaging stage, background IR-imaging after reaction stage, and the experimental closure stage.

Nr.	Instrument	Befehl	Parameter	Nr.	Instrument	Befehl	Parameter
1	Start	(invalid)	(invalid)	20	Heizung	Temperatur	256
2	Gas	Mixtur	Stickstoff,100	21	IRCam	6.Calibration	256
3	Heizung	Temperatur	150	22	Heizung	Temperatur	250
4	Utilities	Warten	30min	23	Utilities	Warten	30min
5	Heizung	Temperatur	250	24	IRCam	Dateinamen	background-1
6	Utilities	Warten	30min	25	IRCam	Integrieren	1000
7	IRCam	Verzeichnis	D:\Daten	26	Gas	Mixtur	Synluft,100
8	IRCam	Dateinamen	250DegC	27	Utilities	Warten	1min30
9	IRCam	Integrationszeit	0.1	28	IRCam	Dateinamen	2min
10	Heizung	Temperatur	246	29	IRCam	Integrieren	1000
11	IRCam	1.Calibration	246	30	Utilities	Warten	2min30
12	Heizung	Temperatur	248	31	IRCam	Dateinamen	5min
13	IRCam	2.Calibration	248	32	IRCam	Integrieren	1000
14	Heizung	Temperatur	250	33	Gas	Mixtur	Stickstoff,100
15	IRCam	3.Calibration	250	34	IRCam	Dateinamen	Nachtbild
16	Heizung	Temperatur	252	35	IRCam	Integrieren	1000
17	IRCam	4.Calibration	252	36	Gas	Mixtur	Stickstoff,60
18	Heizung	Temperatur	254	37	Heizung	Temperatur	30
19	IRCam	5.Calibration	254	38	END	Gas	Stickstoff,0

Table 2.2 An example of the IR-thermography experimental procedure

Because of the time consuming calibration procedure, measurements can only be carried out at fixed temperatures. As standard reaction conditions, 200 °C, 250 °C, 300 °C, 350 °C, 400 °C and 50 ml/min synthetic air (nitrogen used for calibration) flow were used except stated otherwise. A full description of the integration of heat spots on the library by the "Testrig"

software is given by Scheidtman [154]. The temperature increase of each sample in the IR image was quantified with the Testrig software and standardized by relating it to the sample with the highest temperature increase on the plate. The IR image taken by the IR-camera was loaded on the Testrig software consisting of pre-defined library mask. The pre-defined library mask enabled the assigment of the calculated temperature change on each spot to the materials on the library. The software integrated the temperature change on each catalyst spot on the infrared image. The calculated temperature increase on each catalyst spot were normalized to the number of pixels considered in the integration to give the average temperature increase across each catalyst spot on the library. The average temperature increase on each spot was normalized to the average temperature of the spot with maximum increase on the library. These normalized values provided the relative activities of the catalysts on each library. Due to the risk of false positives from the HT-screening experiments, the hits from the HT-screening were prepared conventionally using the same sol-gel recipe but increased quantity of material and tested conventionally. For the conventional screening, a commercial thermogravimetric analyser (Shimadzu TGA-50) was used. If the activities of the HT-screening hits were confirmed conventionally, then the hits were further optimized.

2.2 Catalysts based on Co, Mn, and Ce

2.2.1 High-throughput screening of soot coated library

To start with, catalyst library one was prepared by doping the basic oxides Ce, Mn and Co with 50 different elements. The materials in this first library are denoted as M_3Ce_{97}, M_3Mn_{97} and M_3Co_{97} respectively. The used precursors for each dopant and based element our given in Table 3.1 under the experimental section. Five different reference materials namely: $Pt/Rh/ZrO_2$, Pt/ZrO_2, Pd/ZrO_2, Pd/Al_2O_3, (supplied by our project partner), $Cs_2V_1Fe_2/Al_2O_3$ (a literature catalyst) and 25 catalysts from previous group members were also filled at different positions in the library. The actual position of each material on the library is given in Figure 2.4. The library was decorated with a soot film prior to the IR-screening. The method used to prepare the soot suspension and to coat it on the library is given under the experimental section (3.2). The obtained IR-image of the library at 300 °C is shown in Figure 2.5

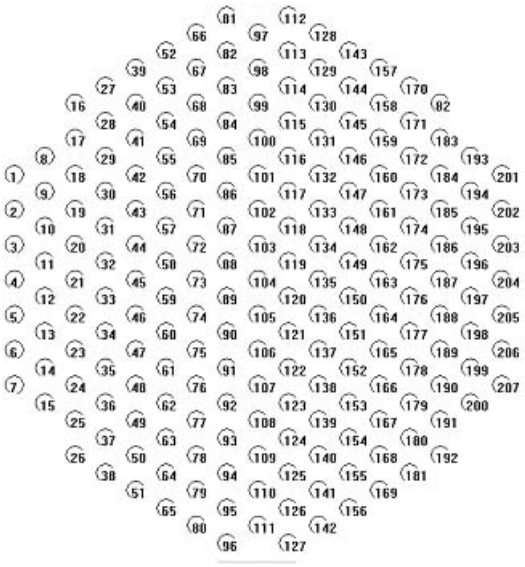

Figure 2.4 Library one filling plan, the actual material indicated by each number is given under section 6.4.

The ten best catalysts on the library are given in Table 2.3 whereby the activities of the catalysts are stated as a function of the best catalyst on the library. The best catalyst so far was the Rb doped Cobalt oxide sample, followed by the Cr_3Co_{97} sample. The best Ceria matrix doped sample was Ag_3Ce_{97}. None of the Manganese oxide doped sample showed considerable activity. All the five reference catalysts included in the library were inactive.

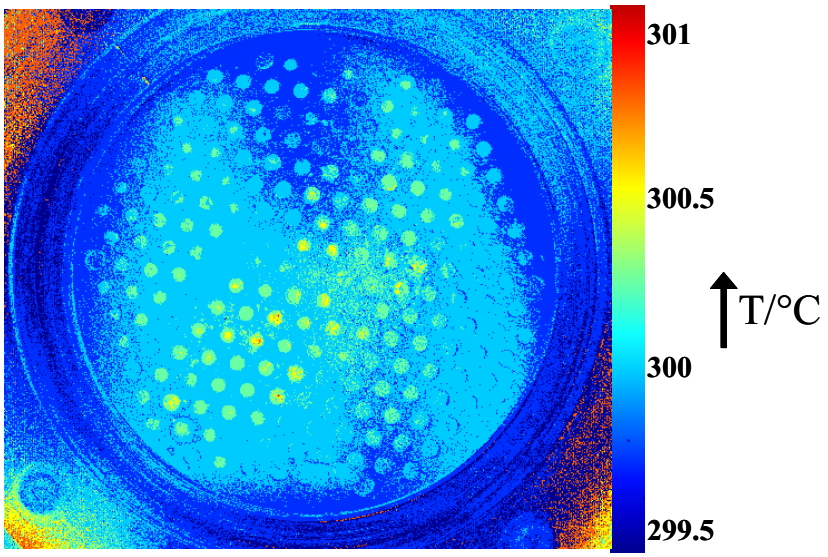

Figure 2.5 The emissivity-corrected IR-thermographic image of library one at 300 °C for the combustion of soot

Catalyst composition	Relative Catalytic activity [%]	Catalyst composition	Relative Catalytic activity [%]
Rb_3Co_{97}	100	Hf_3Ce_{97}	53
Cr_3Co_{97}	94	Sm_3Co_{97}	48
Cd_3Co_{97}	82	Fe_3Ce_{97}	41
Ag_3Ce_{97}	65	V_3Ce_{97}	40
Na_3Co_{97}	64	Ag_3Co_{97}	39

Table 2.3 Catalytic composition and relative activity of the ten best catalysts on library one

2.2.2 Conventional testing of soot coated library one catalysts

Due to the risk of false positives from the high-throughput screening experiments the hits have to be tested conventionally. Therefore promising soot-catalyst mixtures were validated using a Shimadzu TGA-50 thermogravimetric analyser. Because of the complexity of catalytic soot oxidation, even non-active materials on the first library were tested conventionally. Three milligrams of soot were mixed loosely with 12 mg of catalyst in a GC vial with a spatula before being transferred to the TGA crucible. This mixing ensured a loose soot-catalyst contact which is assumed to simulate well the actual soot-catalyst contact in a real diesel exhaust system [155]. Maintaining a fixed soot-catalyst ratio is very important to achieve reproducible results. The mixture was heated from 25 °C to 700 °C at a heating rate of 10 °C/min in a 50 ml/min synthetic air flow. The activity of a catalyst is defined by the combustion temperature, which is the temperature of the TGA curve where 50 % (T_{50}) of the soot is oxidised. Shown in Figure 2.6 is the method used to approximate the T_{50} value. Using the non catalytic oxidation of soot and Cr_3Co_{97} catalysed soot oxidation as reference, the T_{50} value was estimated by linking the 0.5 value on the relative soot weight axis to the soot oxidation curve with a straight line. The intersection of the straight line and the curve is linked to the temperature axis with a straight line. The temperature at the point of intersection of this new straight line and the temperature axis is read as T_{50}. The Cr_3Co_{97} / soot mixture required a slightly lower temperature for soot combustion compared to the non-catalytic soot combustion.

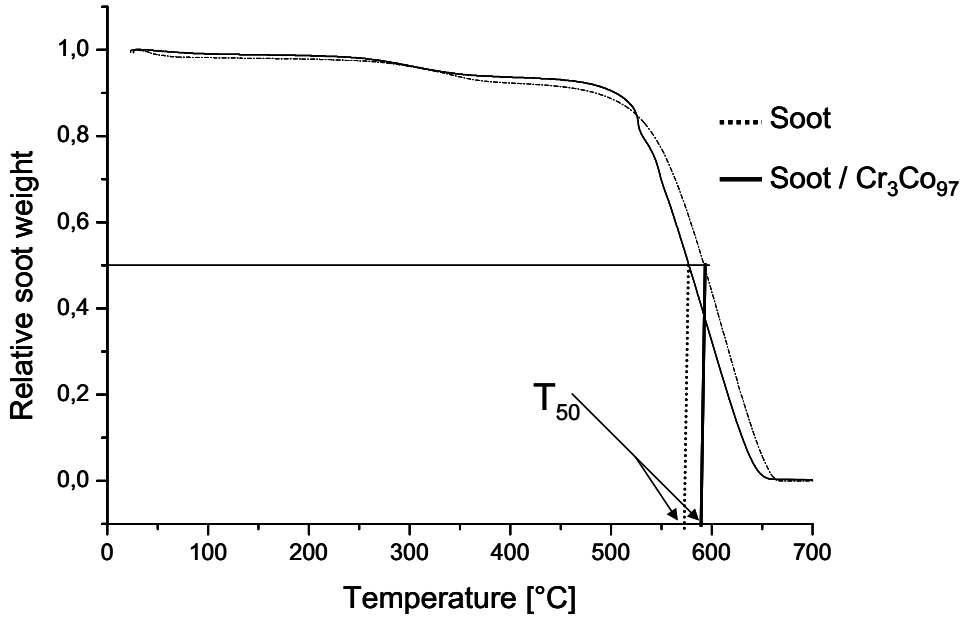

Figure 2.6 Comparison of TGA curves for soot oxidation with and without Cr_3Co_{97} catalysts.

Table 2.4 shows the T_{50} values of some selected catalysts from library one. As shown in this table, the best catalyst was K_3Ce_{97}, followed by Cs_3Co_{97} sample. For these samples, the T_{50} values were 439 °C and 460 °C respectively. Surprisingly, none of these catalysts showed activity during the high-throughput experimentation. One of the possible reasons for this high discrepancy between the HTE and conventional experiment may be the different reaction conditions used. The soot was coated on the catalyst surface using an air brush during the HT experiment and a uniform soot film could not be guaranteed on each catalysts spot. This arrangement may lead to different exposure of the catalyst to the reactant gas and IR observation being made through unreacted soot that lies above since the catalyst promoted combustion may only occur at the soot-catalyst interface. The TGA samples, which were obtained by simply mixing the catalyst and soot may lead to a more exposure of the catalyst to the reaction gas. It was therefore decided, to test catalyst-soot mixtures similar to those used in the TGA-experiments, also in the HTE.

Catalyst composition	T_{50} [°C]	Catalyst composition	T_{50}[°C]
K_3Ce_{97}	439	Zn_3Ce_{97}	546
Cs_3Co_{97}	460	Co_3Ce_{97}	548
Na_3Co_{97}	485	Lu_3Ce_{97}	552
$Cs_2V_1Fe_2$ /Al_2O_3	493	Ge_3Ce_{97}	554
Mn_3Ce_{97}	502	Ca_3Ce_{97}	556
Rb_3Co_{97}	520	Ca_3Mn_{97}	559
Ag_3Ce_{97}	530	W_3Ce_{97}	562
Ba_3Co_{97}	530	V_3Ce_{97}	568
Mo_3Ce_{97}	531	Rb_3Mn_{97}	570
Hf_3Ce_{97}	538	Gd_3Mn_{97}	573
Cd_3Ce_{97}	538	Ti_3Ce_{97}	574
Fe_3Ce_{97}	539	Cr3Co97	578
La_3Ce_{97}	539	Soot	593

Table 2.4 TGA results of selected catalysts from library one for the oxidation of soot with synthetic air. Shown are the catalysts compositions and their corresponding T_{50} temperature values.

2.2.3 Effect of oxygen concentration

Depending on the operation mode, the oxygen concentration in diesel exhaust varies between 5 % and 15 % [156]. This variation in the oxygen concentration can affect the reaction rate. The reaction order in oxygen concentration was found to vary between 0 and 1 in various studies and the reaction rate is generally taken as sole function of oxygen partial pressure [157-159]. In order to determine the effect of oxygen concentration on catalytic soot oxidation, three sets of measurements were conducted whereby the same gas flow rate (50 ml/min) was maintained but the concentration of oxygen varied (21 %, 10.4 %, and 6.4 %). Oxygen concentration variation was achieved by diluting synthetic air with nitrogen. Shown in Figure 2.7 is the TGA plot of the relative soot combustion as a function of temperature for the Zn_3Ce_{97} catalyst. These results show that the combustion temperature of soot shifts to the right as oxygen concentration decreases.

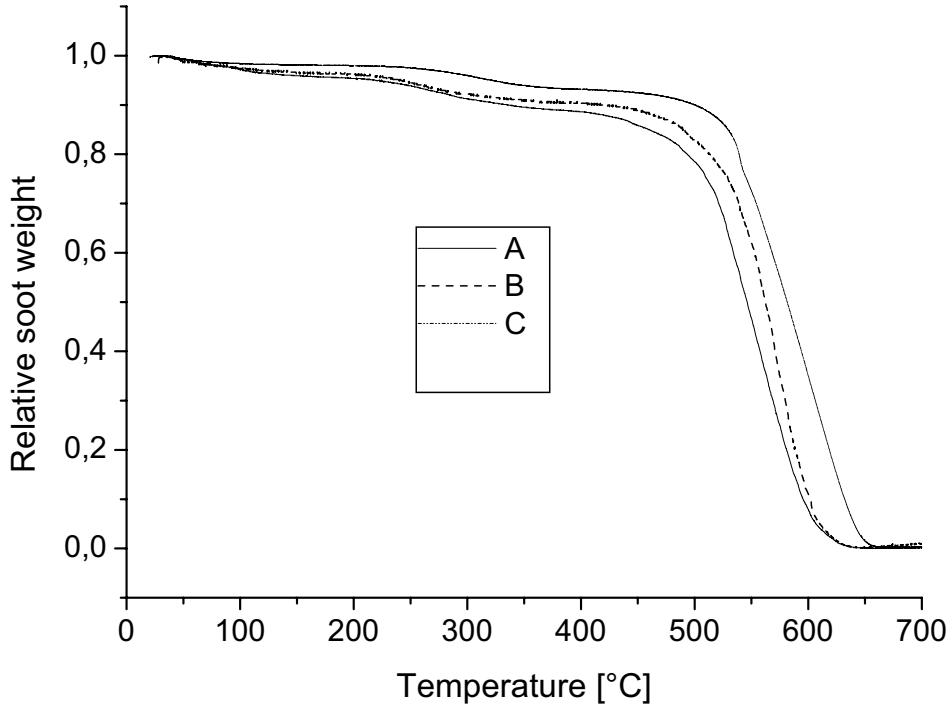

Figure 2.7 The effect of oxygen concentration on Zn_3Ce_{97} catalysed soot combustion at a constant gas flow rate of 50 ml/min. (A: 21 % O_2, B: 10.4 % O_2 and C: 6.4 % O_2)

A temperature difference of about 36 °C existed between the T_{50} values measured when the oxygen concentration was lowered from 21 % to 6.4 %. The data document a positive reaction order in oxygen. These results highlights the importance of a catalyst to function well under varying oxygen content in the reaction gas since soot oxidation catalysts are expected to function well under different oxygen content in diesel exhaust system.

2.2.4 Effect of the oxidizer

In order to determine the use of the catalyst lattice oxygen in soot combustion, TGA experiments were performed with selected catalysts under different gas flow. During one such experiment, five mg of soot was submitted to a temperature ramp from room temperature to 700 °C (10 °C/min) under synthetic air or nitrogen flow at a rate of 50 ml/min. The weight loss data obtained from the TGA are summarized in Table 2.5. For soot combustion with air, no residual ash was recovered which means all of the soot was burned. When soot was treated under nitrogen flow, only 24 weight % of soot was loss. This loss may be explained as coming from the volatile component of soot. For all catalyst/soot samples, it was recorded

that about 20 % decrease occurred when air was used which means that all of the soot was combusted while all catalyst was recovered. When nitrogen was used as the reaction gas, most of the catalysts were not able to burn all of the soot. However the amount of soot left after the experiment was considerably lower than in the case when soot was heated in nitrogen. The $Cu_3Cs_{20}Co_{77}$ and $Cs_{20}Co_{80}$ catalyst also led to considerable soot combustion under inert atmosphere. The $Cu_{10}Cs_{20}Co_{70}$ was able to burn all the soot even under nitrogen. As shown in Figure 2.8 until about 320 °C the sample weight decreases slower in synthetic air than in nitrogen. Above 320 °C the sample weight decreased rapidly in synthetic air with soot combustion almost complete at 450 °C. Soot combustion in nitrogen progressed slowly between 450 °C and 700 °C with the bulk of the combustion occurring between these temperatures. This result clearly indicates the importance of oxygen in the gas stream.

Sample	Catalyst/soot ratio	Feed gas	Total sample weight [mg]	Residual amount [mg]	Residual [%]
Soot	---	Air	5	0	0
soot	---	Nitrogen	5	3.8	76
$Pb_{10}La_5Co_{85}$	4:1	Air	24.5	19.6	80
$Pb_{10}La_5Co_{85}$	4:1	Nitrogen	24.4	22.3	91.4
$Cs_{20}Co_{80}$	4:1	Air	24	19.1	80
$Cs_{20}Co_{80}$	4:1	Nitrogen	24.9	20.9	84
$Cu_3Cs_{20}Co_{87}$	4:1	Air	25	20	80
$Cu_3Cs_{20}Co_{87}$	4:1	Nitrogen	24.1	19.8	82.5
$Cu_{10}Cs_{20}Co_{70}$	4:1	Air	20.5	16.4	80
$Cu_{10}Cs_{20}Co_{70}$	4:1	Nitrogen	20.5	16.3	80

Table 2.5 TGA results indicating the use of lattice oxygen in soot oxidation

Since more soot was combusted when mixed with catalyst under inert atmosphere compared to none catalytic reaction, the used oxygen for the extra combustion most be originating from lattice oxygen.

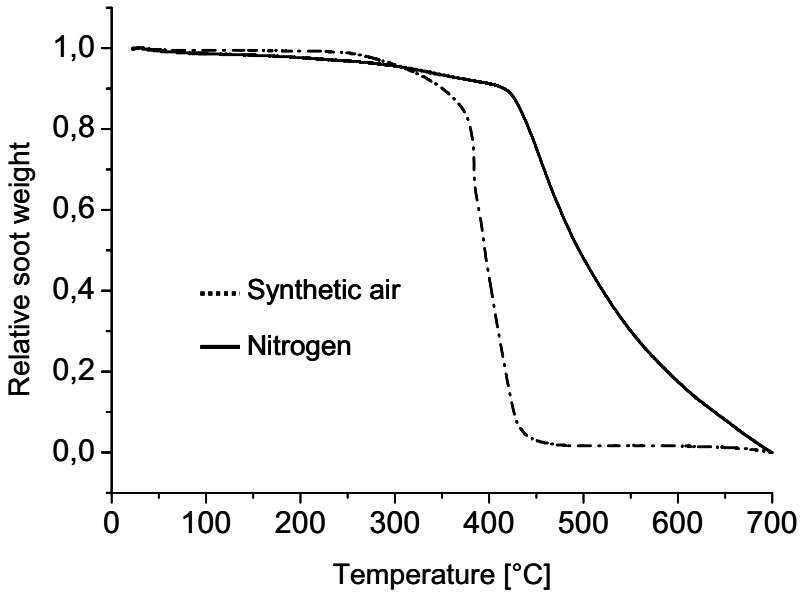

Figure 2.8 TGA curve indicating soot combustion catalysed by $Cu_{10}Cs_{20}Co_{70}$ catalyst in the presence on synthetic air flow or nitrogen flow rate of 50 ml/min

One can postulate from these results that the oxidation process utilizes the lattice oxygen, which is eventually replaced by the gas phase oxygen. This finding may partially explain why the alkali metal doped samples are more active compared to the $Pb_{10}La_5Co_{85}$ sample because they donate their lattice oxygen more freely. Nevertheless, nothing is proven here and future studies in the group may reveal the nature of this conversion.

2.2.5 Catalyst/soot ratio effect

Different catalyst/soot ratios are used in the literature whereby 9:1 and 4:1 are the most often used ratios. In order to determine the effect of the catalyst/soot ratio on catalytic soot combustion, two catalyst/soot ratios (9:1 and 4:1) were prepared by mixing soot and Cs_3Co_{97}. Both samples were mixed using a spatula and later subjected to a temperature ramp under synthetic air flow. The obtained results are depicted in Figure 2.9. Both samples showed almost the same soot combustion profile, with the 9:1 mixture achieving a slightly better combustion. At T_{50}, a temperature difference of 9 °C was recorded between the two mixtures, which was regarded as insignificant. In this study we decided to use a catalyst/soot ratio of 4:1 in order to test our materials in a more severe environment.

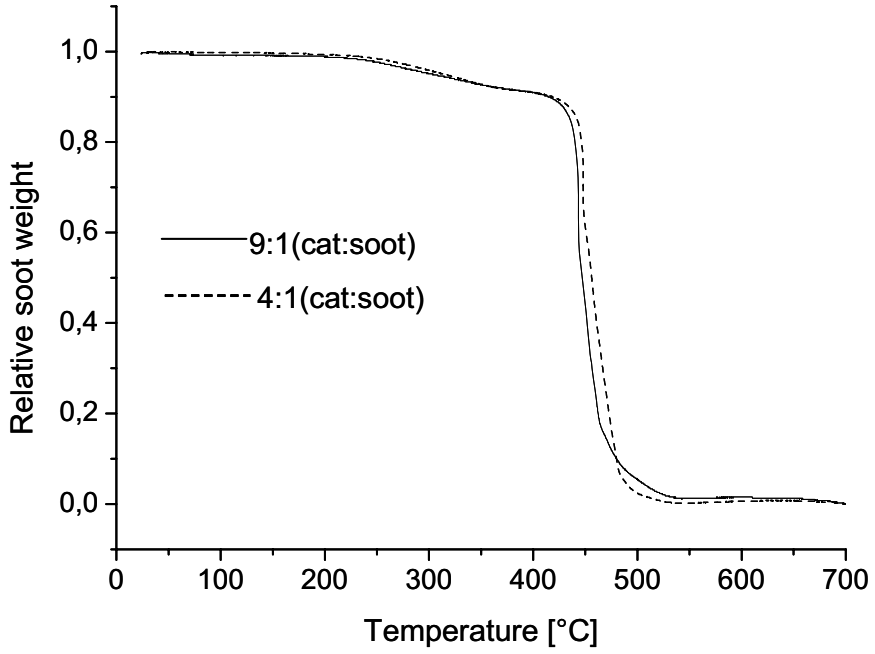

Figure 2.9 TGA curves showing the effect of the catalyst/soot ratio on Cs_3Co_{97} catalysed soot combustion

2.2.6 Effect of catalyst-soot contact on combustion

The type of soot-catalyst contact is one of the factors that influence the catalytic activity of a catalyst on soot combustion. Neeft at el. has defined two types of contact modes, which were named tight and loose contact. Many catalysts which where reported as active in tight contact showed no activity in loose contact. The difference between the tight and loose contact depends on the type of catalyst used [155]. In order to determine the effect of the contact mode on the activity of different catalysts, a tight contact mixture of soot/catalyst was prepared by mixing a 4:1 weight ratio of catalyst and soot first with a spatula and later in a mortar for 10 min. The mixtures were pressed to tablets employing a hydraulic press with a pressure of 50 bars. The tablets were later granulated and subjected to a temperature ramp under synthetic air flow. The loose contact samples where prepared by the method mentioned earlier by simply mixing soot and catalyst with a spatula.

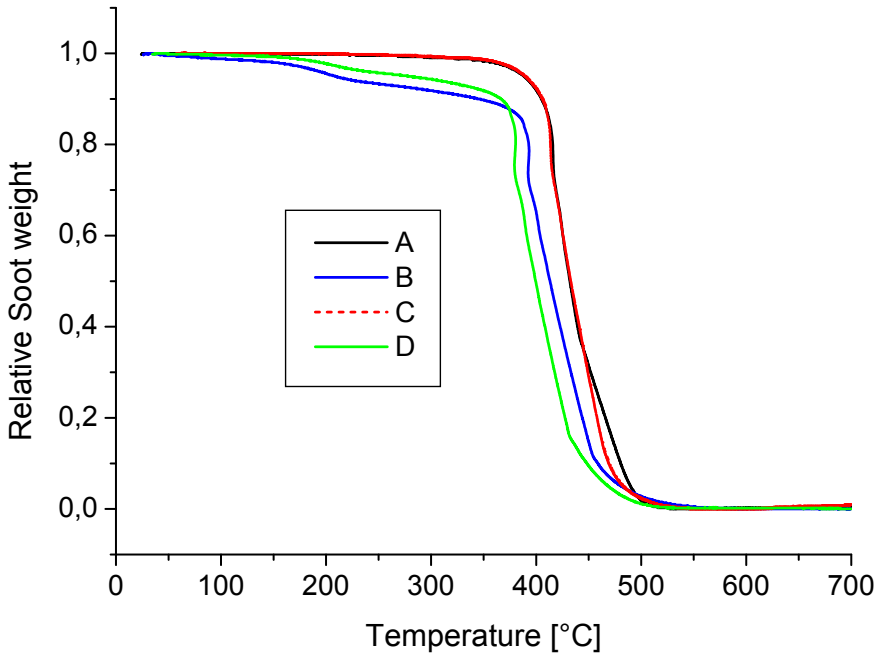

Figure 2.10 TGA curves indicating the effects of the soot/catalyst contacts on soot combustion, where curve A and B depicts soot combustion catalysed by $Cs_{20}Co_{80}$ under loose and tight contact respectively, curve C and D depicts soot combustion catalysed by $Pb_{10}La_5Co_{85}$ under loose and tight contact respectively.

The obtained results for selected catalysts are given in Figure 2.10. It can be clearly seen from this Figure that the catalytic activity of both catalysts were influenced by the contact mode. A T_{50} value difference of up to 33 °C was registered on the $Pb_{10}La_5Co_{85}$ catalyst between the two modes of contact. A lesser T_{50} value difference was registered by the $Cs_{20}Co_{80}$ samples with the tight contact sample showing a value about 18 °C smaller than the loose contact sample. Working under realistic soot-catalyst contact (loose contact) implies that physical phenomena become very important, thus decreasing the overall reaction rate. For evaluation of intrinsic reaction mechanisms, physical phenomena like mass and heat transfer limitations must be minimized. Working under tight contact conditions is obviously not realistic but may be relevant in order to study the intrinsic catalytic chemistry, which may be essential for a rational catalyst design. The findings reported here confirmed that combustion is highly dependent on intimate contact between soot and catalyst. Such a behaviour makes catalyst evaluation a difficult task. Since we wanted to work close to the real soot-catalyst contact in the diesel car exhaust, loose contact was selected.

2.3 Catalyst-soot mixtures libraries

As demonstrated by the high discrepancy between the HTE with thin films and conventional results, a challenging part of the study was the development of a suitable test protocol for catalytic soot oxidation. In heterogeneous catalysis catalytic reactions occur with molecules chemisorbed on the surface at the active site through Langmuir-Hinshelwood or Eley-Rideal type mechanisms. For the combustion of soot there is no carbon vapour and molecular contact between catalyst and soot can not be relied on. Instead the reagent is oxygen, which is activated by the catalyst and oxidizes the soot through a still undefined mechanism. Oxygen spillover may be a possible mechanism. Because the HTE with thin soot films results could not be reproduced, a different approach was considered whereby the powder catalyst and soot were manually mixed (loose contact) with a defined ratio (4:1) and manually transferred in the 206 hexagonally positioned wells in the library plate. A full description of the library preparation process is given under section 3.2.2. Figure 2.11 shows a catalyst-soot mixture library. The advantage of this method compared to aforementioned method is that all mixtures are positioned as powders with comparable filling heights in the wells which reduce potential errors due to their different exposure to reactant gas. However, the pre-mixing method is more time consuming, requiring both catalyst and soot weighing and mixing followed by manual filling of the wells in the library plate, which limits the HT nature of this method.

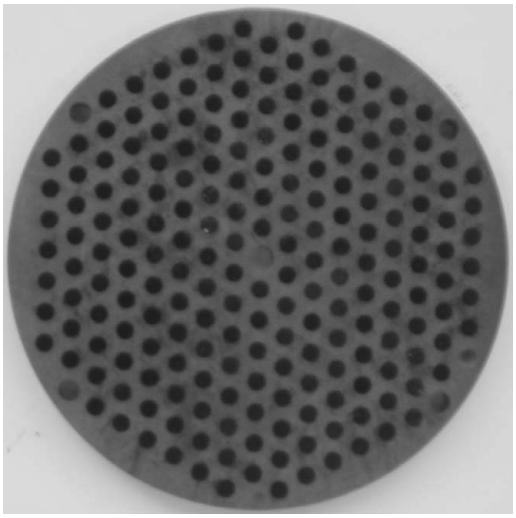

Figure 2.11 An example of a library filled with catalyst-soot mixtures.

2.3.1 High-throughput screening of libraries 2, 3, and 4

The library two, three and four were prepared by doping the three base oxides (Ce, Co and Mn) respectively with 50 selected elements in a molar concentration of 3 %. Co and Mn were doped with the alkali element Cs while Ce was doped with K. The choice of K for Ce was based on promising literature results which suggest that K is a better alkali dopant for Ce. The catalyst and soot were mixed prior to filling in the library. Library two consisted of 50 cerium doped samples, selected catalyst from our group members and five reference catalysts namely: $Pt/Rh/ZrO_2$, Pt/ZrO_2, Pd/ZrO_2, Pd/Al_2O_3, and $Cs_2V_1Fe_2/Al_2O_3$.

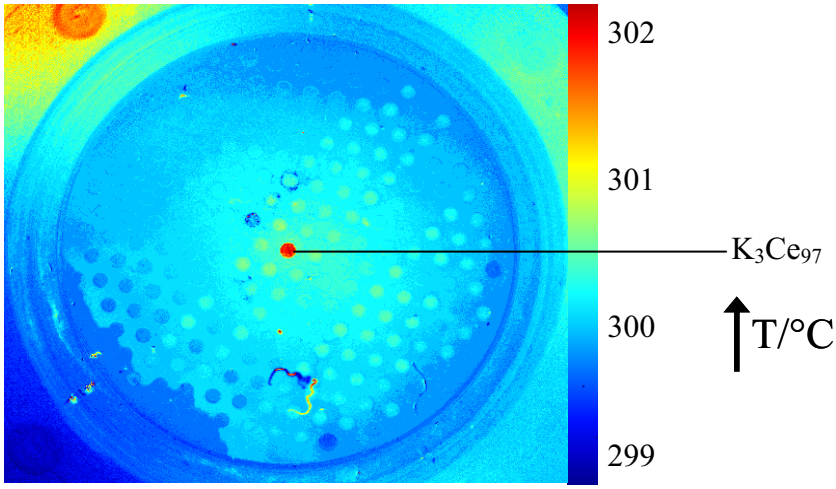

Figure 2.12 The emissivity-corrected IR-thermographic image of library two at 300 °C for the combustion of soot.

The actual position of each catalyst in the library is given under section 6.4. The measured IR-image of the library at 300 °C is depicted in Figure 2.12. As can be seen from this image, only the K_3Ce_{97} sample was active for soot combustion. None of the reference catalysts were active. Because of this result, the subsequent libraries were analysed without any reference material. At this point, this result was highly welcomed since the K_3Ce_{97} previously showed activity during the conventional TGA experiment (see Table 2.4).

Library three which consisted of 50 cobalt doped samples was screened under synthetic air, flow rate 50 ml/min. Shown in Figure 2.13 is the obtained image at 350 °C and the relative activities of the best five catalysts and their compositions. Five samples, Cs_3Co_{97}, Na_3Co_{97}, Rb_3Co_{97}, Ba_3Co, and La_3Co_{97} were identified by IR-thermography as potential low temperature soot oxidation catalysts. Interestingly, these catalysts also showed activity during

the TGA experiments as shown in Table 2.4 above. Both HTE and conventional experiments identified Cs_3Co_{97} catalysts as the best sample. This confirms the fact that the development of soot oxidation catalyst with the high-throughput technique applied here can be achieved.

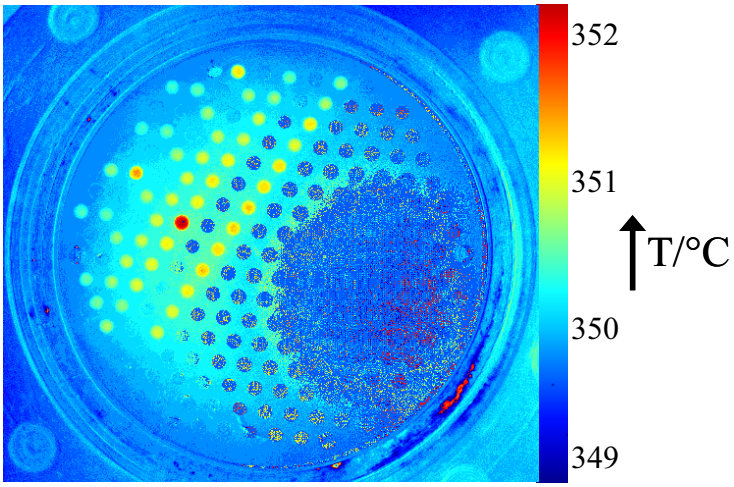

Catalyst Composition	Relative activity
Cs_3Co_{97}	100%
Na_3Co_{97}	70%
Rb_3Co_{97}	60%
Ba_3Co_{97}	48%
La_3Co_{97}	28%

Figure 2.13 (a) The emissivity-corrected IR-thermographic image of library three at 350°C for the combustion of soot. (b) Catalytic composition and relative activity of the five best catalysts on the library.

By doping manganese with 50 different elements (library four) and determining their activity with respect to soot oxidation, it was found that up to 5 samples could combust soot considerably at 300 °C (see Figure 2.14). The best catalyst in this library was La_3Mn_{97} sample.

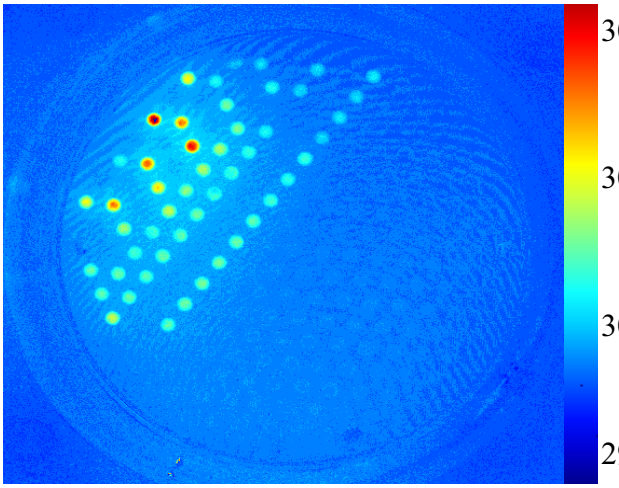

Catalyst Composition	Relative activity
La_3Mn_{97}	100%
Gd_3Mn_{97}	85%
Ti_3Mn_{97}	71%
Rb_3Mn_{97}	70 %
Ca_3Mn_{97}	67%

Fig. 2.14 (a) The emissivity-corrected IR-thermographic image of library 4 at 300°C for the combustion of soot. (b) Catalytic composition and relative activity of the five best catalysts on the library.

2.3.2 Conventional testing of libraries 2, 3, and 4 samples

The best materials from each of these libraries was further characterized with TGA by heating a 4:1 mixture of catalysts and soot from room temperature to 700 °C at a heating rate of 10 °C/min. The obtained results are summarised in Table 2.6.

Catalyst composition	T_{50} [°C]	Catalyst composition	T_{50}[°C]
Cs_3Co_{97}	456	Rb_3Co_{97}	524
Na_3Co_{97}	489	Ba_3Co_{97}	530
K_3Ce_{97}	436	Ag_3Ce_{97}	530
Mn_3Ce_{97}	502	Mo_3Co_{97}	531
La_3Mn_{97}	549	Rb_3Mn_{97}	570
Ca_3Mn_{97}	559	Gd_3Mn_{97}	573

Table 2.6 TGA results of the best catalysts from library 2, 3, and 4 for the combustion of soot with synthetic air

Among the cerium containing samples tested, the K_3Ce_{97} showed the best activity with a T_{50} of 436 °C, followed by Mn_3Ce_{97} with a T_{50} value of 502 °C. These results were in order with those obtained previously (see Table 2.4) and comparable to the HTE results mentioned in Figure 2.12. At this junction, it is logical to suggest that the development of soot oxidation catalyst with the high-throughput technique applied here can be achieved. The presence of cerium compounds at a low concentration in the fuel has been shown to drastically reduce the temperature of the burn-off of soot deposits on the filter, which probably occurs through oxidation of cerium derivatives to finely divided cerium oxide particles which grow in close contact with soot particulate [160]. Upon deposition of these mixtures on the filter CeO_2 acts as an oxidation catalyst to reduce the autoignition temperature of soot particulate, thus allowing on-site filter regeneration [161]. The Cs_3Co_{97} sample from library 3 had a T_{50} of soot at 456 °C. This result was again comparable with the HTE results. However the high activity of the five selected samples from the library four during the HT experiment could not be reproduced by the conventional method. The reason for this failure can not be explained. Compared with the method of soot coating, the mixing method was more meaningful since the HTE results were partially reproduced when the mixing method was applied.

Two alkali metal containing catalysts K_3Ce_{97} and Cs_3Co_{97} were identified both by the IR-thermography as well as by the TGA as potential low temperature soot oxidation catalysts. Cerium oxide is a well known support for diesel soot oxidation [162]. The activity of the CeO_2 has been attributed to its oxygen storage capacity. The cerium oxide may provide surface sites as well as act as an oxygen storage and transport medium [163]. This phenomenon may partially explain the activity of the K_3Ce_{97} catalyst. Querini et al. suggested that K in K/CeO_2 catalysts may act to form a carbonate-type intermediate with the partially oxidized soot, which decomposes and releases CO_2 and that the high mobility of the K compounds due to their relatively low boiling point improves the effective contact between active phases and soot [164]. These results confirm the suggestions given by others that alkali metals are active catalyst components for soot oxidation.

2.3.3 Stability of alkali metal doped catalysts

The fact that a loose soot-catalyst contact was applied makes these catalysts (Cs_3Co_{97} and K_3Ce_{97}) attractive as potential low temperature soot oxidation catalysts. On the other hand, alkali metals are noted for sublimation under the reaction conditions which is advantageous in

that it enhances catalysts mobility and contact but can also results in catalysts loss in the exhaust stream over time. Another disadvantage is that alkali ions tend to leach out of the catalysts in the presence of moisture. One of the conditions of a good catalytic diesel filter catalyst is stability. The challenge in using alkali metal containing catalysts for diesel particulate filter applications is minimizing, if not eliminating the loss of the active species. Therefore the stability of the best catalysts from libraries two and three (K_3Ce_{97}, Cs_3Co_{97} respectively) were accessed conventionally. After a TGA experiment, the same catalysts was reloaded with fresh soot and characterized. These repeated experiments are denoted as runs whereby the same catalyst/soot ratio was used for each run. As shown in Figure 2.15, these materials are relatively stable under the reaction conditions considered. After 13 experimental runs, the Cs_3Co_{97} catalyst maintained its T_{50} value which was 456 °C. The K_3Ce_{97} material witnessed considerable deactivation after run 11. Though K_3Ce_{97} seems to be a good catalyst at first site, the lost of activity after just 11 runs imply this catalyst may not be good enough to be applied on diesel filter. The deactivation of the K_3Ce_{97} observed during multiple TGA cycles is likely due to the loss of potassium through sublimation during the soot oxidation process.

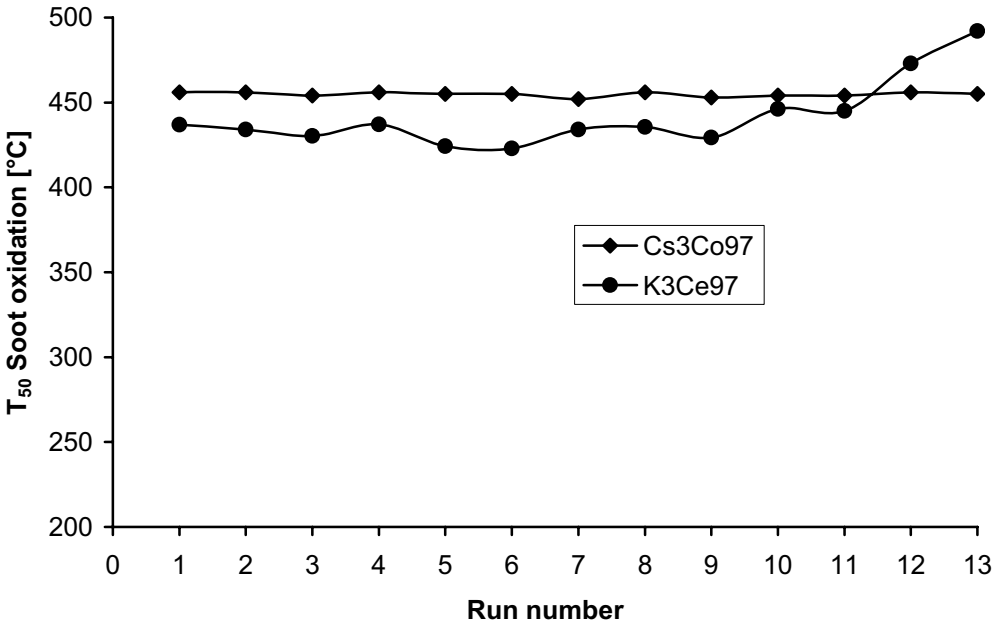

Figure 2.15 Comparison of the stability of Cs_3Co_{97} and K_3Ce_{97} catalysts by a plot of the T_{50} as a function of the number of experimental run.

2.3.4 Composition spread of binary mixed oxides

The given K and Cs content in the Ce and Co oxides, respectively, are likely not the optimum content. To determine the best composition, a composition spread was performed on the best catalysts whereby the samples were prepared conventionally using the syntheses methods given under section 3.1. For the CsCo material, 12 different compositions were considered while 8 KCe compositions were analysed. The samples were analysed by a TGA. Shown in Figure 2.16, is T_{50} of soot combustion as a function of the catalyst composition. The compositions with the best T_{50} values were $K_{15}Ce_{85}$ and $Cs_{20}Co_{80}$ respectively. Addition of a small amount of Cs in Co resulted in a decrease of T_{50} greater than 100 °C. Cs content greater than 40 % do not cause additional significant improvements in the T_{50} value. T_{50} again increased in the case of Co_0Cs_{100} sample. The $Cs_{20}Co_{80}$ sample was able to oxidise soot at T_{50} of 432 °C. In view of the literature [3, 25], it is likely that the activity of this catalyst is due to the synergetic effect of the redox properties of Co and the enhancement of the soot-catalyst contact capability of Cs.

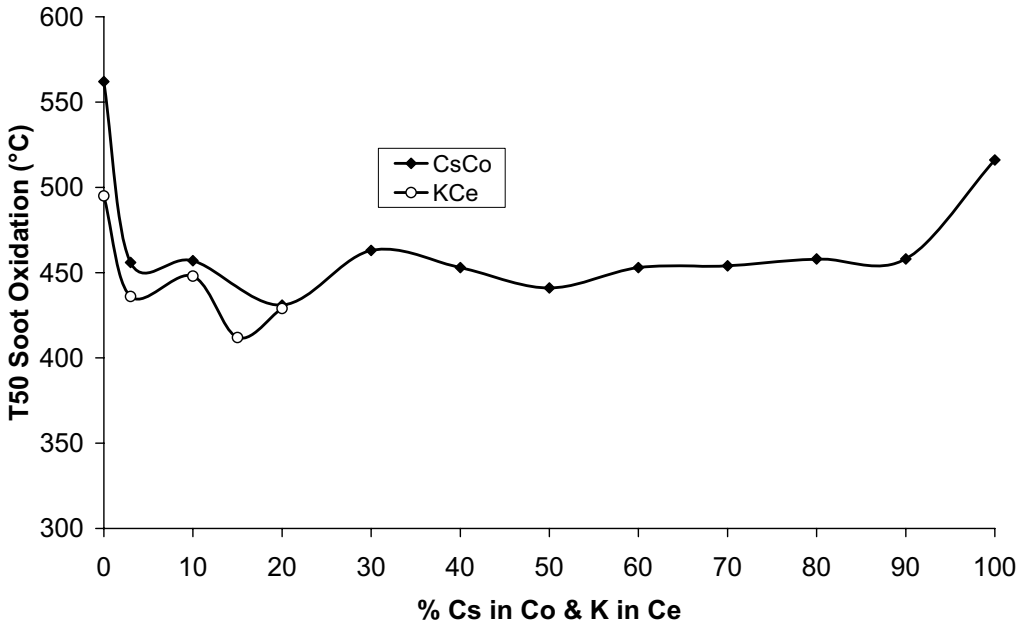

Figure 2.16 The temperature at which 50 % of the soot is combusted vs. catalytic composition

In the case of a KCe composition spread only five samples gave meaningful results. The materials with a K concentration greater than 30 % have been too active causing a rapid combustion of soot leading to peak temperatures. The soot combustion activity of the mixed

oxides was better than that of each individual oxide. Due to their tendency of instant combustion materials with potassium contents ≥ 30 % were not considered in this study, although they may be of interest for practical applications, in which the soot may never reach higher concentrations. Only $K_{15}Ce_{85}$ was considered further.

One of the non alkali metal containing sample found to be active for soot combustion was La_3Co_{97}. To determine the best composition, our industrial partner considered a composition spread of the two elements. Her results suggested that La_5Co_{95} is the best composition. The two samples La_3Co_{97} and La_5Co_{95} were re-synthesized and tested by a TGA for soot combustion. Depicted in Figure 2.17 below is the relative soot weight versus temperature. Clearly, La_5Co_{95} was a better catalyst with a T_{50} of 520 °C while that of La_3Co_{97} was 546 °C.

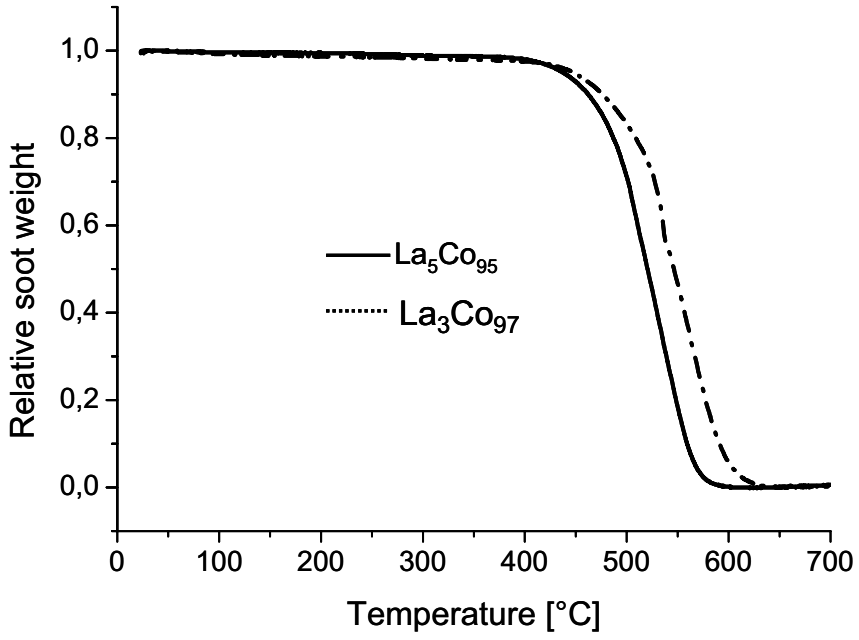

Fig. 2.17 Comparison of TGA curves for soot oxidation with La_3Co_{97} and La_5Co_{95} catalysts

2.4 The effect of alkali metal on the activity of Ce based catalysts

To check the effect of the alkali metals (Li, Na, K, Rb, and Cs) on Ce oxide, the experiments shown in Figure 2.18 were conducted. Samples with different alkali metals content were prepared by a robot and the temperature increase of the individual soot-catalysts mixtures were monitored by IR-thermography. At lower alkali contents (< 10 mole %), all samples behaved similarly (see Figure 2.12). At an alkali metal loading of 50 %, the temperature increase is as follows: Na<K<Rb<Li<Cs. These results suggest that Cs is the most active

alkali dopant for cerium oxide, when its concentration is 50 %, which is in contradiction to the claim by McGinn that K is the most active alkali dopant [26]. For most of the systems, soot combustion increased with increasing alkali metal loading. Galdeano et al. also analysed the effect of alkaline nitrates supported on hydrous zirconium on the rate of catalytic particulate matter combustion [23]. Their alkaline nitrate activity order was K< Li < Cs, which is not very much different from our rating at alkaline nitrate contents of 50 %.

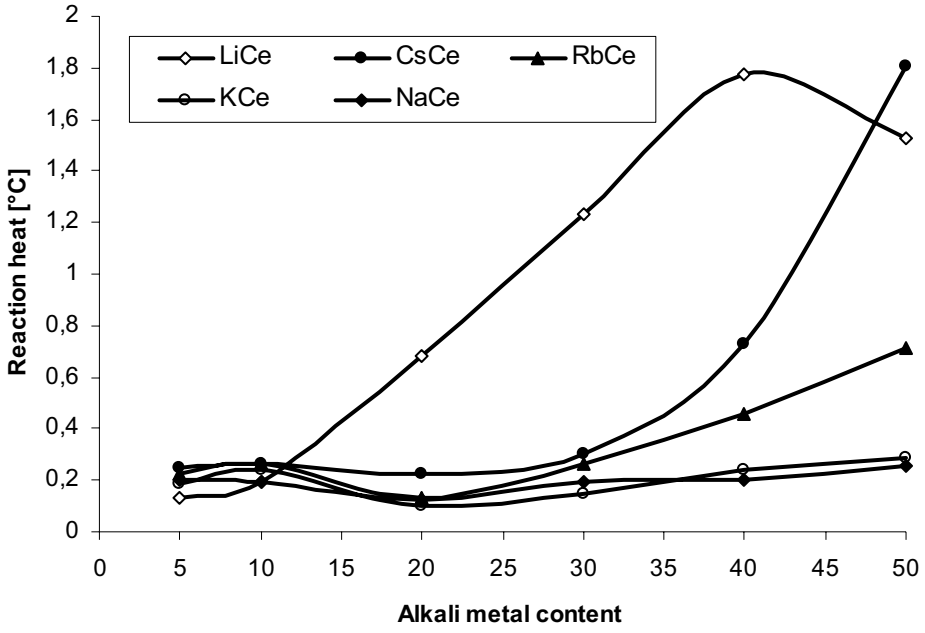

Fig. 2.18 IR-thermography results for alkali-cerium mixed oxides (library 5). A plot of the heat of reaction as a function of alkali metal content.

2.5 Ternary mixtures

2.5.1 Doping of $Cs_{20}Co_{80}$, $K_{15}Ce_{85}$ and La_5Co_{95}

Three selected binary mixed oxides ($Cs_{20}Co_{80}$, $K_{15}Ce_{85}$ and La_5Co_{95}) were further optimised by doping with 50 elements ($M_xCs_{20}Co_{80-x}$, $M_xK_{15}Ce_{85-x}$, and $M_xLa_5Co_{85-x}$), whereby only two concentrations for x (x = 3 and 10 mol %) values have been studied. The libraries are denoted as library six, seven and eight respectively. The used elemental precursors for each library are given under the experimental section. Each of these libraries consisted of 100 samples. The relative activity of the best 10 samples and their compositions from the $M_xCs_{20}Co_{80-x}$ library are shown in Table 2.7, while the IR image of the library at 350 °C under synthetic air is

given in Figure 2.19. The two best catalysts in this library were $Cu_{10}Cs_{20}Co_{70}$ and $Ag_{10}Cs_{20}Co_{70}$ with a relative activity of 100 % and 95 % respectively.

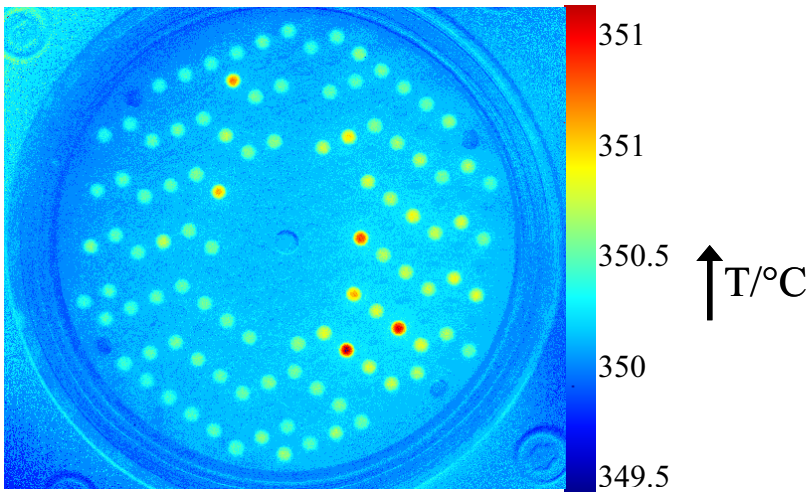

Figure 2.19 The emissivity-corrected IR-thermographic image of library six under synthetic air flow of 50 ml/min at 350 °C

Catalyst composition	Relative Catalytic activity [%]	Catalyst composition	Relative Catalytic activity [%]
$Cu_{10}Cs_{20}Co_{70}$	100	$Ag_3Cs_{20}Co_{77}$	61
$Ag_{10}Cs_{20}Co_{70}$	95	$Se_{10}Cs_{20}Co_{70}$	51
$Na_{10}Cs_{20}Co_{70}$	82	$Pr_{10}Cs_{20}Co_{70}$	50
$Cu_3Cs_{20}Co_{77}$	73	$V_{10}Cs_{20}Co_{70}$	48
$Bi_{10}Cs_{20}Co_{70}$	63	$Cd_{10}Cs_{20}Co_{70}$	46

Table 2.7 The relative activity of the ten best catalysts from library six for the combustion of soot with synthetic air

As was observed during multiple TGA cycles for the combustion of soot, the catalyst K_3Ce_{97} is not stable. The stability of the catalyst may be improved by further doping of the sample. The obtained IR- image of library seven which consisted of $M_xK_{15}Co_{85-x}$ samples is showed in Figure 2.20. Only two catalysts $Pt_{10}K_{15}Ce_{75}$ and $Pt_3K_{15}Ce_{82}$ showed considerable activity for soot combustion at 350 °C. When compared with K_3Ce_{97} catalysts from library two, which showed activity at 300 °C, one can conclude that the addition of a third element only led to activity deterioration. Probably the addition of a third element resulted to a more stable mixed

oxide. A stable oxide is advantageous in reducing catalyst degradation but may lead to poor catalyst soot contact (reduce mobility).

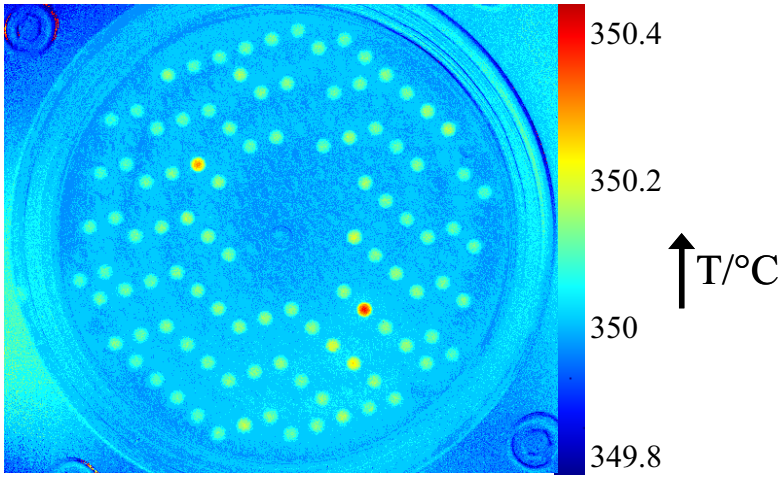

Figure 2.20 The emissivity-corrected IR-thermographic image of library seven under synthetic air flow of 50 ml/min at 350 °C

Catalyst Composition	Relative Activity [%]
$Pt_{10}K_{15}Ce_{75}$	100
$Pt_3K_{15}Ce_{82}$	87
$Fe_{10}K_{15}Ce_{75}$	47
$Cu_{10}K_{15}Ce_{75}$	32
$Ag_{10}K_{15}Ce_{75}$	26

Table 2.8 Relative activity of the five best catalysts from library seven for the combustion of soot with synthetic air

The obtained IR-images for $M_xLa_5Co_{95-x}$ samples under synthetic air at 350 °C and 400 °C are depicted in Figure 2.21 and 2.22 respectively. At 350 °C just one catalyst $Pb_{10}La_5Co_{85}$ was active. By raising the temperature of the library to 400 °C, two other samples $Na_{10}La_5Co_{85}$ and $Ce_{10}La_5Co_{85}$ became active. As expected the activity of the $Pb_{10}La_5Co_{85}$ demished due to reduce soot present. The best catalyst in this library consisted of 10 % Pb, ironically considerable effort is being made to eliminate Pb from industrial use due to its toxicity. One of the probable contributions of Pb to this catalyst could be the formation of a molten phase which assists the catalysts-soot contact because Pb in its metallic form has a very low melting

point (326 °C). Secondly lead is known to make eutectic mixtures with many compounds such as Bi and Sn that can have melting points as low as 150 °C [8]. Such materials, if catalytically active, can be excellent candidates for soot combustion.

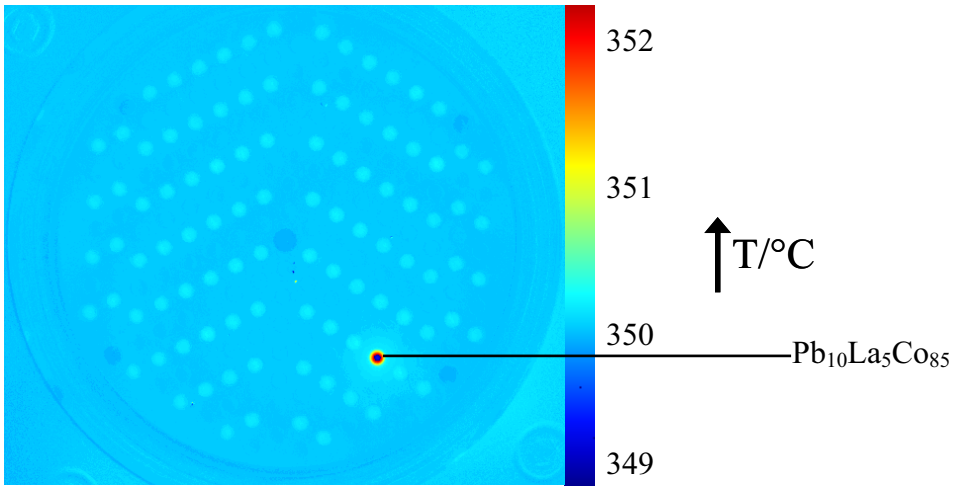

Figure 2.21 The emissivity-corrected IR-thermographic image of library 8 under synthetic air flow of 50ml/min at 350°C

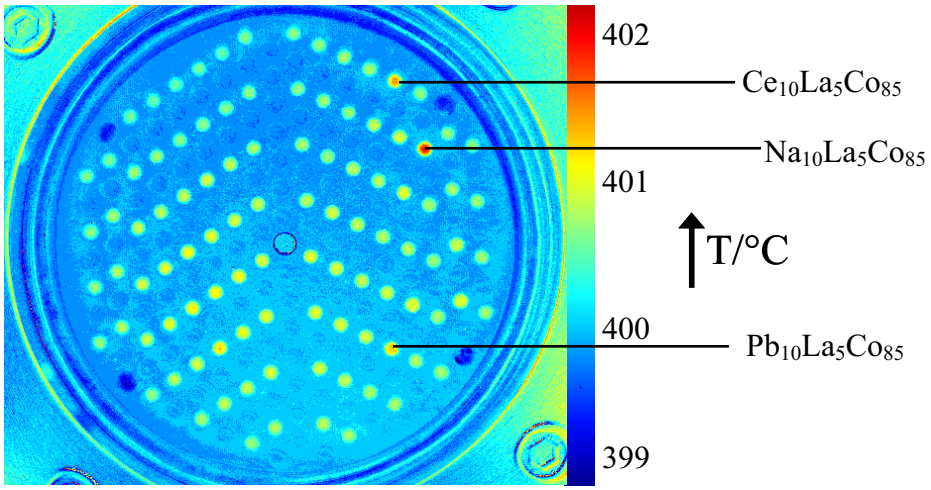

Figure 2.22 The emissivity-corrected IR-thermographic image of library 8 under synthetic air flow of 50 ml/min at 400 °C

2.5.2 Conventional Testing of $M_xK_{15}Ce_{85-x}$, $M_xCs_{20}Co_{80-x}$ and $M_xLa_5Co_{95-x}$ catalysts

After the high-throughput experiments, the activities of the best catalysts on each library were verified conventionally using a thermogravimetric analyzer (TGA). TGA is commonly used to analyse the activity of potential catalysts with respect to soot oxidation by monitoring the weight change of a soot-catalyst mixture or CO_2 and CO evolution from a soot-catalyst mixture when subjected to a temperature program [165]. Table 2.9 summarises the various catalyst compositions and their respective T_{50} values. For the $M_xCs_{20}Co_{80-x}$ samples, the best catalyst was $Cu_3Cs_{20}Co_{77}$ with a T_{50} of 388 °C, followed by the $Cu_{10}Cs_{20}Co_{70}$ catalyst with T_{50} of 396 °C. The doping of $Cs_{20}Co_{80}$ with Cu, Ag, and Bi clearly led to improved catalytic activity. Although the order of merit obtained here does not correlate well with the HT results, the confirmation of the HT results was achieved and new catalysts of improved activity have been discovered. The difference in the order of merit between HT and TG experiments may be due to the fact that different reaction conditions exist during the different reactions. Secondly, though maximum effort was made to maintain a constant mixing procedure, the same catalyst-soot contact is hard to be guaranteed. The catalyst-soot contact greatly influences the combustion temperature for some catalysts.

Catalyst composition	T_{50} [°C]	Catalyst composition	T_{50}[°C]
$Cu_3Cs_{20}Co_{77}$	388	$Bi_{10}Cs_{20}Co_{70}$	423
$Cu_{10}Cs_{20}Co_{70}$	396	$Ag_3Cs_{20}Co_{77}$	424
$Ag_{10}Cs_{20}Co_{70}$	410	$Na_{10}Cs_{20}Co_{70}$	432
		$Cs_{20}Co_{80}$	432
$K_{15}Ce_{85}$	412	$Pt_3K_{15}Ce_{82}$	520
$Pt_{10}K_{15}Ce_{75}$	490	$Fe_{10}K_{15}Co_{75}$	526
$Pb_{10}La_{15}Co_{75}$	433	$Ce_{10}La_{15}Co_{75}$	504
$Na_{10}La_{15}Co_{75}$	490	La_5Co_{95}	520

Table 2.9 TGA results of the best catalysts for the oxidation of soot with synthetic air

As can be seen in Table 2.9, the doping of $K_{15}Ce_{85}$ catalysts never improved the catalyst activity. While the binary mixed oxide $K_{15}Ce_{85}$ was able to oxidise 50 % of soot at 412 °C,

none of the ternary mixed oxide show such activity. The best ternary mixture was $Pt_{10}K_{15}Ce_{75}$ with a T_{50} of 490 °C. The possible reason for this catalyst deterioration could be due to reduced catalyst mobility caused by Pt. However under real conditions in a diesel particulate filter, the Pt containing sample may show better activity. The real diesel exhaust may consist of soot, unburned hydrocarbon and nitrogen oxides. Pt is a well known catalyst for hydrocarbon combustion which may increase the exhaust temperature thereby improving soot combustion. Furthermore Pt is capable of oxidizing NO to NO_2 which is a stronger oxidant than O_2. Nitrogen dioxide can combust soot at a lower temperature than O_2.

The conventional test of the $M_xLa_5Co_{85-x}$ samples revealed that the addition of Pb-, Na-, Ce-oxides in LaCo sample led to improved catalyst activity. As shown in Table 2.9, $Pb_{10}La_5Co_{85}$ has a T_{50} of 433 °C. Compared with the binary catalyst La_5Co_{85} with a T_{50} value of 530 °C, the T_{50} value was reduced by 103 °C. However Pb and its compounds are not welcome in industry because of its toxicity. The high content of Pb in this catalyst may also render it more volatile which may lead to evaporative losses during actual use in a diesel particulate filter. However compared with most reported catalysts for soot combustion, this lead containing compound show excellent activity, therefore it would be interesting to try this material under real diesel exhaust condition. The second best catalyst was $Na_{10}La_5Co_{85}$, with a T_{50} of 490 °C followed by $Ce_{10}La_5Co_{85}$. Both Na and Ce are known in the literature to positively influence soot combustion.

2.5.3 CuCsCo and AgCsCo ternary composition spreads

The activity of a catalyst is not only dependent on the quality of each component but also on their quantity. To determine the best composition of the ternary mixed oxides of $Cu_xCs_yCo_z$, which were found to be active in library 6, a composition spread of the three oxides was synthesized at a 5 mol% increment for each component ($5 \leq x \leq 95$, $5 \leq y \leq 70$, $5 \leq z \leq 95$). This library was synthesized with the same recipe as library 5 and the resulting library is denoted as library 9. The composition and position of each catalyst in the library is given in section 6.4. The library was screened between 200 and 400 °C and the obtained IR-image at 300 °C is given in Figure 2.23 while Table 2.10 depicts the compositions of the best catalysts and their relative activities. Among several active samples, the five best samples in this library were $Cu_{50}Cs_{10}Co_{40}$, $Cu_{75}Cs_{25}$, $Cu_{40}Cs_{30}Co_{30}$, $Cu_{55}Cs_{45}$, and $Cs_{10}Co_{90}$ respectively. No trend could be noticed with respect to the relationship between the catalyst activity and the

concentration of each element. As expected the $Cu_{10}Cs_{20}Co_{70}$ did not show considerable activity at 300 °C. The ternary plot shown in Figure 2.24 clearly depicts the temperature changes with respect to the composition of each material.

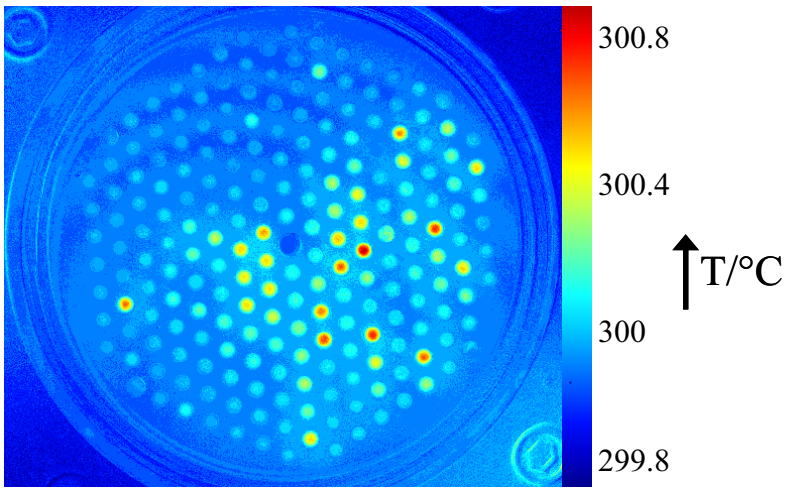

Figure 2.23 The emissivity-corrected IR-thermographic image of library 9 under synthetic air flow of 50 ml/min at 300 °C

Catalyst Composition	Relative Catalytic Activity[%]	Catalyst Composition	Relative Catalytic Activity[%]
$Cu_{50}Cs_{10}Co_{40}$	100	$Cu_{70}Cs_{30}$	75
$Cu_{75}Cs_{25}$	87	$Cu_{45}Cs_{25}Co_{30}$	72
$Cu_{40}Cs_{30}Co_{30}$	85	$Cu_{35}Cs_{25}Co_{40}$	71
$Cu_{55}Cs_{45}$	81	$Cu_{40}Cs_{35}Co_{25}$	70
$Cs_{10}Co_{90}$	75	$Cu_{30}Cs_{35}Co_{35}$	65

Table 2.10 Catalyst composition and relative activity of the ten best catalysts on the library 9

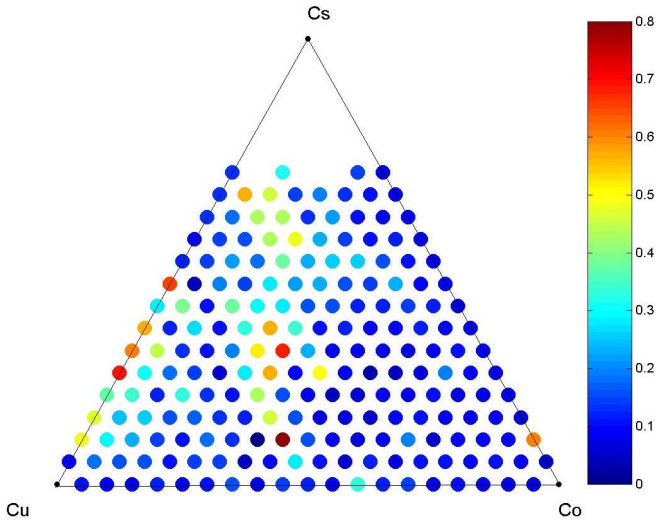

Figure 2.24 Catalytic activity of the $Cu_xCs_yCo_z$ ternary composition spread library 9 ($5 \leq x \leq 95$, $5 \leq y \leq 70$, $5 \leq z \leq 95$) reaction condition 50 ml/min synthetic air flow, reaction temperature 300 °C)

To determine the best composition of the ternary mixed oxides of $Ag_xCs_yCo_z$, which were found to be active in library 6, a composition spread of the three oxides was synthesized at a 5 mol% increment for each component ($5 \leq x \leq 95$, $5 \leq y \leq 70$, $5 \leq z \leq 95$). This library is denoted as library 10. Figure 2.25 is a ternary plot of the heat of reaction of each catalyst-soot spot. The red spots on the diagram represents catalysts with high soot oxidation activity. This plot suggest that all the three elements were necessary for the catalytic activity. However, all the major active samples contained a high cobalt content.

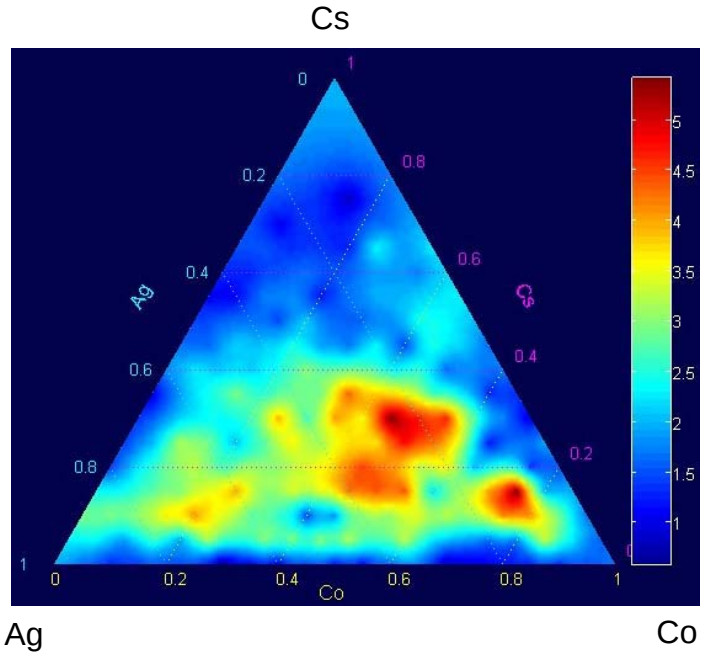

Figure 2.25 The relative catalytic activity of the $Ag_xCs_yCo_z$ ternary composition spread library 10 ($5 \leq x \leq 95$, $5 \leq y \leq 75$, $5 \leq z \leq 95$, reaction condition 50 ml/min synthetic air flow and temperature 300 °C)

2.5.4 Conventional testing of library 9 samples

In order to validate the soot oxidation activities of the best catalysts of library 9 discovered through the high-throughput experimentation technique, the temperature dependent soot weight change was determined by TGA. Table 2.11 summarizes the T_{50} of the best catalysts. The high activities of some samples shown during the HTE could not be reproduced conventionally. However, four catalysts $Cu_{40}Cs_{30}Co_{30}$, $Cu_{45}Cs_{25}Co_{30}$, $Cu_{50}Cs_{10}Co_{40}$, and $Cu_{35}Cs_{25}Co_{40}$, showed T_{50} of 330 °C, 336 °C, 350 °C and 361 °C which were better than that of $Cu_3Cs_{20}Co_{77}$ and $Cu_{10}Cs_{20}Co_{70}$ catalysts (388 °C and 396 °C) reported earlier. Clearly, we were able to achieve catalytic activity improvement through composition spread.

Catalyst Composition	T_{50} [°C]
$Cu_{40}Cs_{30}Co_{30}$	330
$Cu_{45}Cs_{25}Co_{30}$	336
$Cu_{50}Cs_{10}Co_{40}$	350
$Cu_{35}Cs_{25}Co_{40}$	361

Table 2.11 TGA results of the four best catalysts from library 9 for the oxidation of soot.

2.5.5 The effect of the calcination temperature

Diesel soot oxidation catalysts are expected to work in a changing environment under real condition. These catalysts are expected to withstand temperatures as high as 1000 °C or more. To investigate the effect of the calcination temperature on the catalytic activity, selected catalysts ($Cs_{20}Co_{80}$, $Cu_3Cs_{20}Co_{77}$, $Cu_{10}Cs_{20}Co_{70}$, $Pb_{10}La_5Co_{85}$) found to be active for soot combustion were synthesized conventionally and calcined at four different temperatures (400, 500, 600, and 700 °C). Figure 2.26 reports the T_{50} versus calcination temperature. T_{50} of the soot utilised in this study during the uncatalyzed experiment is about 600 °C. All the considered catalysts were able to combust soot at a much reduced temperature irrespective of the calcination temperature. The T_{50} values for the $Cs_{20}Co_{80}$ and $Cu_3Cs_{20}Co_{77}$ samples increased with increasing calcination temperature. Figure 2.26 shows that the activities of $Cu_{10}Cs_{20}Co_{70}$ and $Pb_{10}La_5Co_{85}$ were also dependent on the calcination temperature with each catalyst showing superior activity when calcined at 700 °C. The fact that the reported catalysts were still very active after calcination at 700 °C makes them attractive for application in diesel exhaust systems.

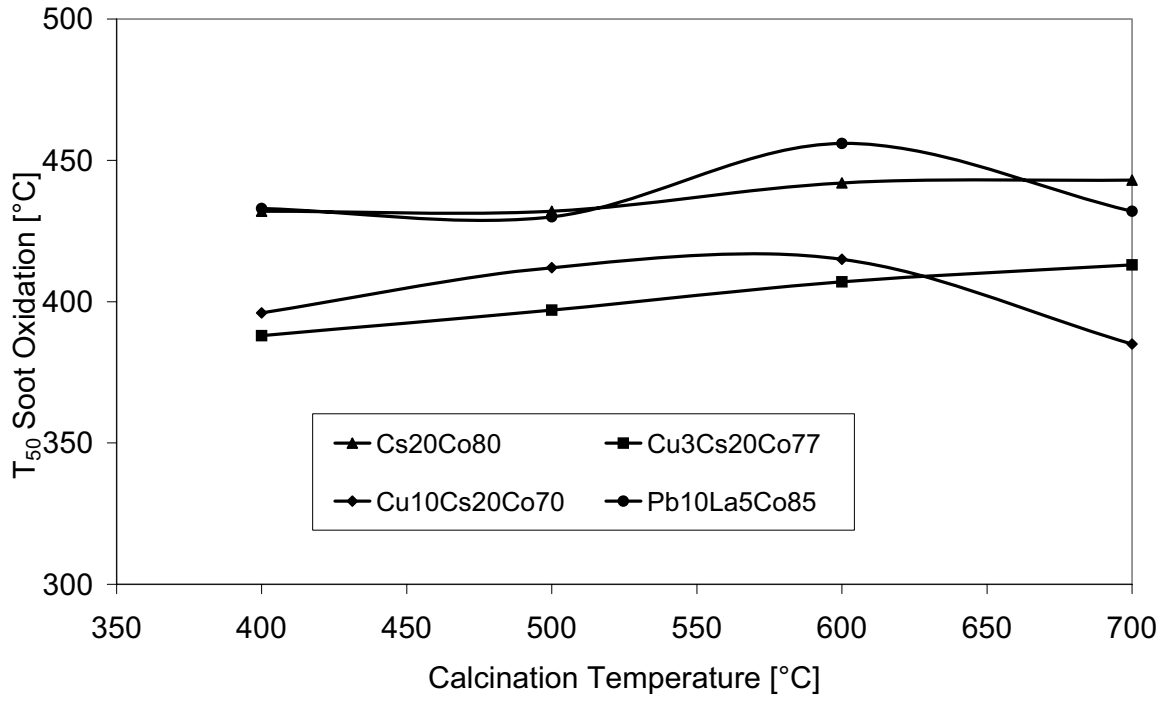

Figure 2.26 The temperature at which 50 % of soot is oxidized as a function of the calcinations temperature.

Shown in Figure 2.27 is a summary of the combinatorial process used in the development of soot oxidation catalysts based on Co-, Mn-, and Ce-oxides. Initially, the based oxides Co, Mn, and Ce were doped with 50 different elements from the periodic table and the hits mixed oxides identified. A binary composition spread of the hit mixed oxide was performed. A ternay mixture was achieved by doping the binary oxide with a third element. Finally a ternary composition spread of the best ternary mixed oxide was performed.

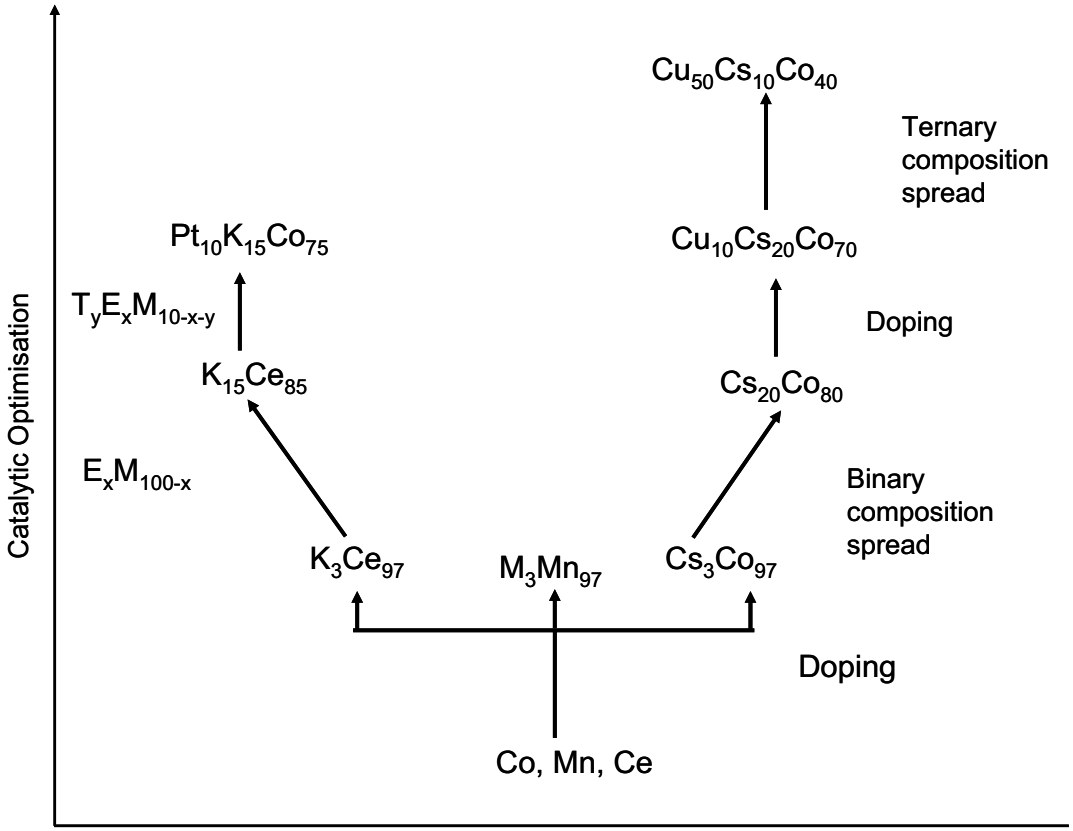

Figure 2.27 A summary of the combinatorial development of soot oxidation catalysts based on Co, Ce and Mn.

2.6 High dimensional sample preparation and screening

2.6.1 High-throughput screening

High-throughput methods allow the rapid syntheses of many different materials, which can be used to screen large sample spaces. This advantage of HTE was explored to synthesize high dimensional materials from reported active oxides in the literature. Using this approach, a pentanary composition spread of five different metal oxides was investigated. The used elements in this study were: Ce, Cr, Co, Cu, Fe, K, La, Mn, Mo, and V. The applied precursors and their concentrations are given in Table 3.3. All these elements in their single phase or mixed phases are given in literature as potential soot oxidation catalysts. Our aim here was to develop new complex catalysts from these single oxides. To search these complex spaces most efficiently, our search was limited to just 126 samples for each five elements, whereby the composition of each element was varied from 0-100 % at 20 % interval.

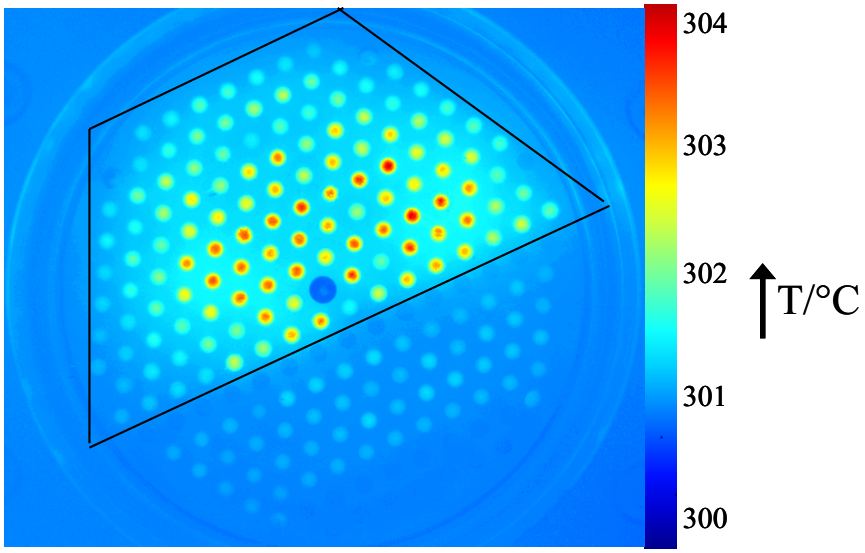

Figure 2.28 The emissivity–corrected IR-thermographic image of catalyst library 11 at 300 °C for the combustion of soot.

Catalyst Composition	Relative Activity [%]	Catalyst Composition	Relative Activity [%]
$Co_{80}Cr_{20}$	100	$Fe_{40}Cu_{40}Ce_{20}$	85
$Fe_{40}Co_{20}Cr_{20}Ce_{20}$	94	$Cu_{80}Ce_{20}$	83
$Fe_{60}Cu_{20}Ce_{20}$	93	$Fe_{40}Co_{20}Cr_{20}$ Cu_{20}	82
Co_{100}	90	$Cr_{40}Co_{20}Cu_{20}Fe_{20}$	81
$Cu_{60}Ce_{20}Fe_{20}$	90	$Ce_{40}Co_{20}Cu_{20}Fe_{20}$	80

Table 2.12 Catalytic composition and relative activity of the ten best catalysts on the library

Shown in Figure 2.28 is the IR-image obtained by testing the Ce, Co, Cr, Cu, and Fe containing library at 300 °C. The 126 materials from the pentanary composition spread are contained in the rectangle drawn on the library surface. As can be observed from this image a few catalyst were active for soot combustion at 300 °C under synthetic air. In Table 2.12, the activities of the best 10 samples in the library are given relative to the activity of the best sample in the library. The best candidate here was a binary mixed oxide consisting of Co and Cr. The pentenary mixed oxide ($Fe_{20}Co_{20}Cr_{20}Cu_{20}Ce_{20}$) was found to be inactive. As expected the single oxide cobalt oxide was also found to be active. In order to visualize the effect of the composition variation of different elements, four elements from the five were visualised successively using a quaternary visualization programme written by Sieg [166]. Details about this visualization tool can be seen in her dissertation. As can be clearly seen from the quaternary plots, none of the single metal oxide apart from Co was active for soot combustion at 300 °C. The effect of the four elements on each plot was different. The quaternary plot with least active samples was the Cu, Fe, Cr and Co combination. Here just three samples showed activity towards soot combustion and just one contained all the four elements. This comprehensive mapping of the composition spaces documents, that there are no unidentified areas of catalyst compositions of exceptional catalytic activity.

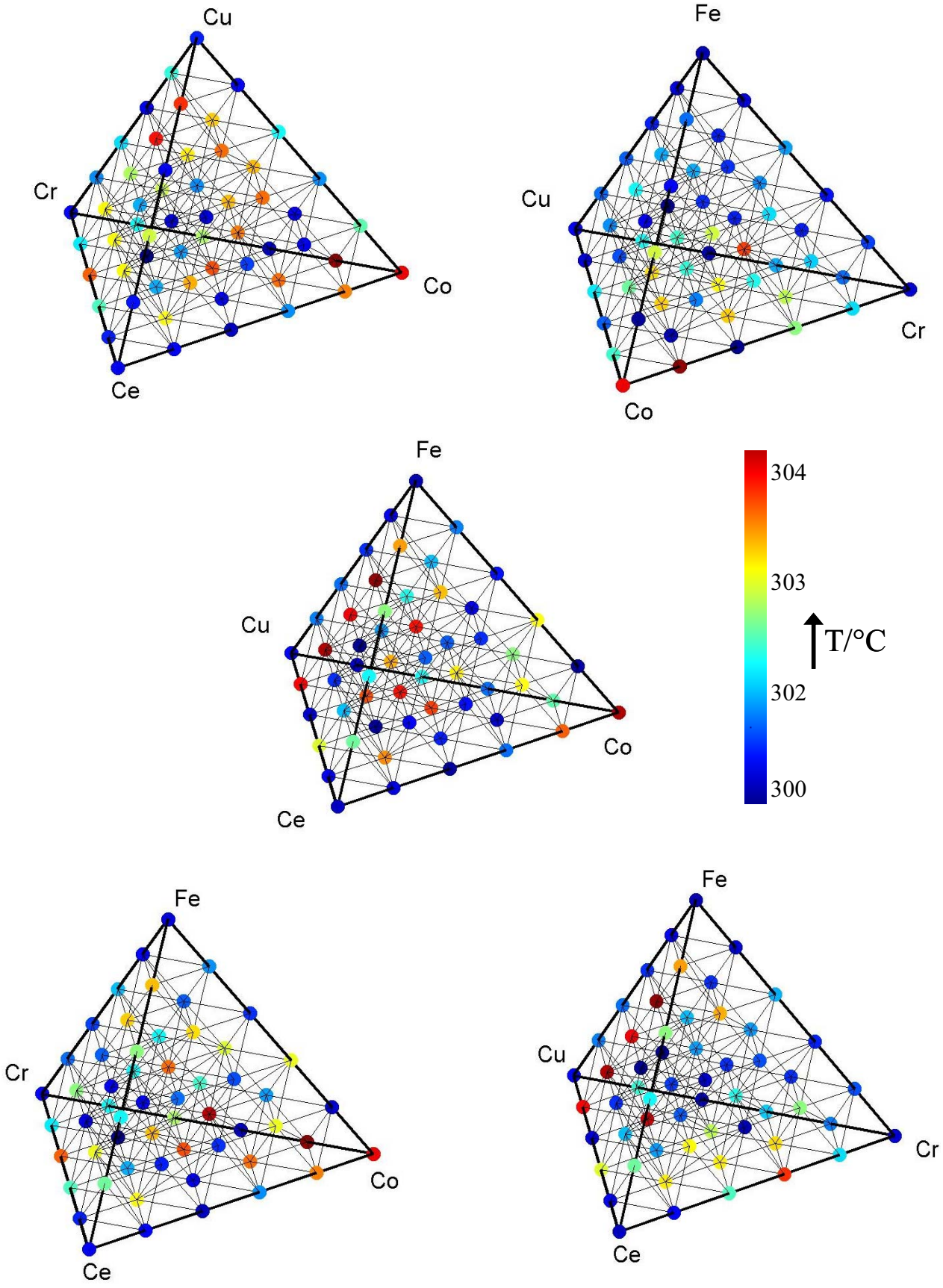

Figure 2.29 Visualisation of the activity of the CrCuCeCoFe pentenary library using a quartenary plot.

Another pentanary library consisting of Ce-, Co-, V-, La- and Mo-mixed oxides was synthesized and screened with the IR camera. The obtained IR-image is depicted in Figure 2.30 below. Quite a few catalysts in this library were active for soot combustion. As shown in Figure 2.30 b, the best catalyst in this library was $Ce_{40}Co_{20}V_{20}La_{20}$, followed by $Ce_{60}Co_{20}La_{20}$ with a relative activity of 71 %. No single metal oxide sample was among the best 10 samples and just one binary mixed oxide ($Ce_{80}La_{20}$) was active.

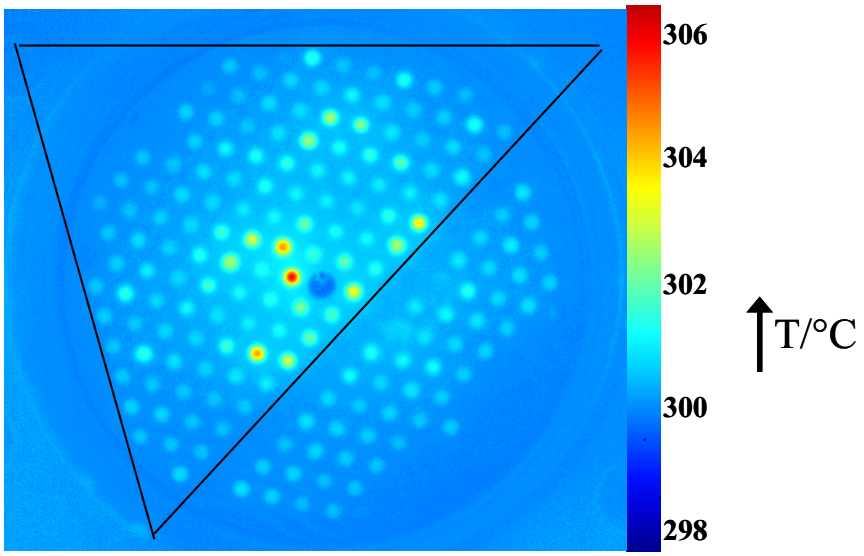

Catalyst Composition	Relative Activity [%]	Catalyst Composition	Relative Activity [%]
$Ce_{40}Co_{20}V_{20}La_{20}$	100	$La_{60}Co_{20}Mo_{20}$	24
$Ce_{60}Co_{20}La_{20}$	71	$Ce_{40}Mo_{40}La_{20}$	21
$Ce_{60}Co_{20}Mo_{20}$	52	$V_{40}Mo_{20}La_{40}$	20
$Co_{40}Ce_{20}La_{20}Mo_{20}$	30	$La_{40}V_{20}Co_{20}Mo_{20}$	17
$Ce_{80}La_{20}$	27	$Co_{40}Ce_{20}V_{20}La_{20}$	16

Figure 2.30 The emissivity–corrected IR-thermographic image of catalyst library 12 at 300°C for the combustion of soot. (b) Catalytic composition and relative activity of the ten best catalysts on the library

A composition spread of five different elements (Cr, Cu, Fe, Mn and Mo) was screened under synthetic air at 300 °C. The IR-image obtained under these reaction conditions is shown in Figure 2.31. Also included in this library are 76 samples from the composition spread of Ce, Cu, K, Fe, and La. Shown in the Table 2.13 are the relative activity of the best samples from the library. The best sample in this library was $Fe_{40}Mn_{40}Mo_{20}$. The best material among the

Ce, Cu, K, Fe, and La samples was $Ce_{40}Cu_{40}Fe_{20}$ with a relative activity of 85 %. No pentanary nor quaternary sample was found active in this library. Worth mentioning is that nearly all active materials from the Cr, Cu, Fe, Mn and Mo composition spread samples contained Mn-oxide suggesting the importance of Mn-oxide in the catalytic activity of these samples. However a clear trend of catalytic activity with respect to Mn-oxide content was not identified. Surprisingly, just one sample containing K was among the best materials from the Ce, Cu, K, Fe, and La samples. The special activity of alkaline ions detected with Ce and Co containing mixed oxides is not seen here, which is an argument against any general effect of alkaline ions on soot oxidation catalysis.

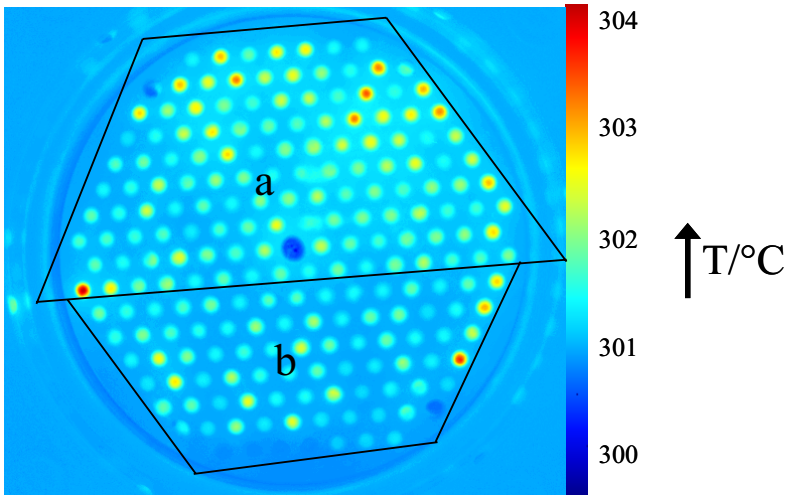

Figure 2.31 The emissivity–corrected IR-thermographic image of catalyst library 13 at 300°C for the combustion of soot. Section (a) consist of 126 samples from CrCuFeMnMo and section (b) consist of 76 samples from CeCuKFeLa composition spread.

Catalyst Composition	Relative Activity [%]	Catalyst Composition	Relative Activity [%]
$Fe_{40}Mn_{40}Mo_{20}$	100	$Cu_{60}Fe_{20}Mn_{20}$	65
$Cr_{40}Fe_{40}Mn_{20}$	72	$Cr_{20}Mn_{60}Mo_{20}$	63
$Fe_{20}Mo_{80}$	71	$Cr_{40}Mn_{60}$	62
$Mn_{80}Mo_{20}$	69	$Cu_{20}Mn_{80}$	61
$Mn_{60}Mo_{40}$	68	$Cu_{60}Mn_{40}$	61
$Ce_{40}Cu_{40}Fe_{20}$	85	$Ce_{20}K_{40}La_{40}$	57
$Ce_{20}Cu_{80}$	67	$Ce_{20}Fe_{80}$	51
$Cu_{40}Fe_{60}$	59		

Table.2.13 Relative catalytic activity of the best samples in library 13

2.6.2 Conventional experiment for libraries 11, 12, and 13 samples

In order to confirm the activity of the active samples discovered via high-throughput experimentation, the activity of these samples were validated in conventional TGA experiments. In the TGA experiments a 4:1 catalyst/soot mixture was heated from 25 °C to 700 °C at a heating rate of 10 °C/min under synthetic air flow. The weight loss of the mixture as a function of temperature was recorded. The obtained results given in Table 2.14 show the T_{50} value of the best catalysts and their composition from library 11.

Catalyst Composition	T_{50} [%]
$Fe_{40}Ce_{20}Co_{20}Cr_{20}$	494
$Cr_{40}Fe_{20}Co_{20}Cu_{20}$	509
$Ce_{60}Co_{20}Cu_{20}$	509
$Co_{80}Cr_{20}$	541
$Fe_{40}Co_{40}Ce_{20}$	542
$Fe_{60}Cu_{20}Ce_{20}$	546
$Fe_{40}Ce_{40}Co_{20}$	562
Co_{100}	564
$Ce_{40}Co_{20}Cu_{20}$	569
$Cu_{80}Ce_{20}$	574

Table 2.14 The T_{50} temperature of the best catalyst from library 11

Among the active samples, $Fe_{40}Ce_{20}Co_{20}Cr_{20}$ was the best, with a T_{50} of 494 °C. The T_{50} of all other catalysts were larger than 500 °C. Though the materials which were active during HT-

experiments were again active during TGA experiments, the low temperature of combustion during HT-experiment were not confirmed in the TGA measurements. Because of the high T_{50} value obtained during TGA measurements, these samples were not considered further. It is well known in literature that none alkali metal containing mixed oxides will combust soot substantially only above 400 °C. The obtained results here are a further proof of this known tendency.

The TGA results of the lead samples from library 12, which consisted of Ce, Co, V, La and Mo, are given in Table 2.15. The $Ce_{60}Co_{20}Mo_{20}$ catalyst showed the best T_{50} which was 490 °C. No other catalyst from the HT experiment reached a T_{50} below 500 °C. The best HT-catalyst, $Ce_{40}Co_{20}V_{20}La_{20}$, has a T_{50} of 528 °C, which is about 38 °C higher than the $Ce_{60}Co_{20}Mo_{20}$ catalyst. The discrepancy between the high-throughput and the TGA results can be attributed to the different reaction conditions under which these reactions are performed, for example a temperature ramp is used during TGA experiments while the catalytic activities are screened at a constant temperature during the IR-thermography experiments. However the catalysts which were active during the HT experiments also showed activity during TGA experimentation which was most important.

Catalyst Composition	T_{50} [°C]
$Ce_{60}Co_{20}Mo_{20}$	490
$Ce_{60}Co_{20}La_{20}$	514
$La_{60}Mo_{20}Co_{20}$	521
$Ce_{40}Co_{20}V_{20}La_{20}$	528
$Ce_{80}La_{20}$	537
$Ce_{40}Co_{40}La_{20}$	556

Table 2.15 T_{50} temperature of the best catalyst from library 12

To confirm the activity of the hits from library 13 samples, again TG analyses were performed. As can be seen from Table 2.16, the material with the best T_{50} was $Fe_{40}Mn_{40}Mo_{20}$ (502 °C). No catalyst showed T_{50}-values below 500 °C.

Catalyst composition	T_{50} [°C]	Catalyst composition	T_{50}[°C]
$Fe_{40}Mn_{40}Mo_{20}$	502	$Cu_{80}Ce_{20}$	556
$Fe_{40}Cr_{40}Mn_{20}$	513	$Mo_{80}Fe_{20}$	563
$Mn_{60}Mo_{40}$	530	$Cu_{60}Mn_{40}$	568
$Cu_{60}Fe_{20}Mn_{20}$	549		
$Ce_{40}Cu_{40}Fe_{20}$	524	$La_{40}K_{40}Ce_{20}$	568
$Cu_{80}Ce_{20}$	538	$Fe_{80}Ce_{20}$	576

Table 2.16 T_{50} temperatures versus catalytic compositions

2.6.3 Ternary Composition Spread of CeCoMo

The ternary mixed oxide $Ce_{60}Co_{20}Mo_{20}$ as stated above was found to be active for soot combustion during HT experiment and as can be seen under TGA results, the catalyst was validated. This promising result motivated us to have a closer look at the relationship between the concentration of each metal oxide in the ternary mixed oxide and the ability of the sample to combust soot. Therefore further experiments were performed to determine the best composition of the ternary oxide Ce, Co, and Mo whereby each element composition was varied from 5-100 % at 5 % interval. Only 195 samples were synthesized and characterised for soot combustion because some samples were intentionally not synthesized in order to be able to test all the samples in one library. Shown in Figure 2.32 is the IR-image of this ternary composition library.

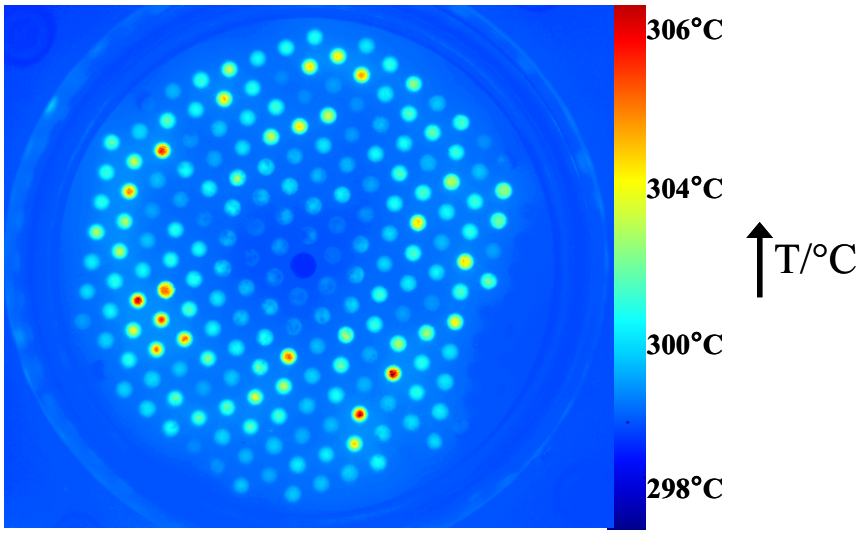

Figure 2.32 The emissivity –corrected IR-thermographic image of catalyst library 14 at 300 °C for the combustion of soot.

Catalyst Composition	Relative Activity [%]	Catalyst Composition	Relative Activity [%]
$Ce_{10}Co_{65}Mo_{25}$	100	$Ce_{50}Co_{45}Mo_{5}$	80
$Ce_{50}Co_{15}Mo_{35}$	98	$Ce_{50}Co_{45}Mo_{5}$	72
$Ce_{60}Co_{20}Mo_{20}$	95	$Ce_{45}Co_{10}Mo_{45}$	71
$Ce_{25}Co_{60}Mo_{15}$	92	$Ce_{45}Co_{35}Mo_{20}$	70
$Ce_{20}Mo_{80}$	90	$Ce_{25}Co_{5}Mo_{70}$	60

Table 2.17 Catalytic composition and relative activity of the ten best catalysts on library 14

Among several active samples, the three best samples in this library were $Ce_{10}Co_{65}Mo_{25}$, $Ce_{50}Co_{15}Mo_{35}$, and $Ce_{60}Co_{20}Mo_{20}$ respectively, therefore just two samples were more active compared to the $Ce_{60}Co_{20}Mo_{20}$ sample. No trend could be noticed with respect to the relationship between the catalyst activity and the concentration of each element. The most import trend observed here was that all the three oxides were important for the catalytic activity. Just one binary mixed oxide ($Ce_{20}Mo_{80}$) was among the 10 best catalyst in this library. The actual catalytic phase responsible for the activity of the ternary mixed oxides is not clear at this stage.

2.6.4 Conventional experiment

The best materials from the CeCoMo library were further analysed conventionally using a TGA equipment. A defined catalyst-soot ratio was mixed with a spatula, loaded in a TGA crucible and subjected to a temperature ramp under synthetic air flow. The recorded sample weight change as a function of temperature was used to determine T_{50}. Shown in Table 2.18 are the T_{50} values and the compositions of the best samples.

Catalyst Composition	T_{50} [°C]		T_{50} [°C]
$Ce_{50}Co_{15}Mo_{35}$	451	$Ce_{50}Co_{45}Mo_{5}$	530
$Ce_{60}Co_{20}Mo_{20}$	492	$Ce_{25}Co_{5}Mo_{70}$	547
$Ce_{20}Mo_{80}$	502	$Ce_{45}Co_{10}Mo_{45}$	555
$Ce_{25}Co_{60}Mo_{15}$	511	$Ce_{45}Co_{35}Mo_{20}$	556
$Ce_{10}Co_{65}Mo_{25}$	522	$Ce_{50}Co_{45}Mo_{5}$	558

Table 2.18 Catalytic composition versus T_{50}.

Only catalyst $Ce_{50}Co_{15}Mo_{35}$ (T_{50} 451 °C) was more active compared to the $Ce_{60}Co_{20}Mo_{20}$ sample. No trend could be noticed with respect to the relationship between catalyst activity and the elemental concentration. However the most active catalyst contained a high concentration of Ceria. Ceria is a well known oxide for soot combustion with its activity attributed to its oxygen storage and release potential. The only binary oxide ($Ce_{20}Mo_{80}$) among the best ten catalyst, had a T_{50} value of 502 °C.

2.7 Catalytic search around the composition of known catalyst from the literature

2.7.1 High-throughput screening

The catalyst $Cs_2V_1Fe_2/Al_2O_3$ prepared by the impregnation of α-Al_2O_3 powder with an aqueous solution of inorganic salts was given by Neri et al. as a potential soot combustion catalyst [20]. It was decided to search for potential catalysts around the composition space of this known catalyst. The sol-gel method used for the preparation of the samples is given under the experimental section. The applied strategy involved the replacement of one of the metals in the catalyst with 50 different metals selected from the periodic table. The general formulae of the samples were $M_2V_1Fe_2/AlO_x$ and $M_2V_1Cs_2/AlO_x$ whereby M denotes the 50 elements used for doping. The idea here was to test if a superior catalyst could be synthesized by simply varying one of the elements and the synthesis method of a known catalyst. The molar ratio of the various metals (20:10:20), the molar ratio of the mixed metal and the support (50:50) were left constant as in the literature catalyst but different support precursor (aluminium tri-sec-butylate) was used. Fifty samples with a general formula $M_2V_1Fe_2/AlO_x$ were synthesized and their catalytic activity tested with IR-camera (library15).

The IR-image obtained is given in Figure 2.33 below. Few catalysts with their relative activity given in Table 2.19 were found to catalyse soot combustion at 350 °C. The most active sample was the $Rb_2V_1Fe_2/AlO_x$ material followed by the $Ru_2V_1Fe_2/AlO_x$ sample. Among the seven active samples, only one ($Cu_2V_1Fe_2/AlO_x$) was free of alkali- and noble metals. Six samples were observed to show a better activity compared with the $Cs_2V_1Fe_2/AlO_x$ sample. In this study the K doped sample was found to be more active compared with the Cs doped sample which is in contradiction to the results by Neri et al who also compared the two

catalysts. However one should be careful in comparing catalysts which were synthesized using different syntheses methods and test protocols.

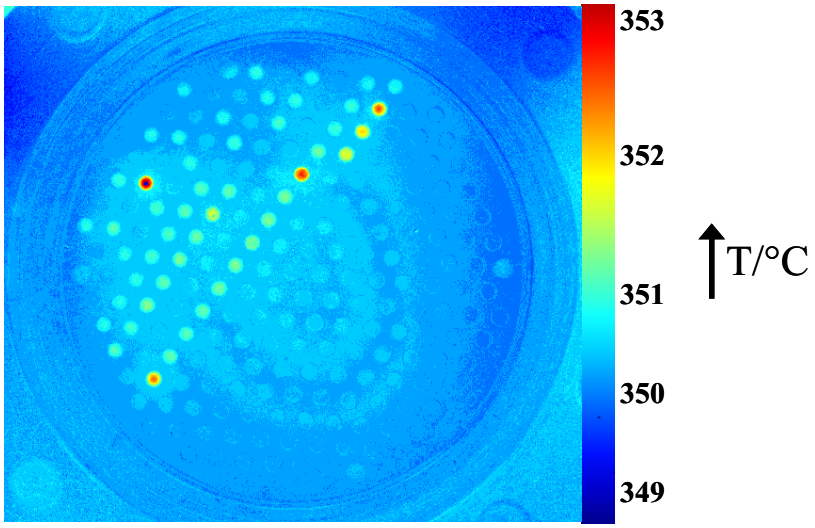

Figure 2.33 The emissivity–corrected IR-thermographic image of catalyst library 15 at 350 °C for the combustion of soot.

Catalyst Composition	Relative Catalytic Activity[%]	Catalyst Composition	Relative Catalytic Activity[%]
$Rb_2V_1Fe_2/AlO_x$	100	$Rh_2V_1Fe_2/AlO_x$	30
$Ru_2V_1Fe_2/AlO_x$	79	$Cs_2V_1Fe_2/AlO_x$	24
$Cu_2V_1Fe_2/AlO_x$	51		
$K_2V_1Fe_2/AlO_x$	34		
$Ir_2V_1Fe_2/AlO_x$	32		

Table 2.19 Catalytic composition and relative activity of the 7 best catalysts on the library

Furthermore fifty samples were synthesized with a general formula $M_2V_1Cs_2/AlO_x$ and screened with IR-camera at 350 °C under synthetic air flow (library 16). As can be seen from the IR-image given in Figure 2.34, just three catalysts showed considerable activity. The triangle indicate the section of the library that was filled with $M_2V_1Cs_2/AlO_x$ samples. The relative activity of the ten best samples are given in Table 2.20.

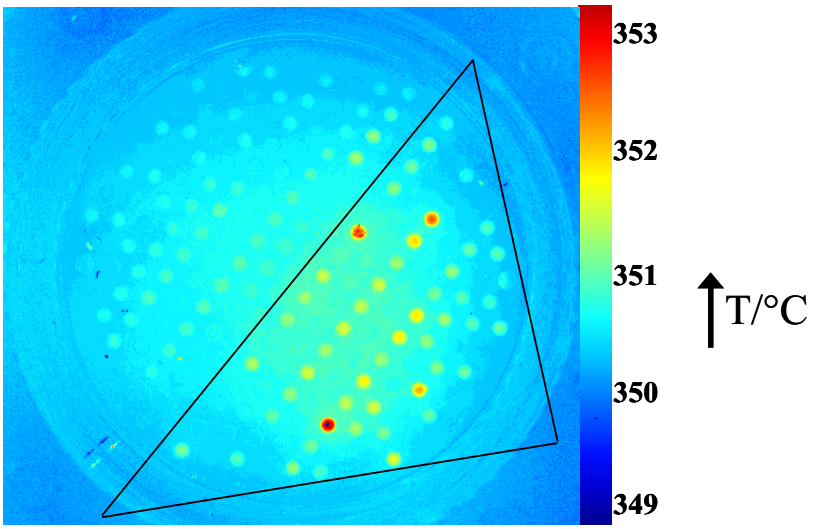

Figure 2.34 The emissivity–corrected IR-thermographic image of catalyst library 16 at 350°C for the combustion of soot.

Catalyst Composition	Relative Catalytic Activity[%]	Catalyst Composition	Relative Catalytic Activity[%]
$Cr_2V_1Cs_2/AlO_x$	100	$Fe_2V_1Cs_2/AlO_x$	52
$Cu_2V_1Cs_2/AlO_x$	97	$Ru_2V_1Cs_2/AlO_x$	50
$K_2V_1Cs_2/AlO_x$	92	$Ca_2V_1Cs_2/AlO_x$	47
$Na_2V_1Cs_2/AlO_x$	65	$In_2V_1Cs_2/AlO_x$	41
$Cd_2V_1Cs_2/AlO_x$	62	$Ba_2V_1Cs_2/AlO_x$	38

Table 2.20 Catalytic composition and relative activity of the ten best catalysts on library 16

2.7.2 Conventional experiments for library 15 & 16

The hits from libraries 15 and 16 were further characterised by TGA equipments. The results obtained are summarised in Table 2.21. The catalysts which were active during the high-throughput experiments were again active during conventional experiment. The best catalyst among the materials tested from library 15 was $Cs_2V_1Fe_2/AlO_x$ which showed a T_{50} of 432 °C. This confirmed the high activity of the original composition reported by Neri [20]. All the materials with high soot oxidation activity contained either alkali metals or noble metal except $Cu_2V_1Fe_2/AlO_x$ with a T_{50} value of 531 °C. Surprisingly the catalyst with the best activity during HT-experiment ($Rb_2V_1Fe_2/AlO_x$) did not show considerable activity under TGA experiment. The reason for this failure is not clear at this stage.

Catalyst	T_{50} [°C]	Catalyst	T_{50} [°C]
$Cs_2V_1Fe_2/AlO_x$	432	$Cu_2V_1Fe_2/AlO_x$	531
$Ru_2V_1Fe_2/AlO_x$	480	$Rh_2V_1Fe_2/AlO_x$	553
$Ir_2V_1Fe_2/AlO_x$	486		
$Cr_2V_1Cs_2/AlO_x$	399	$Ru_2V_1Cs_2/AlO_x$	454
$K_2V_1Cs_2/AlO_x$	406	$La_2V_1Cs_2/AlO_x$	456
$Cu_2V_1Cs_2/AlO_x$	416		

Table 2.21 TGA results of the best catalysts from library 15 and 16.

The best catalyst from library 16 samples was $Cr_2V_1Cs_{20}/Al_2O_3$ which oxidized 50 % of soot at 399 °C.This catalyst thus displayed a higher activity than the original Neri catalyst. No other catalyst showed a T_{50} value less than 400 °C.

2.8 Effect of nitrogen monoxide on soot combustion

The catalysts $Pb_{10}La_5Co_{85}$ and $Cu_{10}Cs_{20}Co_{70}$ were identified by both high-throughput and TGA experiments as potential low temperature soot oxidation catalysts. In order to further access the catalytic behaviour of these promising candidates, catalytic studies were carried out in a flow reactor using temperature programme oxidation. The description of the used fixed bed reactor and the operational conditions are given under the experimental section (3.5.3).

The product gas from the reactor was analysed by CO and CO_2 gas sensors. Initially, 90 mg of the catalyst was activated in the reactor under 50 ml/min synthetic air flow at 300 °C. The activated catalyst was mixed with 10 mg of soot in a crucible with a spatula to obtain the so call loose contact mixture and filled in the reactor. The catalyst-soot mixture was held in the reactor by a frit. The temperature of the catalyst-soot mixture was eventually increased from 200 °C to 500 °C at a heating rate of 2 °C/min in a 100 ml/min model gas flow. For these catalysts, two model gas were applied whereby model one contained 50 ml of synthetic air and 50 ml of nitrogen why model two consisted of 50 ml of synthetic air and 4000 ppm NO in 50 ml of nitrogen. Diesel exhaust gas is made up of soot, hydrocarbon as well as NO_x, therefore we decided to examine the effect of NO on the activity of our catalysts. Shown in Figure 2.35 is a comparison of the CO_2 evolution from the $Cu_{10}Cs_{20}Co_{70}$ (calcined at 700 °C)

catalyst-soot mixture against temperature with and without NO presence. From these curves it is difficult to suggest that NO had any influence on the combustion of soot. One would expect a decrease in the temperature necessary for soot combustion if NO was oxidized to NO_2 by this catalyst. NO_2 is a known strong oxidant for soot combustion. The small difference in the two curves is seemingly an experimental reproducibility effect. Interestingly, this catalyst has T_{50} of 396 °C which is not too different from the temperature at which the maximum of CO_2 was produced. As can be seen clearly from the two curves in Figure 2.35, the maximum CO_2 production temperature was 380 °C in the case where NO was present in the reactant gas and 390 °C in the case without NO present. No carbon mono-oxide was detected during the experiment which further highlights the potential of this catalyst as a good soot combustion catalyst in diesel exhaust gas.

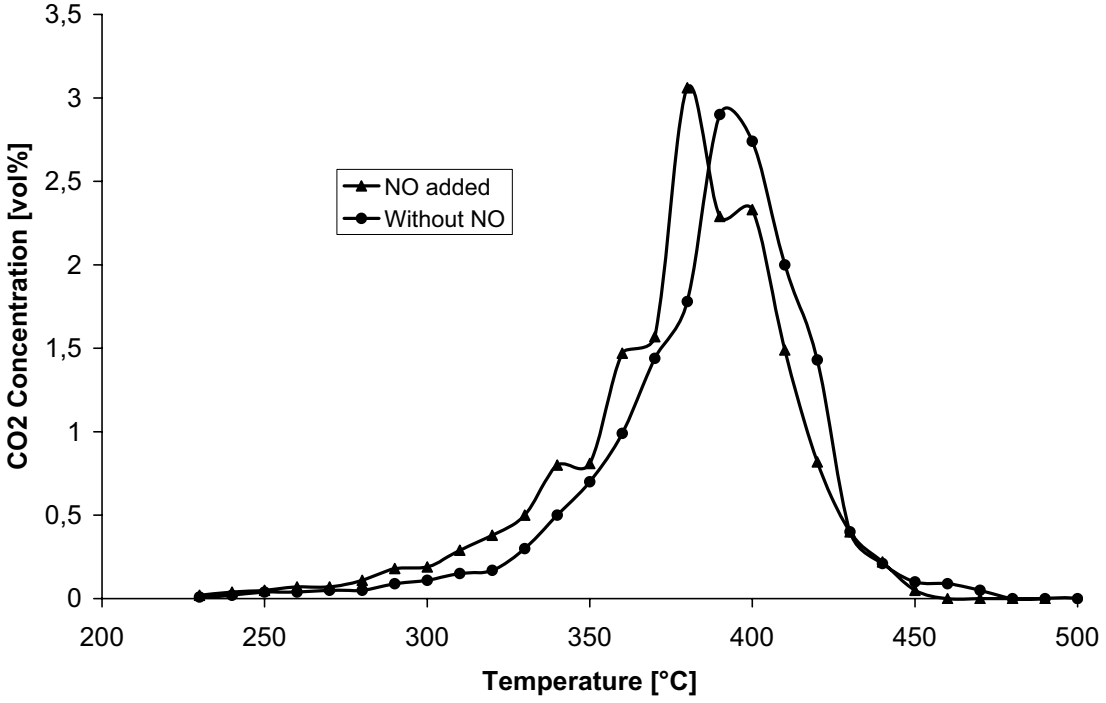

Figure 2.35 Formation of CO_2 during temperature programme oxidation of soot over $Cu_{10}Cs_{20}Co_{70}$ catalyst.

The achieved results from $Pb_{10}La_5Co_{85}$ (calcined at 700 °C) catalyzed soot combustion are given in Figure 2.36. When NO was absent in the reactant gas, the temperature of maximum CO_2 evolution is 410 °C. The performance of $Pb_{10}La_5Co_{85}$ is increased in a substantial way by dosing NO in the reactant gas. The catalyst exhibited a maximum CO_2 evolution already at 380 °C. This observation suggests a strong effect of NO. NO is not known as a soot oxidizing agent, but the oxidation of NO to NO_2 is said to have a tremendous effect in reducing the soot

combustion temperature, since NO_2 is a strong oxidant. This reaction is exploited in Johnson Matthey`s continuously regenerating technology (CRT) [167]. In a continuously regenerating particulate system, a noble metal based catalyst is placed upstream of a diesel particulate filter to cause the oxidation of NO to NO_2, which causes the system to be expensive. The replacement of the noble metal based catalyst with a noble metal free mixed metal is an urgent research topic. It has been proposed by R. Vijay et al. that Co_3O_4 has the ability to convert NO to NO_2 [109]. Probably the $Pb_{10}La_5Co_{85}$ catalyst is able to convert some of the NO present to NO_2 which led to the improved catalytic activity of the catalyst observed during this reaction.

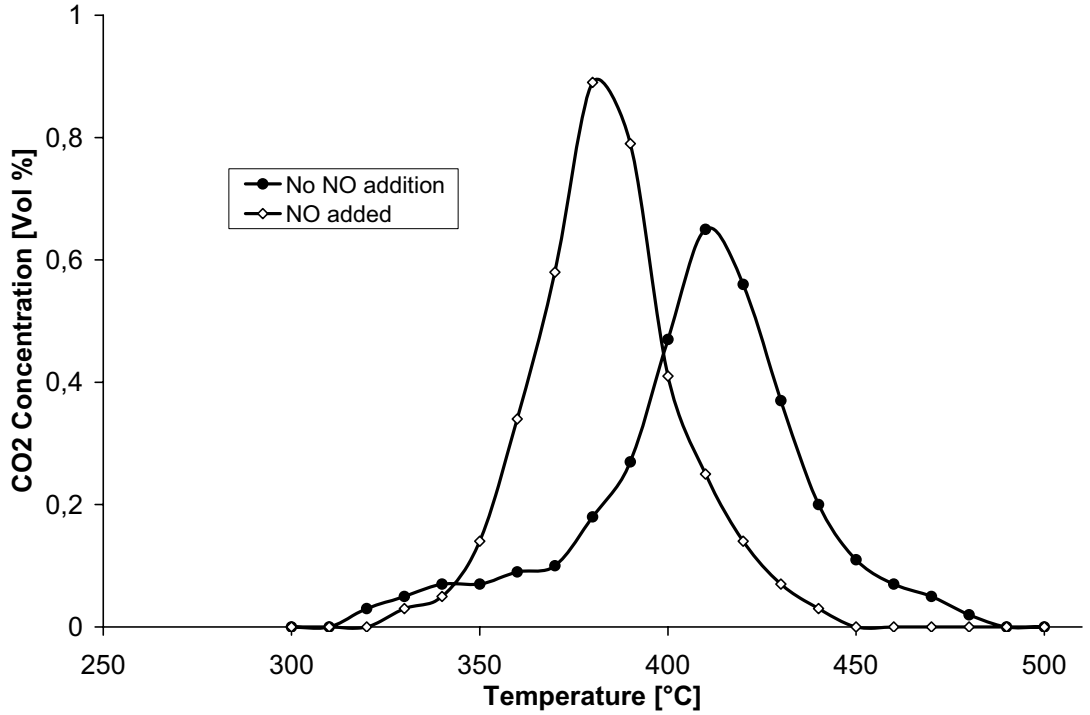

Figure 2.36 Formation of CO_2 during temperature programme oxidation of soot over $Pb_{10}La_5Co_{85}$ catalyst.

In a summary, the ability of the $Cu_{10}Cs_{20}Co_{70}$ and $Pb_{10}La_5Co_{85}$ catalysts to oxidize soot in the presence of NO were verified in a temperature programme reaction apparatus. The strong activities of these catalysts in combusting soot, which was achieved during ec-IR thermography and TGA measurements were again confirmed in a fixed-bed reactor. The temperature at which maximum CO_2 was produced was found to be close to T_{50}. NO was found to have little effect on $Cu_{10}Cs_{20}Co_{70}$ catalytic soot combustion. On the other hand, the introduction of NO in $Pb_{10}La_5Co_{85}$ catalytic soot combustion was found to have a profound effect on soot combustion. Both catalysts mentioned here are indeed potential low

temperature soot oxidation catalysts in diesel exhaust. However the measurements made here are less complete because other substances present in diesel exhaust such as water vapour and SO_2 may have adverse effect on this catalyst. Therefore it would be interesting to study the effect of such substances on these catalysts. Secondly, a quantitative assessment of the reaction product was not possible during this study. Neither N_2 nor NO_2 formation during NO assisted catalytic soot combustion could be analysed. Therefore for future work it is highly recommended to analyse possible NO oxidation or reduction on these catalysts.

2.9 Selective Oxidation of Alcohol

The catalytic oxidation of alcohols to carbonyl compounds has attracted much attention both in the industrial processes and in organic syntheses. However, alcohols are traditionally oxidized with stoichiometric oxidants such as dichromate and permanganate which produces enormous amounts of metal salts as wastes. Therefore, a catalytic process that operates under mild reaction conditions and allows for high selectivity is highly desirable. In our group, a lot of materials have been synthesized using the sol-gel method and tested for different oxidation reactions by different group members. These available samples together with those synthesized individually were screened for their possible catalytic activity in oxidizing 2-heptanol to 2-heptanone by molecular oxygen.

The selective oxidation of 2-heptanol to 2-heptanone was carried out in a 20-ml round-bottomed two-neck glass flask equipped with a reflux condenser, a magnetic stirrer and a gas inlet allowing a flow of oxygen to bubbled into the reaction mixture. Typically, a mixture of 2-heptanol (690 μmol) and 200 mg of catalyst was charged in the reactor. The reactor was placed in an oil bath, which was preheated to a predefined temperature (80 °C, 90 °C, 120 °C), while it was vigorously stirred. The temperature of the reactor was allowed to equilibrate for 10 minutes, after which, 10 ml/min of molecular oxygen was bubbled into the reaction mixture through a mass flow controller. Samples were withdrawn from the reaction mixture at appropriate time intervals (1h, 1.5h, 2h, and 3h), diluted with acetone and centrifuged at a rate of 4000 U/min for 10 min. The reaction product was later separated from the catalyst by carefully pipetting the liquid, after the catalyst powder settled on the flask bottom. The obtained sample was further diluted with a 50:1 volume ratio of acetone to sample (to prevent detector saturation) and analysed with a GC-MS system. Initially, the catalytic activity of $Pt_{0.5}Al_1Mn_{6.7}Co_{91.8}$ for the oxidation of 2-heptanol at different reaction time was investigated

by analysing the reaction product at different reaction times under the same reaction temperature (90 °C). The obtained results are given in Table 2.22.

Time [h]	Conversion [%]	Selectivity [%]
0.25	12.3	80.5
0.5	14.8	85
1	16.9	91.5
2	17.5	95.7

Table 2.22 Oxidation of 2-heptanol to 2-heptanone by molecular O_2 catalysed by $Pt_{0.5}Al_1Mn_{6.7}Co_{91.8}$ at 90 °C

The $Pt_{0.5}Al_1Mn_{6.7}Co_{91.8}$ catalyst was efficient for the oxidation of 2-heptanol to 2-heptanone. The oxidation was found to increase with increasing batch time, with maximum conversion achieved after 2 hours. The selectivity of 2-heptanol to 2-heptanone was also observed to increase with batch time, with a maximum after 2 hours. Interestingly, after 2 hours reaction time, very few by-products were presence. The main by-product was 4-hydoxyl-4-methyl-2-Pentanone with a selectivity of 3.5 %.

The stability of the $Pt_{0.5}Al_1Mn_{6.7}Co_{91.8}$ catalyst with respect to its activity was investigated, whereby the catalyst recovered after the reaction was again calcined and reused (denoted as used catalyst). The obtained results which are shown in Figure 2.37, is a plot of the conversion of 2-heptanol and its selectivity to 2-heptanone at 120 °C. Clearly, the catalytic activity was increasing with increasing batch time up to 120 min. After this time the conversion of 2-heptanol decreased with increasing batch time. Maximum conversions of 25 % and 24 % were achieved for the fresh and the used catalyst respectively after 120 min batch time. The used catalyst selectivity towards 2-heptanone was found to be slightly better. However the difference was too small, therefore no conclusion can be drawn.

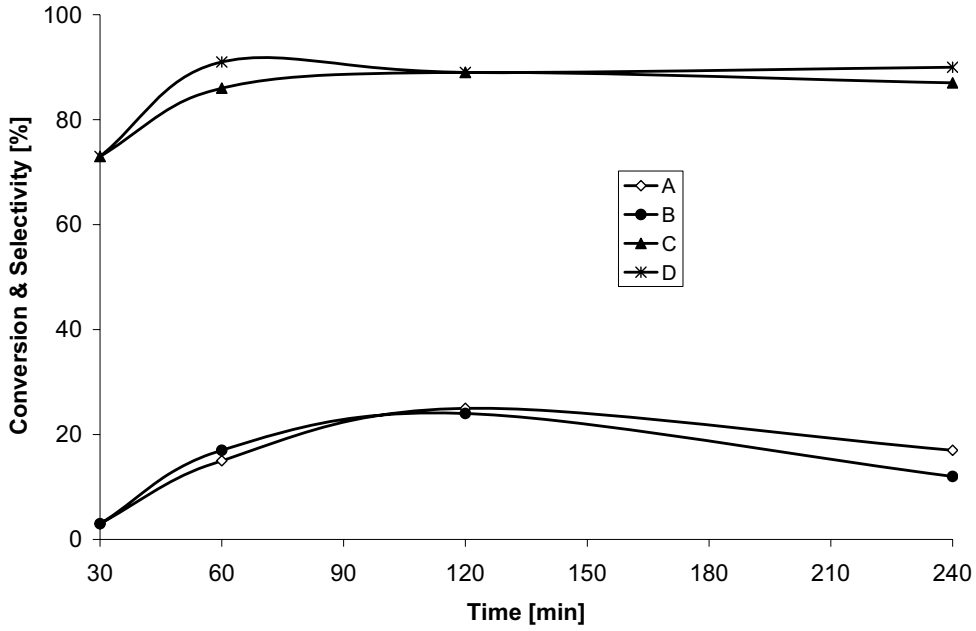

Figure 2.37 Selective oxidation of 2-heptanol to 2-hetanone with O_2 catalysed by $Pt_{0.5}Al_1Mn_{6.7}Co_{91.8}$ (120°C): (A) oxidation with fresh catalyst, (B) oxidation with used catalyst (C) 2-heptanone selectivity with fresh catalyst, (D) 2-heptanone selectivity with used catalyst.

These results suggest that the $Pt_{0.5}Al_1Mn_{6.7}Co_{91.8}$ catalyst maintained its activity after the first reaction which is encouraging in terms of a possible recycling of the catalyst. However, the achieved conversion is still low. The possible solvent effect on the catalytic oxidation of 2-heptanol was also assessed. Toluene 10 times the volume of the alcohol was added into the reaction mixture. Table 2.23 presents catalytic activity and selectivity in the oxidation of 2-heptanol by molecular oxygen over $Pt_{0.5}Al_1Mn_{6.7}Co_{91.8}$ catalyst with and without toluene present in the reaction mixture at 90 °C. The conversion of 2-heptanol was found to proceed slightly better in the presence of a solvent. However, the 2-heptanone selectivity achieved under solvent assisted reaction was poor. For both reactions, the main by-product identified was 4-hydroxyl-4-methyl-2-pentanone.

Time [h]	Solvent	Conversion [%]	Selectivity [%]
1		17	92
2		18	97
3		19	95
1	Toluene	18	57
2	Toluene	28	35
3	Toluene	22	50

Table 2.23 $Pt_{0.5}Al_1Mn_{6.7}Co_{91.8}$ oxidation of 2-heptanol to 2-heptanone by molecular oxygen with and without toluene solvent.

Table 2.26 is a representative summary of some of the various samples which were examined and their corresponding conversion and selectivity. Among these samples, the $Cr_{50}Co_{50}$ catalyst resulted in a 2-heptanol conversion of 30.7 % and a selectivity of 49 %. Though this catalyst conversion was relatively high, its selectivity towards 2-heptanone formation was poor. Best catalyst was the $Pt_2Cr_{49}Ce_{49}$ with a conversion of 18.1 % and a selectivity of 89 % after 8 hours of reaction time.

Catalyst	Time [h]	Conversion[%]	Selectivity [%]
Pt/ZrO_2	1	4.5	70
$Pt_2Cr_{49}Ce_{49}$	8	18.1	89
$Cr_{50}Ce_{50}$	3	30.7	49
$CsVFe/Al_2O_3$	3	4.5	0
$K_{15}Ce_{75}$	3	0.75	0
Cs_3Co_{97}	3	1.25	0
$Co_{30}Cu_{70}$	3	0.5	0
$Rb_3Co_{19}Mn_{78}$	3	0.78	0
$Pt_1Ce_{14}Ni_{85}$	3	0.91	0
$Pt_{0.5}K_3Ce_{96.5}$	3	0.8	0

Table 2.24 Catalytic oxidation of 2-heptanol to 2-heptanone by molecular oxygen at 90 °C.

One of the possible reasons for the poor catalytic activity of the considered catalysts in this study is the possible deactivation of the catalysts by water present in the reaction mixture. In order to exclude catalytic deactivation caused by water, molecular sieve acting as a water trap was included in one of the reaction mixture containing $Cr_{50}Ce_{50}$ catalysts. It should be mentioned that further optimisation of the reaction conditions of the oxidation of 2-heptanol

by some of the mentioned catalysts here was carried out by Rende. The results can be found in her thesis [168]. Figure 2.38 is a comparison between the reaction conducted without molecular sieve and reaction conducted in the presence of molecular sieve (3Å).

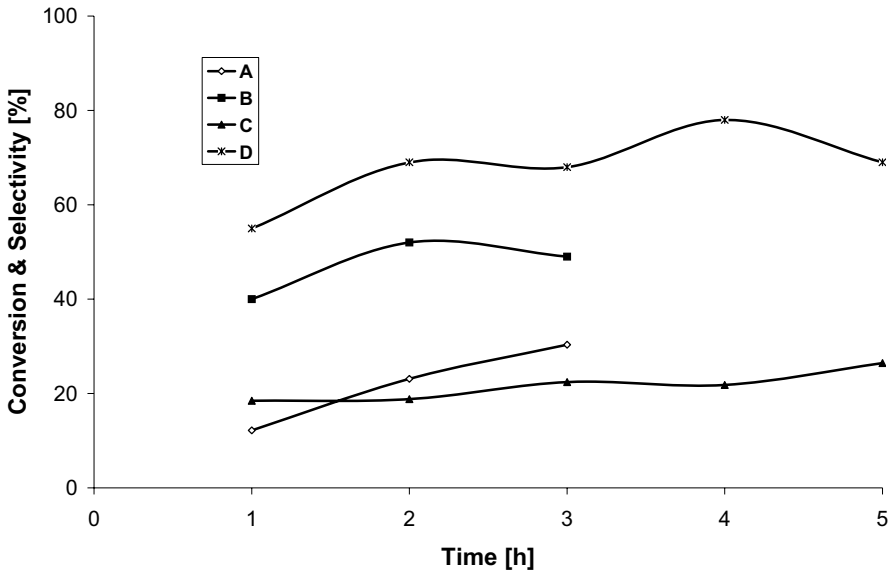

Figure 2.38 Oxidation of 2-heptanol to 2-heptanone with molecular oxygen catalysed by $Cr_{50}Ce_{50}$ catalyst at 90 °C, A and B are the conversion and selectivity without molecular sieve, C and D are the conversion and selectivity in the presence of molecular sieve.

As can be seen in Figure 2.38, the $Cr_{50}Ce_{50}$ catalyst was active under both reaction conditions. The alcohol was oxidized more slowly in the present of molecular sieve. After one hour of reaction time, more alcohol (18.5 %) was oxidized in the presence of molecular sieve. After a reaction time of 2 and 3 hours respectively, more alcohol was oxidize in the absence of molecular sieve with a maximum conversion of 30,4 %. However the alcohol selectivity towards 2-heptanone was generally better in the reaction mixture containing molecular sieve. The selectivity increased from 55 % to 69 % after one and two hours of reaction time respectively, but it remained almost constant up to five hours of reaction. Generally, the catalytic oxidation of alcohols by molecular oxygen is performed under relatively high pressure (0.5-2 MPa). However, alcohols have been successfully oxidized by molecular oxygen under atmospheric pressure, but the noble metals such as Ru-complex are necessary [169]. This study has shown that $Cr_{50}Ce_{50}$, $Pt_2Cr_{49}Ce_{49}$, and $Pt_{0.5}Al_1Mn_{6.7}Co_{91.8}$ are potential alcohol oxidation catalyst under mild conditions.

2.10 Catalyst Characterisation

The BET surface areas of the lead catalysts were determined by physisorption measurements after calcinations, but prior to reaction. X-ray powder diffraction studies were performed with a Huber G670 Guinier camera using CuKα_1 radiation (λ=1.54056Å). Lattice parameter refinement was done by full pattern Rietveld refinement with the program TOPAS [170] using the fundamental parameters approach [171]. The determined BET surface area for selected materials is given in Table 2.25. Also the BET surface area of the used soot was measured, which was found to be 159.9 m^2/g. The specific surface areas of all the selected catalysts were found to be more than 20 m^2/g. Since only samples with two different concentrations were examined, no conclusion on the effect of Cs concentration on surface area can be made. Interestingly, addition of a third element (Cu, Ag) to the CsCo catalyst increased its specific surface area. Since these catalysts also showed increased soot oxidation activity, it is logical to assume that increased surface area had a positive effect on the catalytic activity. The doping of LaCo sample with Pb led to a decrease in the sample surface area. This finding suggest that a different factor should be responsible for the improved catalytic activity observed after doping with Pb.

Catalyt	BET surface area (m^2/g)
K_3Ce_{97}	39.8
Cs_3Co_{97}	31.4
$Cs_{20}Ce_{80}$	31.9
$Cu_{10}Cs_{20}Co_{70}$	34.8
$Ag_{10}Cs_{20}Co_{70}$	35.4
$Pb_{10}La_5Co_{85}$	24.5
La_5Co_{95}	47.2
$Cs_2Fe_2V_1/Al_2O_3$	92.2
Soot	159.9

Table 2.25 BET specific surface area of selected catalyst and soot

The XRD pattern of the binary K-Ce sample is given in Figure 2.39. The XRD measurement reveals only CeO_2 as crystalline compound with a cubic fluorite type structure (JCPDS 75-076). No additional peaks indicating the presence of other phases could be detected. From the X-ray diffraction pattern small amounts of amorphous phases cannot be excluded in this catalyst. CeO_2 is a well known support for diesel soot combustion [172, 173]. One of the most important role of CeO_2 in catalytic redox reactions is to provide surface sites and to act as

oxygen storage/transport medium by the redox pair Ce^{4+}/Ce^{3+}. Two factors can explain the activity of the K_3Ce_{97} towards soot combustion: the first is the availability of Ce^{4+} sites and the second is the ability of the material to donate its oxygen.

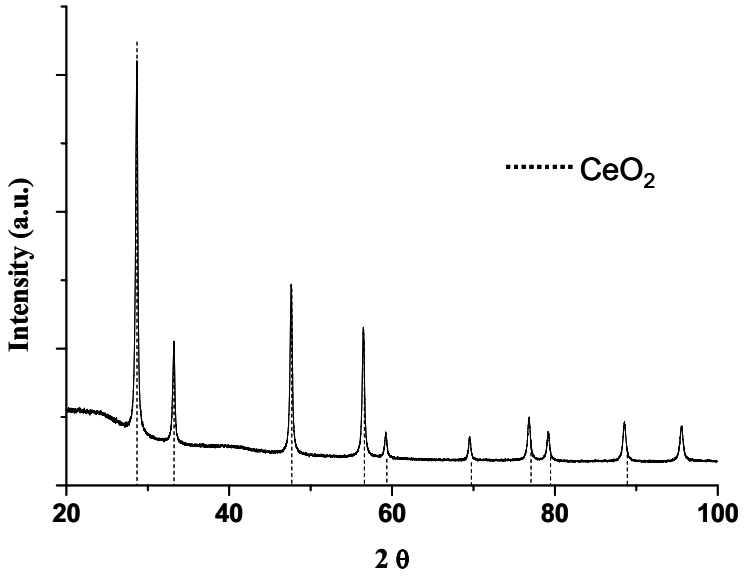

Figure 2.39 Powder X-ray diffraction pattern of K_3Ce_{97} catalyst

The phase composition and morphology of the K_3Ce_{97} catalyst was further analysed by transmission electron microscope equipped with an energy dispersive x-ray analyser. The sample contains crystalline (particle size 5-15 μm) and amorphous particles. The representative TEM image shown in Figure 2.40, clearly demonstrate the presence of ceria oxide with no morphological diversity. EDX analysis reveals the existence of only Ce particles with no evidence of K. Probably, the failure to detect potassium was due to its low content (3 %).

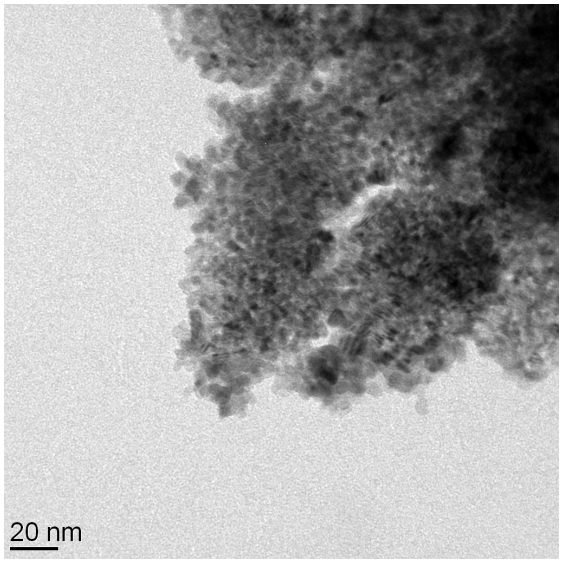

Figure 2.40 Representative TEM image of K_3Ce_{97} catalyst

In order to verify the formation of solid solutions in active samples based on Cobalt oxide, we recorded and analysed the XRD pattern of these samples. Shown in Figure 2.41 are the XRD patterns of selected samples before reaction with soot (fresh samples) and after reaction with soot (after reaction samples). All the samples showed major peaks at about 2 Θ = 31.3° and 36.9° which indicates the presence of a spinel–type Co_3O_4 phase in these samples. The XRD pattern of $Cs_{20}Co_{80}$ for both fresh and the after reaction samples were almost the same. Their major difference was in their full width at half maximum, whereby the after reaction sample full width at high maximum decreased, which suggests that the crystallinity increased after the reaction with the soot. Taking into account that the $Cu_{10}Cs_{20}Co_{70}$ catalyst was very active for soot combustion, in order to identify the changes that happened to this catalyst during the reaction, and also for detection of the phases formed, this catalyst was also characterized by XRD after the raection. Clearly peaks can be seen at : 2 Θ = 31.3° and 36.9° which are due to the Co_3O_4 phase, 2 Θ = 21.6° and 30.7° which are due to a CsCl phase and small peaks at 2 Θ = 35.6° and 38.9° indicating a CuO phase. A comparison of the fresh and the after reaction sample shows an improve crystallinity after the soot oxidation test. The sharpness of the major peaks increased with decreased full weight at half maximum compared to the fresh sample. The activity of the CsCo catalyst was found to increase when the concentration of Cs was increased from 3 mole % to 20 mole %. The corresponding XRD pattern of the two samples are indicated as (c) and (e) in Figure 2.41 respectively. Both samples showed the presence of a spinel-type Co_3O_4 phase and a CsCl phase, with no mixed phases identified.

The $Cs_{20}Co_{80}$ catalyst contained more CsCl than the Cs_3Co_{97} catalyst, which may have improved the catalyst-soot contact leading to better catalytic activity.

The activities of the above mentioned samples appear to be related to the presence of the Co_3O_4 phase which was identified in all the samples. The reducibility of Co_3O_4 may be responsible for the catalytic activity. The relatively weak bond strength of the Co-O bond in Co_3O_4 increases the availability of lattice oxygen. The presence of CsCl in the sample possibly increases the catalyst-soot contact by conferring surface mobility. Also CsCl could act to preserve the redox capacity of cobalt when calcined at 400 °C and may prevent the sintering of Co_3O_4. The addition of a third element Cu and Ag lead to the inclusion of the CuO and Ag_2O phases in the samples respectively. The reducibility of the Co_3O_4 crystallites is known to be enhanced by the presence of a CuO phase [174]. The lower temperature of soot combustion observed for $Cu_{10}Cs_{20}Co_{70}$ may be associated with the enhanced reducibility of Co_3O_4 towards soot combustion.

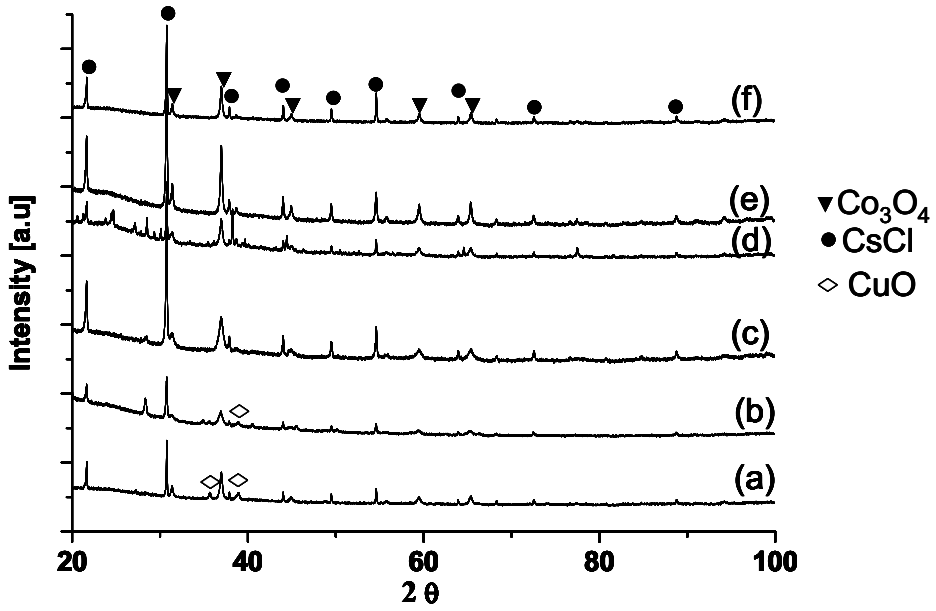

Figure 2.41 Powder XRD patterns of (a) $Cu_{10}Cs_{20}Co_{70}$ after reaction sample, (b) $Cu_{10}Cs_{20}Co_{70}$ fresh sample (c) Cs_3Co_{97} sample (d) $Ag_{10}Cs_{20}co_{70}$ fresh sample (e) $Cs_{20}Co_{80}$ fresh sample and (f) $Cs_{20}Co_{80}$ after reaction sample

The catalysts La_5Co_{95} and $Pb_{10}La_5Co_{85}$ were identified as potential soot oxidation catalyst. In order to identify the phases present in these samples, XRD measurements were conducted and the obtained XRD pattern is depicted in Figure 2.42. In sample (a) which was a binary mixed

oxide of La and Co, only one phase Co_3O_4 could be identified. Plot (b) denotes the pattern of the $Pb_{10}La_5Co_{85}$ sample which was calcined at 400 °C. Also only one phase Co_3O_4 was present with very small particles. The crystallinity of this sample was very poor, which may be attributed to the third element added. It seems logical to attribute the superior soot combustion activity to the presence of Co_3O_4, however, solely on that basis one would expect the La_5Co_{95} sample to be more active than $Pb_{10}La_5Co_{85}$, instead, the reverse was true, which points against Co_3O_4 as active phase

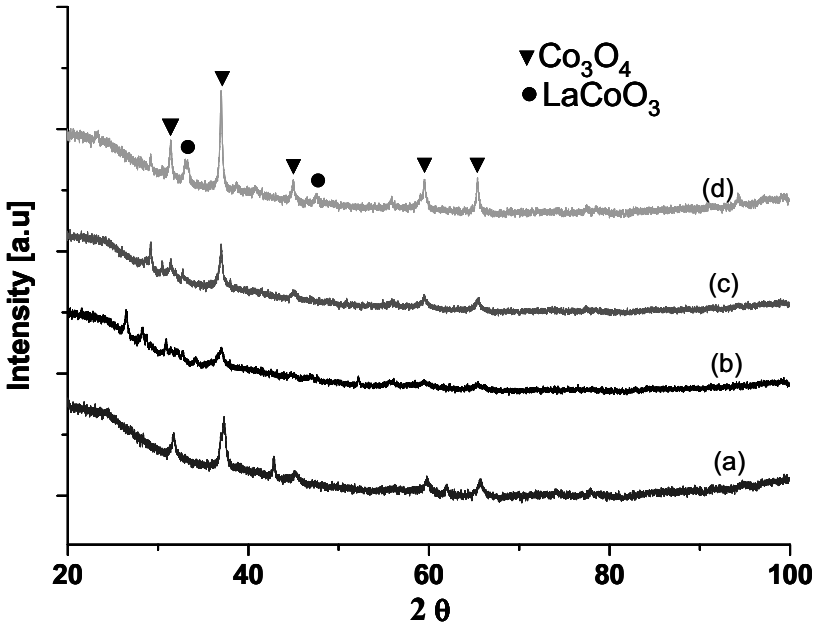

Figure 2.42 Powder XRD patterns of (a) La_5Co_{95} calcined at 400 °C, (b) $Pb_{10}La_5Co_{85}$ calcined at 400 °C, (c) $Pb_{10}La_5Co_{85}$ calcined at 600 °C, and (d) $Pb_{10}La_5Co_{85}$ calcined at 700 °C with likely peak phase assignment.

Also examined was the effect of the calcination temperature on the crystallinity of the $Pb_{10}La_5Co_{85}$ catalyst. All the samples irrespective of the calcination temperature showed the presence of Co_3O_4 phase. Clearly, the crystallinity of the sample was increasing with increasing calcinations temperature. In addition to the phase identified in all samples, the mixed phase $LaCoO_3$ was identified in the sample calcined at 700 °C. The calcination temperature was found to have little effect on the catalytic activity of this catalyst towards soot combustion, which is an argument against $LaCoO_5$ as active phase

Further characterisation of the La_5Co_{95} and $Pb_{10}La_5Co_{85}$ catalysts were performed using a transmission electron microscope (TEM) which was couple to an electron dispersive x-ray analyser (EDX). The TEM image of the $Pb_{10}La_5Co_{85}$ sample is shown in Figure 2.43. The TEM image indicates that the crystalline content in the sample is high. The EDX data shown in Table 2.26 which were measured at specific points, reveals a good correlation between the expected elemental distribution ($Pb_{10}La_5Co_{85}$) and the observed elemental distribution. A relatively homogeneous elemental distribution was achieved in the nano-range. This observation suggested a homogeneous distribution of the various constituent of the catalyst. In addition, no indication of domain formation was obtained.

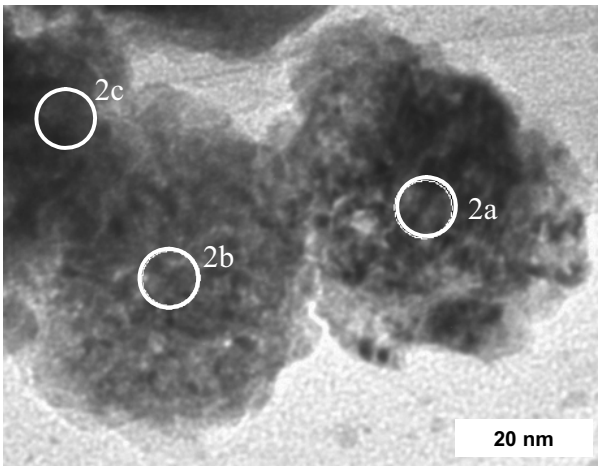

Figure 2.43 TEM-image of the $Pb_{10}La_5Co_{85}$ catalyst with markings indicating EDX analyses points.

Position	Co-K (Atomic %)	La-L (Atomic %)	Pb-L (Atomic %)
2a	88.04	4.44	7.53
2b	91.4	4.5	4.09
2c	84.3	4.68	11.02

Table 2.26 Results of the EDX analyses of $Pb_{10}La_5Co_{85}$ catalyst at specific points.

Figure 2.44 is a micrograph obtained from the TEM measurement on the La_5Co_{95} catalyst. The micrograph confirms the crystallinity of La_5Co_{95} which was reported by XRD-measurement. The EDX analysis confirms a homogeneous distribution of the metals with no

indication of domain formation. Some regions of high contrast can be recognised in the micrograph which where confirmed by EDX analysis as having a slightly higher content of cobalt.

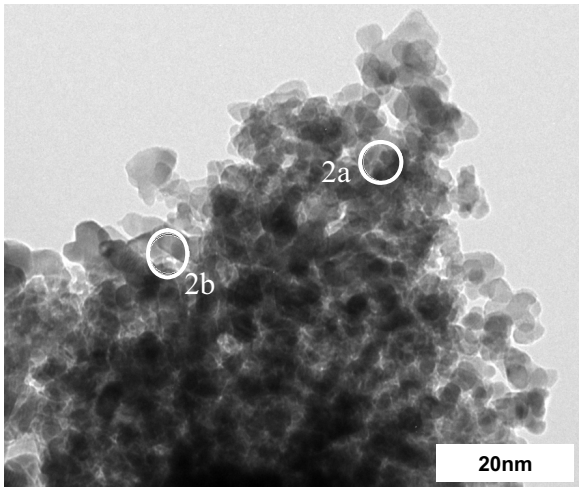

Figure 2.44 TEM-image of the La_5Co_{95} catalyst with markings indicating EDX analyses points.

Position	Co-K (Atomic %)	La-L (Atomic %)
3a	94.42	5.58
3b	94.76	5.24

Table 2.27 Results of the EDX analyses of La_5Co_{95} catalyst at specific points

3 Experimental Section

In this section, the various synthesis methods used to synthesize the catalysts which were examined in the course of this work will be discussed. First, high-throughput syntheses of catalyst libraries will be discussed and the chemicals used will be mentioned. All in all, 16 catalyst libraries were synthesized. Furthermore the conventional methods used to synthesize the catalysts studied here will be discussed in detail. Last but not the least, the experimental setup and procedure for both high-throughput and conventional experimentations will be discussed.

3.1 High-throughput syntheses of catalyst libraries

3.1.1 Cobalt- and Mn-based catalyst libraries

The same sol-gel recipe was used for the syntheses of catalyst libraries with Co and Mn as matrix. Using this recipe, seven libraries (part of 1, 3, 4, 6, 8, 9, 10), which consisted of binary (M_3Co_{97}, M_3Mn_{97}) and ternary ($M_xCs_{20}Co_{80-x}$, $Cu_xCs_yCo_z$ and $Ag_xCs_yCo_z$) materials were synthesized. The corresponding metal propionates were applied as precursors for the basic oxides (cobalt(II)- and manganese(II)-propionate). The syntheses of the propionates are given in section 3.2. The commercially available chemical precursors given in Table 3.1 were applied as dopants. The matrix stock solution was prepared by dissolving cobalt(II)- or manganese(II) propionates in methanol at a concentration of 1 M. All dopants except otherwise stated, were dissolved in methanol at a concentration of 0.1 M. Using the Python programming language, a parameterized recipe was written which was later exported to the library design software Plattenbau. Based on this parameterized recipe, the software Plattenbau calculates the volumes of the different solutions of the sol components as required for the preparation of individual samples. It automatically generates an optimized pipetting list, which when imported to a commercial pipetting robot (Zinsser Analytic, Lissy), to control its operation.

The preparation of La_3Co_{97} will be used as an example to demonstrate the automatic library synthesis procedure. Initially, the sample amount (300 µmol) and the reagent list consisting of the reagent names and concentrations were defined in the Plattenbau software. For example, the composition of the lanthanum nitrate (0.03) is defined in the Plattenbau sample list and the composition of cobalt(II) propionate (0.97) is calculated by the software. Using

the imported recipe, the require amount of each component of the sample was calculated which was; n(La)= 9 µmol, n(Co)= 291 µmol, n(4-hydroxy-4-methyl-2-pentanone = 900 µmol and n(Methanol)= 15 mmol. From the given reagents and their concentration under the Plattenbau reagent list, the corresponding required volume of each component of the product sample was calculated and a pipetting list generated which was exported to a pipetting robot. The reagent rack containing the stock solutions and the synthesis rack (50 vials) filled with 2 ml GC vials were positioned on the robot workbench. The preparation of La_3Co_{97} for example was performed by pipetting the following volumes of single solutions in sequence: methanol (226.6 µl), 4-hydroxy-4-methyl-2-pentanone (112 µl), cobalt propionate (291 µl), and Lanthanum nitrate (90 µl, 9 µmol) in a 2 ml vial. With the completion of the pipetting process the entire rack was placed on an orbital shaker (Heidolph, Titramax 100) for 1 hour. Note the actual volume of methanol to be pipetted was 607.6 µl, from this volume the 291 µl from cobalt(II) propionate solution and 90 µl from lanthanum nitrate solution were subtracted. Later the rack was dried for 5 days at room temperature. After drying, the samples were placed in a calcination rack and introduced in an oven. Finally the samples were heated from room temperature to 400 °C at a rate of 1 °C/min under static air atmosphere, calcined there for 5 h and allowed to cool in the same atmosphere. The calcined samples in the GC vials were crushed and mixed with a spatula.

A slide modification was introduced in the syntheses of the $M_xCs_{20}Co_{80-x}$ materials. Again M denotes the dopant (50) and x its atomic %, hereby two x values (3, 10) were considered. Briefly the preparation of $Cu_3Cs_{20}Co_{77}$ was as follows: methanol (226.6 µl), 4-hydroxy-4-methyl-2-pentanone (112 µl), cobalt propionate (231 µl), copper nitrate (90 µl, 9 µmol), and a 60 µl of a 1 M caesium chloride solution were pipetted in a 2 ml vial. The drying and calcination procedures were the same as above.

3.1.2 Ce-based catalyst libraries

The sol-gel recipe used to synthesized catalyst libraries with cerium nitrate as the matrix is explained in this section. Four libraries (part of 1, 2, 5, and 7) based on this recipe were synthesized. The general recipe for the synthesis of M_3Ce_{97} was as follows;

3 . M : 97. Ce : 3 .(100) Complexing Agent : 0.02. (100) Propionic acid.

M = one of the 50 dopants

The matrix- and dopants- precursors used as well as their concentration are given in Table 3.1. The synthesis of La_3Ce_{97} for example was as follows, 90 µl (9µmol) of a 0.1 M solution of lanthanum nitrate was dosed by the pipetting robot in a GC vial. 291µL of a 1 M solution $Ce(NO_3)_3 \cdot 6H_2O$ in methanol was added in the vial. Finally 111.7 µl (8.06 M) solution of a mixture of propionic acid (sol-gel catalyst) and 4-hydroxyl-4-methyl-2-pentanone as complexing agent was added in the vial. The sol was homogenised by stirring on an orbital shaker for one hour, after which, the sample was dried for 5 days at 40 °C. The obtained gel was successively calcined in an oven at 400 °C, using a heating rate of 0.2 °C/min and kept at this temperature for 5 h.

Table 3.1 Summary of the chemicals, the solvents and the concentrations of the precursors used in synthesizing library 1-10.

Chemical	Solvent	c [mol/L)	Chemical	Solvent	c [mol/L)
$AgNO_3$	M	0.1	$Mg(NO_3)_2 \cdot 6H_2O$	M	0.1
$Al(NO_3)_3 \cdot 9\ H_2O$	M	0.1	$Mn(NO_3)_2 \cdot 4H_2O$	M	0.1
$B(OH)_3$	M	0.1	Mn(II)-propionate[e]	M	1
$Ba(NO_3)_2$	W	0.1	$Mo[OCH(CH_3)_2]_5$	I	0.1
$Bi[C_4H_9CH(C_2H_5)COO]_3$	M	0.1	$NaNO_3$	M	0.1
$Ca(NO_3)_2 \cdot 4\ H_2O$	M	0.1	$Nd(NO_3)_3 \cdot 6\ H_2O$	M	0.1
$Cd(NO_3)_2 \cdot 4\ H_2O$	M	0.1	$Pb(CH_3CO_2)_2$	W	0.1
$Ce(NO_3)_2 \cdot 6\ H_2O$	M	0.1	$Pr(NO_3)_3 \cdot 5\ H_2O$	M	0.1
$Ce(NO_3)_3 \cdot 6\ H_2O$[a]	M	1	$PtBr_4$	W	0.1
$Co(NO_3)_2 \cdot 6\ H_2O$	M	0.1	$Rb[CH_3COCHCOCH_3]$	M	0.1
Cobalt(II)-propionate[b]	M	1	$RuCl_3$	W	0.1
$Cr(NO_3)_3 \cdot 9\ H_2O$	M	0.1	$SbCl_3$	M	0.1
CsCl	W	0.1	$Sc(NO_3)_3 \cdot 5\ H_2O$	M	0.1
CsCl[c]	W	1	SeO_2	M	0.1
$Cu(NO_3)_2 \cdot 3\ H_2O$	M	0.1	$Si(OC_2H_5)_4$	M	0.1
$Dy(NO_3)_3 \cdot 5\ H_2O$	M	0.1	$Sm(NO_3)_3 \cdot 6\ H_2O$	M	0.1
$Er(NO_3)_3 \cdot 5\ H_2O$	M	0.1	$Sn[OCH(CH_3)_2]_4$	M	0.1
$Eu(NO_3)_3 \cdot 6\ H_2O$	M	0.1	$Sr(NO_3)_2$	M	0.1
$Fe(NO_3)_3 \cdot 9\ H_2O$	M	0.1	$Ta(OC_2H_5)_5$	M	0.1
$Ga(NO_3)_3 \cdot xH_2O$	M	0.1	$Tb(NO_3)_3 \cdot x\ H_2O$	M	0.1
$Gd(NO_3)_3 \cdot 6H_2O$	M	0.1	$TeCl_4$	M	0.1
$Ge[OCH(CH_3)_2]_4$	M	0.1	$Ti[OCH(CH_3)_2]_4$	M	0.1
$HfCl_4$	M	0.1	$Tm(NO_3)_3 \cdot 6\ H_2O$	M	0.1
$Ho(NO_3)_3 \cdot 5\ H_2O$	M	0.1	$V[CH_3COCHCOCH_3]_3$	M	0.1
$In(NO_3)_3 \cdot 5\ H_2O$	M	0.1	$W[OCH(CH_3)_2]_6$	M	0.1
KNO_3	W	0.1	$Y(NO_3)_3 \cdot 6\ H_2O$	M	0.1
$La(NO_3)_3$	M	0.1	$Yb(NO_3)_3 \cdot x\ H_2O$	M	0.1
$La(NO_3)_3$[d]	M	1	$Zn(NO_3)_2 \cdot 4\ H_2O$	M	0.1
$Lu(NO_3)_3 \cdot xH_2O$	M	0.1	$ZrO(NO_3)_2 \cdot x\ H_2O$	M	0.1

M, I and W indicating methanol, isopropanol and water respectively.

[a] used to synthesize libraries: part of 1, 2, 5, and 7

[b] used to synthesize libraries: part of 1, 3, 6, 8, 9, and 10

[c] used to synthesize libraries: 6, 9, and 10

[d] used to synthesize library: 8

[e] used to synthesize library: 3

3.1.3 Libraries 11, 12, 13 and 14 Synthesis

The synthesis method used to synthesize the library 11, 12, 13, and 14 catalysts is described in this section. The general recipe for the synthesis of $A_aB_bD_dE_eF_f$ was as follows;

a . A : b . B : d . D : e . E : f . F : 3 . (a + b + c + d + e)CA : 0.04 (a + b + c + d + e) Prop.

A, B, D, E, F = metal precursor
a, b, d, e, f = varied between 0, 20, 40, 60, 80, and 100 mmol
CA = Complexing agent
Prop. = Propionic acid

For the synthesis of CoMoCe ternary composition spread for example, cobalt- and cerium-nitrates were dissolved in methanol at a concentration of 1 M while molybdenium isopropoxide was dissolved in isopropanol at a concentration of 1 M. The preparation of $Co_{20}Mo_{40}Ce_{40}$ for example was as follows: 60 µl (60 µmol) of the cobalt nitrate stock solution was pipetted in a 2 ml vial. Furthermore, 120 µl (120 µmoll) of molybdenum isopropoxide solution and 120 µl (120 µmol) cerium nitrate solution were added. Finally 112.5 µl (900µmol) of a 8 M mixture of 4-hydroxyl-4-methyl-2-pentanone as complexing agent and propionic acid was added. The mixture was stirred for one hour and later dried at 40 °C for 5 days to allow gel formation and catalyst drying. Successively, the samples were calcined in an oven at 400 °C, using a heating rate of 0.2 °C/min and kept at this temperature for 5 h under static atmosphere. The precursors and their concentrations applied in the syntheses of these libraries are summarised in Table 3.2.

Chemical	Solvent	c [m/L]	Chemical	Solvent	c [m/L]
$Ce(NO_3)_3 \cdot 6\ H_2O$	I	1	$Cu(NO_3)_2 \cdot 3\ H_2O$	M	1
$Co(NO_3)_2 \cdot 6\ H_2O$	I	1	$Mn(NO_3)_2 \cdot 4H_2O$	I	1
$Fe(NO_3)_3 \cdot 9\ H_2O$	M	1	KNO_3	W	1
$Mo[OCH(CH_3)_2]_5$	I	1	$OV[OCH(CH_3)_2]_3$	I	1
$Cr(NO_3)_3 \cdot 9\ H_2O$	I	1	$La(NO_3)_3$	I	1

Table 3.2 scheme showing the chemicals and their concentration used to synthesize libraries 11, 12, 13, and 14. M, I, W, denotes methanol, isopropanol, and distilled water respectively.

3.1.4 Libraries 15 and 16 synthesis

Libraries 15 and 16 were synthesized following the method described in detail by T. Wolter [175]. The general recipe is given below while the used matrix and dopants precursors are summarised in Table 3.3.

20 M + 10 $OV(O^{i}Pr)_3$ + 20 $Fe(NO_3)_3 \cdot 9H_2O$ + 50 $Al(O^{sec}Bu)_3$ + 300 $C_6H_{12}O_2$ + 6500 $^{i}PrOH$ + 100 H_2O + 6 HCl_{conc}

M = 50 dopants

These libraries were synthesized manually because of the instability of the alkoxide used. For example the aluminium tri-sec-butylate solution was observed to precipitate after 10 min at room temperature. The preparation of $Cu_2V_1Fe_2/AlO_x$ for example was carried out by pipetting the following volumes of single solutions in the following sequence: 74.1 µl (600 µmol) of 4-hydroxy-4-methyl-2-pentanone, 200 µl (40 µmol) of a 0.2 M copper nitrate solution, 20 µl (20 µmol) of vanadium (V) oxy tri-isoproxide solution, 40 µl (40 µmol) of iron nitrate solution, 100 µl (100 µmol) of aluminium tri-sec-butylate solution, 435 µl of isopropanol, 3.6 µl of distilled water, and 0.44 µl of concentrated hydrochloric acid. The mixture is stirred for 2 h and dried at room temperature for three days before calcination. The applied calcination programme is shown below.

RT $\xrightarrow{0.5\ °C/min}$ 250°C (5 h) $\xrightarrow{0.5\ °C/min}$ 400°C (5 h) $\xrightarrow{2°C/min}$ RT

Table 3.3 Summary of the chemicals, the solvents and the concentrations of the precursors used in synthesizing library 15 and 16.

Chemical	Solvent	c [mol/L]	Chemical	Solvent	c [mol/L]
$AgNO_3$	I	0.2	$Mn(NO_3)_2 \cdot 4H_2O$	I	0.2
$Al[C_2H_5CH(CH_3)O]_3$	I	1	$Mo[OCH(CH_3)_2]_5$	I	0.2
$B(OH)_3$	I	0.1	$NaNO_3$	I	0.2
$Ba(NO_3)_2$	I	0.2	$NbCl_5$	I	0.2
$Ca(NO_3)_2 \cdot 4\ H_2O$	I	0.2	$Nd(NO_3)_3 \cdot 6\ H_2O$	I	0.2
$Cd(NO_3)_2 \cdot 4\ H_2O$	I	0.2	$Ni(NO_3)_3.6H_2O$	I	0.2
$Ce(NO_3)_2 \cdot 6\ H_2O$	I	0.2	$Pr(NO_3)_3 \cdot 5\ H_2O$	I	0.2
$Cr(NO_3)_3 \cdot 9\ H_2O$	I	0.2	$RhCl_3.3H_2O$	W	0.2
CsCl	W	0.2	$RuCl_3$	W	0.2
CsCl[a]	W	1	$RbNO_3$	W	0.2
$Cu(NO_3)_2 \cdot 3\ H_2O$	I	0.2	$SbCl_3$	I	0.2
$Dy(NO_3)_3 \cdot 5\ H_2O$	I	0.2	$Sc(NO_3)_3 \cdot 5\ H_2O$	I	0.2
$Er(NO_3)_3 \cdot 5\ H_2O$	I	0.2	SeO_2	I	0.2
$Eu(NO_3)_3 \cdot 6\ H_2O$	I	0.2	$Si(OC_2H_5)_4$	I	0.2
$Fe(NO_3)_3 \cdot 9\ H_2O$	I	0.2	$Sm(NO_3)_3 \cdot 6\ H_2O$	I	0.2
$Fe(NO_3)_3 \cdot 9\ H_2O$[b]	I	1	$Sn[OCH(CH_3)_2]_4$	I	0.2
$Ga(NO_3)_3 \cdot xH_2O$	I	0.2	$Ta(OC_2H_5)_5$	I	0.2
$Gd(NO_3)_3 \cdot 6H_2O$	I	0.2	$Tb(NO_3)_3 \cdot x\ H_2O$	I	0.2
$Ge[OCH(CH_3)_2]_4$	I	0.2	$TeCl_4$	I	0.2
$HfCl_4$	I	0.2	$Ti[OCH(CH_3)_2]_4$	I	0.2
$Ho(NO_3)_3 \cdot 5\ H_2O$	I	0.2	$Tm(NO_3)_3 \cdot 6\ H_2O$	I	0.2
$In(NO_3)_3 \cdot 5\ H_2O$	I	0.2	$OV[OCH(CH_3)_2]_3$	I	1
$IrCl_3$	W	0.2	$W[OCH(CH_3)_2]_6$	I	0.2
KNO_3	I	0.2	$Y(NO_3)_3 \cdot 6\ H_2O$	I	0.2
$La(NO_3)_3$	I	0.2	$Yb(NO_3)_3 \cdot x\ H_2O$	I	0.2
LiNO3	I	0.2	$Zn(NO_3)_2 \cdot 4\ H_2O$	I	0.2
$Lu(NO_3)_3 \cdot xH_2O$	I	0.2	$ZrO(NO_3)_2 \cdot x\ H_2O$	I	0.2
$Mg(NO_3)_2 \cdot 6H_2O$	I	0.2			

[I] Isopropanol

[W] Water

[a] Used to synthesize library 16

[b] Used to synthesize library 15

3.2 Libraries preparation

3.2.1 Soot coated library preparation

The catalysts powders obtained from calcination were grounded in HPLC-vials and manually transferred into the 206 hexagonally positioned wells in the library plate. The soot paste which was later coated on powder catalyst library was prepared according to the recipe given by our industrial partner. The paste was prepared as follows: nine milligram of soot (Printex U) was mixed with 60 ml of water in a glass beaker. 50.96 ml of isopropanol was added to the mixture which was continuously stirred with a magnetic stirrer. Finally 0.9 ml of polyxyethylen 20 sorbitan monolaurate (Tween 20) was added in the mixture. Polyxyethylen 20 sorbitan monolaurate was added to increase the adhesive property of soot. However it also increases the hydrocarbon content in soot. Increase hydrocarbon content in soot is known to have a positive effect on the soot oxidation temperature because hydrocarbons are more easily oxidized than soot. The suspension was further stirred for 1 h. Before the commencement of the coating process, the library was first wetted with isopropanol to prevent the powder from being scattered during the process. A commercial air brush from Satagraph Corporation which was attached to an Aspera T2134A 103BC01 compressor was used to coat a soot film on the library. Each library was sprayed for 5 min. The library covered with a soot film was dried at 60 °C for 6 h and later at 120 °C for 3 h to cause the evaporation of isopropanol and water. The dried library was later screened in an IR-thermographic experiment.

3.2.2 Preparation of Soot-catalyst mixtures libraries

8 mg of catalyst powder was added in 2 mg of soot in an HPLC-vial. The mixture was loosely stirred with a spatula for 2 min in order to achieve a loose soot-catalyst contact. The mixture was transferred in the 206 hexagonally positioned wells in the library plate. Care was taken to ensure equal filling heights of the soot-catalyst mixtures in the wells.

3.3 Conventional Syntheses of catalysts

3.3.1 Cobalt (II)-propionate

The synthesis of cobalt (II)-propionate was based on a recipe given by J. Saalfrank in his dissertation [176]. 10g (84.1 mmol) of cobalt carbonate and 150 ml (2 mol) of propionic acid were mixed in a 250 ml round bottom glass flask. The flask was equipped with a magnetic stirrer and connected to a reflux condenser. The mixture was boiled in an oil bath at 150 °C for 4 h. After the mixture was a little cooled, it was filtered by a filter paper to separate the un-dissolved $CoCO_3$. Propionic acid was distilled from the mixture by rotating evaporator at 50 °C and 30 mbar. The achieved red paste was dried under vacuum for several hours at room temperature. Elemental analysis (CHN-analysis) was conducted on the sample to determine its composition. The results are given in Table 3.4

	C	H	N
Theoritical composition (%)	35.14	4.91	
Measured composition (%)	35.55	5.09	0.06

Table 3.4 Elemental analysis of cobalt (II)-propionate.

3.3.2 Manganese (II)-propionate

The synthesis of manganese (II)-propionate followed the method described in detail by J. Saalfrank [176]. 10g (39.8 mmol) of $Mn(NO_3)_2 \cdot 4H_2O$ and 150 ml (2 mol) of propionic acid were mixed in a 250 ml round bottom glass flask. The flask was equipped with a magnetic stirrer and connected to a reflux condenser. The mixture was boiled in an oil bath at 150 °C for 1 h, after which, the reflux condenser was detached from the mixture. The open mixture was further boiled at the same temperature. In the course of boiling in an open glass flask, propionic acid was added to replace the propionic acid that evaporated. After the colour of the solution changed from dark brown to light brown, propionic acid was distilled from the mixture using a rotating evaporator at 50 °C and 30 mbar. The achieved brownish paste was dried at 130 °C in an oven.

3.3.3 Catalysts based on Co and Mn

The same recipe was applied to syntheses mixed oxides based on cobalt and manganese as already indicated under high-throughput syntheses. The synthesis of La_3Co_{97} will be used to demonstrate the synthesis procedure. 4-Hydroxyl-4-methyl-2-pentanone (1.86 ml) and methanol (3.78 ml) were placed in a 20 ml vial. Furthermore, 4.85 ml of a 1 M Cobalt propionate solution in methanol, 1.5 ml of a 0.1 M lanthanum nitrate solution in methanol were added while stirring. The resulting solution was stirred for 1 hour, to obtain a homogeneous sol and dried for 5 days at room temperature for gelation. Subsequently the gel was heated (heating rate of 1°C /min) to 400 °C, calcined there for 5 h and later cooled to 30 °C at a cooling rate of 2 °C/min.

3.3.4 Catalysts based on Ce

The recipe used to syntheses catalysts based on cerium has been given earlier under the HT-synthesis. Based on this recipe, 5mmol of K_3Ce_{97} catalyst was synthesized as follows. 4-hydroxyl-4-methyl-2-pentanone (1.86ml) was placed in a 20 ml vial. To this solution, a 4.85 ml of a 1 M cerium nitrate solution in methanol and 1.5 ml of a 0.1 M potassium nitrate solution in distilled water were added while stirring. Finally 7.48 µl of propionic acid was added. The resulting solution was stirred for 1 hour, to obtain a homogeneous sol. Later the sol was dried for 5 days at 40 °C for gelation. Successively, the gel was calcined in an oven at 400 °C, using a heating rate of 0.2 °C/min and kept at this temperature for 5h.

3.3.5 Synthesis of $Cs_2V_1Fe_2/Al_2O_3$ based on the impregnation method

The sample was prepared based on the method applied by G. Neri et al. [20]. An α-Al_2O_3 powder was impregnated with an aqueous solution of inorganic salts. For example 10 mmol of sample was prepared by dissolving 233.96 mg of NH_4VO_3, 648 mg of $FeCl_3$, and 673.44 mg of CsCl in distilled water. The mixture was thoroughly mixed with a stirrer for I h, after which, 1555.4 mg of α-Al_2O_3 was added in the mixture. The suspension was heated at 80 °C under stirring for 1 h, dried at 105 °C for 2 h. Finally the powder was calcined at 400 °C under static air for 4 h.

3.3.6 Catalyst based on Al

The same recipe given under the HT syntheses section for the synthesis of materials based on aluminium oxide was used here with little modification. For example the synthesis of $Cu_{20}V_{10}Fe_{20}Al_{50}$ was as follows: 1.85 ml (15 mmol) of 4-hydroxyl-4-methyl-2-pentanone was dispensed in a 100 ml glass beaker. While stirring, 20 ml of 2-propanol was added in the beaker. 1 ml (1mmol) of a 1 M iron nitrate solution was added. Furthermore, 0.5 ml (0.5 mmol) of a 1 M solution of vanadium (V) oxy tri-isopropoxide was added. To the mixture, 2.5 ml (2.5mmol) of a 1 M solution of aluminium butylate was added. Successively, 0.9 ml (5 mmol) of distilled water and 10.95 µl (0.3 mmol) of concentrated hydrochloric acid were added dropwise. The mixture was further stirred for 2 h and dried at room temperature for 3 days. The powder obtained was calcined using the temperature programme shown below.

$$RT \xrightarrow{0.5\ ^\circ C/min} 250^\circ C\ (5\ h) \xrightarrow{0.5\ ^\circ C/min} 400^\circ C\ (5\ h) \xrightarrow{2^\circ C/min} RT$$

3.4 High-throughput library screening

3.4.1 Experimental setup for IR-Thermography

The emissivity-corrected IR-thermography was applied for the parallel screening of the catalytic activity of powder catalysts. The flow diagram of the experimental setup is given in Figure 3. 1. The setup can be divided into three sections, namely: gas-dosing section, catalytic activity detection section, and system control and data acquisition. The gas dosing section consists of stainless steel pipe-lines and mass flow controllers. The mass flow controllers from the company MKS were used to dose the reactant gas in the reactor. The detection section consisted of an IR-camera and the reactor. The IR-camera used for the parallel detection of the heat of reaction was from the company Thermosensorik Corp. This camera was equipped with a 640*480 pixel PtSi-FPA detector. The Pt-silizide detector used here was very important especially for calibration which requires stable IR-detector. It is important to mention that the pixel signals of Li-antimonite or MCT-detector based cameras tend to drift, which can falsify the calibration procedure needed to determine small temperature changes. The camera was mounted on a stand directly above the IR-reactor. The IR-reactor containing the catalyst library was closed with a Sapphire glass which is transparent to infrared radiation (electromagnetic spectrum range between 0.17-6 µm). Section three consist of mass flow

regulator and magnetic valve regulator, as well as and a computer for the entire system control and data acquisition.

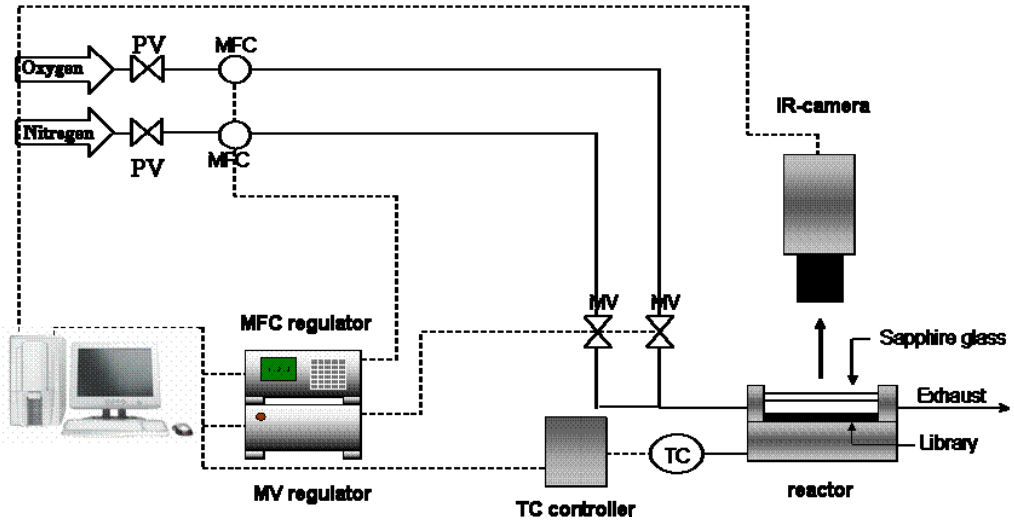

Figure 3.1 Flow sheet of the IR-thermography setup. PV = plug valve, MFC = mass flow controller, TC = thermocouple and MV = magnetic valve.

Shown in Figure 3.2 a and b is the representative cross section of the reactor highlighting the gas inlet (5) and gas outlet (12) respectively. The reactor made from steel has a large opening where the library is placed during the experiment. Furthermore, the reactor has a heating plate beneath the reaction chamber (3). This arrangement ensures an isothermal temperature distribution across the library during reactions. A thermocouple connected to the reactor is used to adjust the reactor temperature. Generally, the temperature profile will affect not only the chemical reaction but also adsorption, desorption and transport mechanisms. The balanced reactor equations could be made easier if isothermal conditions are achieved. Eight holes (5) drilled on the upper part of the reactor block, are used to transport the reactant gas stream to the reaction chamber. The actual dosing of the reactant gas to the reaction chamber is through a steel ring with evenly distributed holes (diameter = 0.5 mm) around the ring. The reaction product leaves the reaction chamber through a central hole on the library and finally leaves the reactor through one effluent gas (12) drill at the lower part of the reactor. A full description of the reactor was also given elsewhere [177].

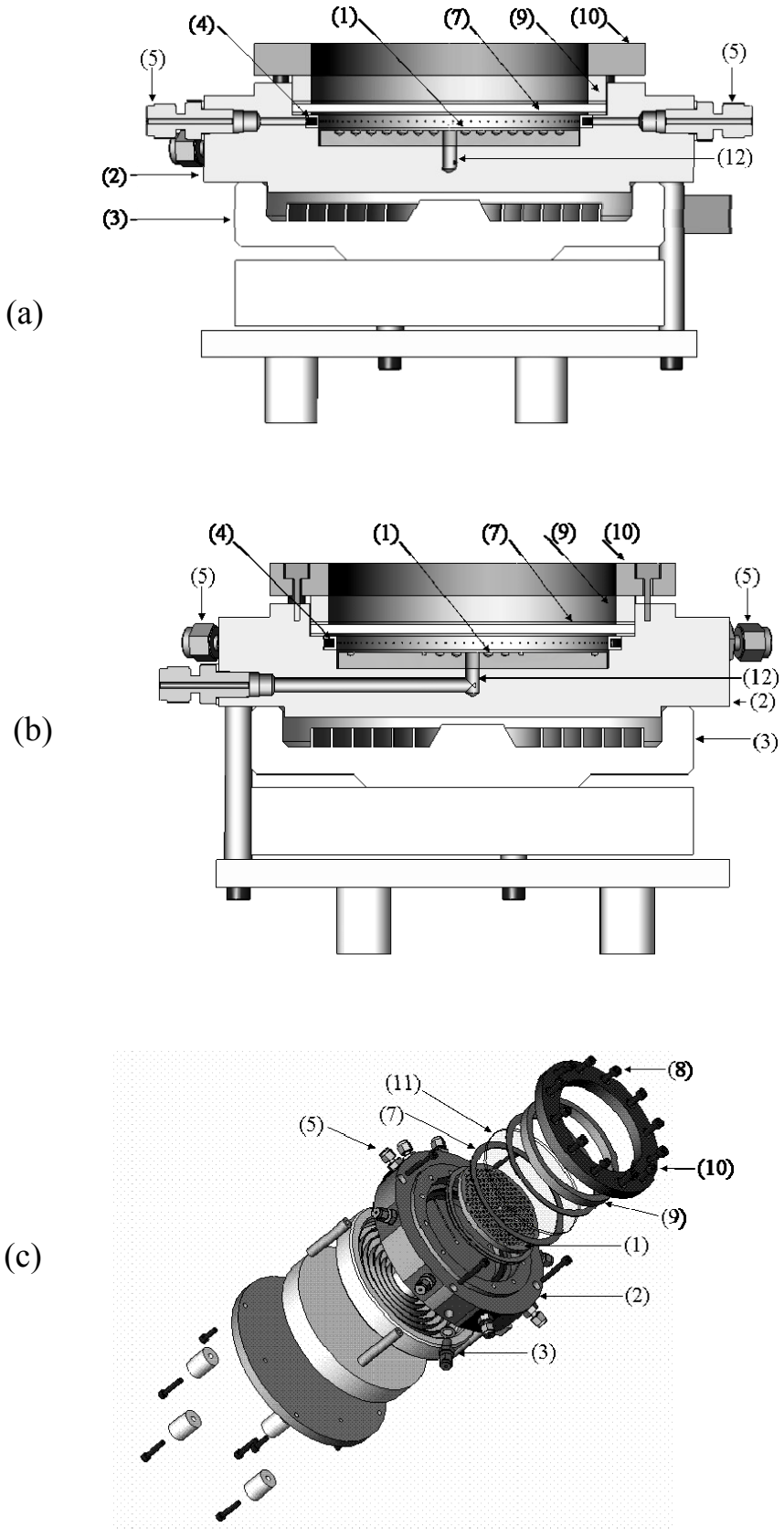

Figure3.2 Cross section of the IR-thermography reactor, a and b showing gas inlet and outlet respectively, c is the explosive diagram of the reactor.

3.4.2 Experimental procedure

IR-thermography was deployed to screen for catalytic activity of mixed oxides for the oxidation of soot by synthetic air. The catalyst library filled with sample powders was mounted in the IR-reactor. In some cases, the library was first coated with a soot film before introduction into the reactor (see 3.3). The high-throughput process was completely automated, controlled by the TestRig software. Before the high-throughput screening, the screening conditions and sequence was defined in the Testrig software as shown in one of the used protocols below (Table 3.5). The important steps are summarised here. Initially, the library is heated to the desired temperature under 50 ml/min nitrogen flow. The temperature is set to a temperature which is 4 °C below the desired reaction temperature and six point calibration started. During the calibration, the emissivity of the samples in the library as well as the detector sensitivity are measured between 4 °C below and 6 °C above the reaction temperature. The temperature difference between two each two measurements is 2 °C. Throughout the calibration process, a constant nitrogen flow of 50 ml/min is maintained. The measured detector sensitivity and samples emissivity, are used to correct the detector sensivity and samples emissivity at the desired reaction temperature. After calibration, the reaction temperature is adjusted to the desired temperature and an IR image of the library is taken. This image is subtracted as the background image from the subsequent images.

Nr.	Instrument	Befehl	Parameter	Nr.	Instrument	Befehl	Parameter
1	Start	(invalid)	(invalid)	20	Heizung	Temperatur	256
2	Gas	Mixtur	Stickstoff,100	21	IRCam	6.Calibration	256
3	Heizung	Temperatur	150	22	Heizung	Temperatur	250
4	Utilities	Warten	30min	23	Utilities	Warten	30min
5	Heizung	Temperatur	250	24	IRCam	Dateinamen	background-1
6	Utilities	Warten	30min	25	IRCam	Integrieren	1000
7	IRCam	Verzeichnis	D:\Daten	26	Gas	Mixtur	Synluft,100
8	IRCam	Dateinamen	250DegC	27	Utilities	Warten	1min30
9	IRCam	Integrationszeit	0.1	28	IRCam	Dateinamen	2min
10	Heizung	Temperatur	246	29	IRCam	Integrieren	1000
11	IRCam	1.Calibration	246	30	Utilities	Warten	2min30
12	Heizung	Temperatur	248	31	IRCam	Dateinamen	5min
13	IRCam	2.Calibration	248	32	IRCam	Integrieren	1000
14	Heizung	Temperatur	250	33	Gas	Mixtur	Stickstoff,100
15	IRCam	3.Calibration	250	34	IRCam	Dateinamen	Nachtbild
16	Heizung	Temperatur	252	35	IRCam	Integrieren	1000
17	IRCam	4.Calibration	252	36	Gas	Mixtur	Stickstoff,60
18	Heizung	Temperatur	254	37	Heizung	Temperatur	30
19	IRCam	5.Calibration	254	38	END	Gas	Stickstoff,0

Table 3.5 An example of the IR-thermographic experimental protocol

Before the start of the reaction measurement, the gas flow is switched to synthetic air at a flow rate of 50 ml/min. The first reaction IR image of the library is taken after 2 min reaction time. Subsequent images are taken after 5, 10, 15, 20, and 30 minute. After this measurement, the gas flow is again switched to nitrogen and an IR image of the library taken, which was used to check possible sample emissivity changes after reaction. The same procedure is repeated at different temperatures (200-, 250-, 300- and 400 °C). The temperature increase of each sample in the IR image is quantified by the TestRig software. The temperature of each sample was standardized by relating it to the sample with highest temperature increase on the plate.

3.5 Conventional Experiment

3.5.1 Thermogravimetric analysis

The lead materials from the high-throughput experiments were prepared conventionally and their catalytic activities were verified using a Shimadzu TGA-50 thermogravimetric analyser. A picture of the used TGA device is given in Figure 3.3. Basically, the TGA consists of an oven where the heating of the sample is performed, a balance for the measurement of the weight change, a mass flow controller for gas dosing and an attached computer for system control and data acquisition.

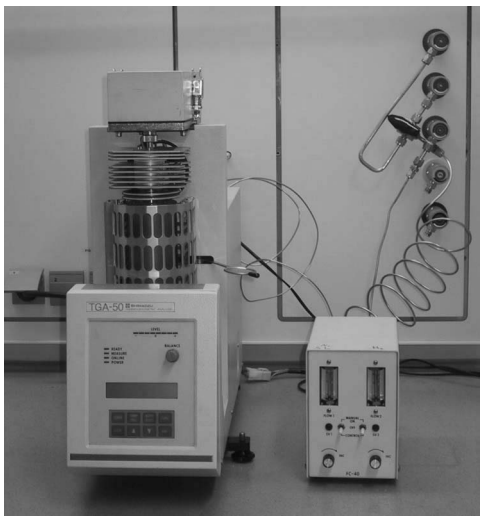

Figure 3.3 A picture of the used thermogravimetric analyser (Schmadzu T50)

Prior to the thermogravimetry analysis, a separate sample of each conventionally prepared catalyst material has been heated at a heating rate of 10 °C/min to 700 °C under 50 ml/min nitrogen flow to identify potential material`s specific weight changes that may mask the TGA signal resulting from soot oxidation. This was important since most catalysts were calcined at 400 °C and residual organics may still be present. However some of the catalysts, especially at the initial state of this work were not subjected to this pre-treatment procedure because 400 °C was assumed to be enough to burn off the hydrocarbons. After the pre-conditioning step, 3 mg of soot were mixed loosely (as in most HT-experiments) with 12 mg of catalyst in a GC vial with a spatula before being transferred to the TGA crucible. In some cases a catalyst-soot weight ratio of 20:5 was applied. This mixing ensured a loose soot-catalyst contact. The mixture was heated from 25 °C to 700 °C at a heating rate of 10 °C/min in a 50 ml/min synthetic air flow. The activity of a catalyst is defined by the combustion temperature, which is the temperature of the TGA curve where 50 % (T_{50}) of the soot is oxidised. To verify the reproducibility of the results, several TGA experiments were conducted at least twice, where the mixture with the soot was not taken from the same batch, but prepared individually.

3.5.2 Tight contact sample preparations and testing

The tight catalyst-soot samples were prepared my mixing a 4:1 weight ratio of catalyst and soot initially with a spatula. The mixture was later thoroughly mixed in a ball mill for ten minutes. The obtain mixture was pressed to a tablet by applying a pressure of 50 bar using a hydraulic press from Enerpac Corporation. The tablet was ground manually and the obtained powder was subjected to a temperature ramp of 10 °C/min from room temperature to 700 °C in the TGA equipment.

3.5.3 Fix bed reactor

The activities of two best catalysts were verified in a fix bed reactor. A simplified flow scheme of the used laboratory plant is given in Figure 3.4 below. The set-up can be divided into three main parts: gas dosing, fix bed reactor and data acquisition. The main part of the plant is the fix bed reactor made from Duran glass (L = 39.2 cm, $Ø_i$ = 1.3 cm) which is placed inside a heating mantle during the experiment. The heating mantle controlled by a thermocouple was used to heat the reactor. The catalyst is held in place by a frit inside the reactor. The necessary gases (N_2, synthetic air and 4000 ppm NO in N_2) are dosed by mass

flow controllers from the company Bronkhorst Hi-Tech. A three way valve was used to control the direction of circulation of the reactant gas into the reactor or through the by-pass pipe-line. A thermocouple used to measure the catalyst bed temperature was connected to the bed via a T-piece at the top of the reactor. The effluent gas from the reactor is analysed by CO and CO_2 gas special sensors from the company GFG. The CO and CO_2 gas sensors were equipped with an infrared measuring cell of type IR24.

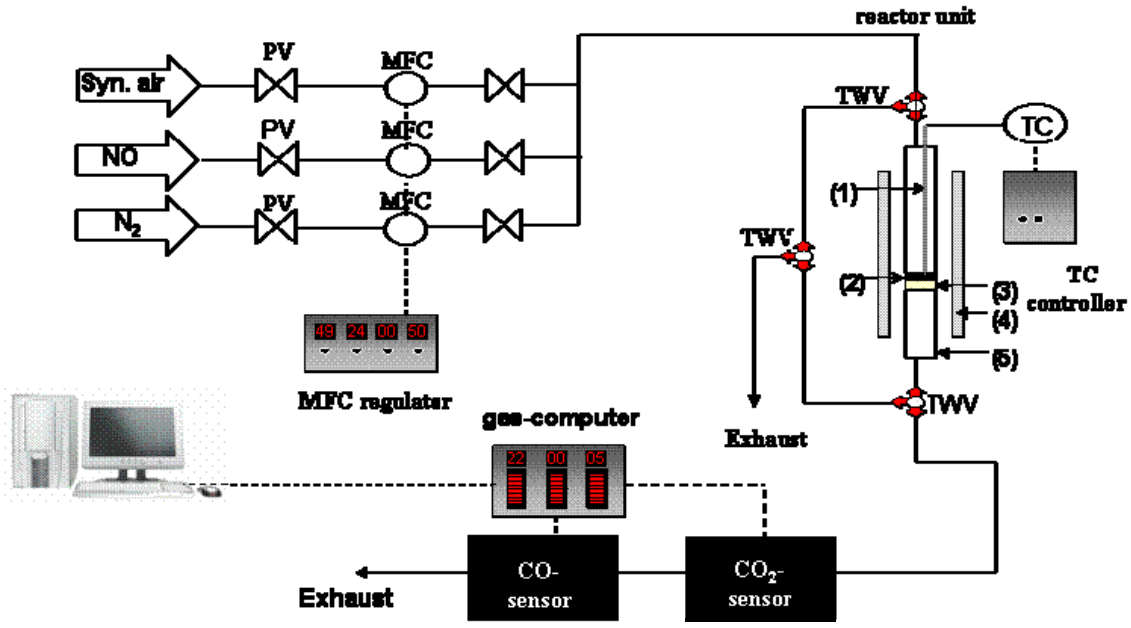

Figure 3.4 Scheme of the flow reactor equipment. (PV = plug valve, MFC = mass flow controller, TC = thermocouple, TWV = three way valve)

3.5.4 Experimental procedure

In every experiment, 90 mg of catalyst with a particle size of 100-200 µm was dispersed into the reactor tube. The reactor was placed in the experimental setup, connected to the rest of the setup and a thermocouple was placed at the catalyst bed. The catalyst was in-situ activated at 300 °C with 100 ml/min synthetic air for 1 h. After cooling, the activated catalyst was dispersed in a crucible and mixed with 10 mg of soot using a spatula. The catalyst-soot mixture was reloaded in the reactor which was then mounted again with the rest of the setup. The reactor temperature was increased to 200 °C. The reactant gas used to calibrate the sensors was passed via the bypass line while the reactor temperature was allowed to

equilibrate. After the set temperature was reached, the reactant gas (100 ml/min) flow was switched from by-pass to the reactor. 10 min was allowed to enable the gas flow to stabilise. The reactor was further heated from 200 to 500 °C at a heating rate of 2 °C/min while the composition of the product gas stream was manually registered from the sensors` readings at predefined time intervals. The same experimental procedure was applied for different reactant gas compositions. The reactant gas compositions used are summarised in Table3.6.

Gas mixture	O_2 [Vol.-%]	N_2 [Vol. %]	NO [Vol.%]
1	10	90	
2	10	89.8	0.2

Table 3.6 Scheme of gas composition used in the flow reactor experiments

3.5.5 Selective oxidation of 2-heptanol

Custom made round-bottom two-neck glass flask reactor was applied for the selective oxidation of 2-heptanol to 2-heptanone. Figure 3.5 represent the used setup. One of the openings on the reactor was connected to a reflux condenser, while the other opening was used to dose oxygen in the reactor. The reactor was heated by an oil bath which was placed on a magnetic stirrer/heating plate. A magnetic stirrer placed in the reactor was used to homogenise the reaction mixture. The reaction procedure was as follows: a mixture of 2-heptanol (690 µl), 200 mg of catalyst and a magnetic stirrer were charged in the reactor. The reactor was connected to the reflux condenser and placed in an oil bath, which was preheated to a certain temperature. The temperature of the reactor was allowed to equilibrate for 10 min, after which, 10 ml/min of molecular oxygen was bubbled into the reaction mixture through a mass flow controller.

Samples were withdrawn from the reaction mixture at appropriate time intervals (1h, 1.5h, 2h, and 3h), diluted with acetone and centrifuged at a rate of 4000 U/min for 10 min. The reaction

product was later separated from the catalyst by carefully pipetting the liquid suspending on the catalyst. The obtained sample was further diluted with a 50:1 volume ratio of acetone to prevent detector saturation, analysed with a GC-MS system. The GC-MS measurements were done with the aid of Mrs Höltzen. In some reactions 6.9 ml of toluene was added in the reaction mixture to act as a solvent. Also to simulate reaction under water free condition, the 2-heptanol used was dried with 1 g molecular sieve (3Å), added in the reaction mixture for one day before the reaction.

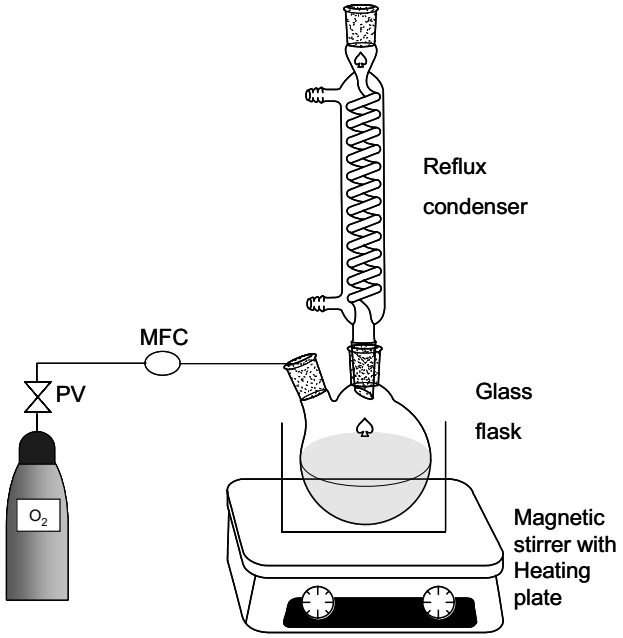

Figure 3.5 Scheme of the setup used for the selective oxidation of alcohol. (PV = plug valve, MFC = mass flow controller)

3.6 Catalyst characterisation

3.6.1 X-Ray diffraction

X-Ray diffractometry is a technique used for determining the atomic structure and the crystallinity of a solid crystalline material. This technique involves the beaming of monochromatic x-ray on a lattice. The reported X-ray patterns in this work were performed with a Huber G670 Guinier camera using Cu $K\alpha_1$ radiation (λ=1.54056Å) in the range of 2 Θ = 4° - 100°. Before the analysis, the catalyst sample was ground to fine powder and coated on a sellotape slat. Lattice parameter refinement was done by full pattern Rietveld refinement

with the program TOPAS [170] using the fundamental parameters approach [171] with the aid of K. Stöwe.

3.6.2 Transmission electron microscopy / Energy dispersive x-ray analysis

A transmission electron microscope from Jeol Corporation of type JEOL JEM-2011 (LaB6 emitter, 200kV accelerator voltage) was used to characterise the catalysts. An EDX-analyser with SiLi-detector from the Oxford Instrument coupled to the TEM was applied to analyse points on the TEM image. For the analysis, fine particles catalyst powder is suspended in methanol. A copper grid (400 mesh, Ø = 3 mm) coated with carbon is deep in to the solution and later subjected to an electron beam. The measurements were realised with the help of J. Schmauch from the technical physics department.

3.6.3 Physisorption measurement

The method of low temperature N_2 adsorption is used to determine the pore volume, pore radius distribution and the surface area of a solid sample under the assumption of different models. The BET surface areas and the pore radius of the lead catalysts were determined by physisorption measurements after calcinations but prior to reaction. The equipment used was of type Carlo Erba Soptomatic 1990 from Fisons Instrument Corporation. These measurements were realized with the help of R. Nagel and C. Thome. Prior to the measurement, the sample contained in the burrette was heated at 200 °C and evacuated overnight until a vacuum of about 1 mPa is reached. After evacuation, the burrette was cooled by liquid nitrogen to -196 °C and the measurement started. During the measurement, the burrette pressure is increased up to the environmental pressure while the adsorption data are recorded. Subsequently, the pressure in the burrette was decreased down to 300 Torr while the desorption data are recorded. The specific surface are was calculated based on the BET-method. The pore radius distribution for mesoporous materials are calculated based on the BJH-method while that of microporous materials was calculated based on the Horvath-Kawazoe.

4 Summary and Conclusion

The main objective of this work was to discover and improve new catalysts for the combustion of soot preferentially with low or no noble metal. Diesel soot is one of the major environmental pollutants especially in the developed world where the number of cars running on diesel engine is tremendously on the raise. While engine modification was enough to allow diesel cars pass the previous legislation such as Euro 3, it is clear that such modifications are not enough to allow the certification of future diesel cars. The automobile industries are now concentrating their efforts in developing after-treatment systems. The most promising approach in eradicating diesel soot from diesel exhaust emission is the application of particulate filters that trap the soot from the exhaust. Though the particulate filter have offered a break-through in trapping diesel soot, it comes at a price because the trapped soot increases the filter back pressure which concomitantly leads to an increase in fuel consumption. A clever way of preventing filter plugging is to apply oxidation catalyst on the filter system that will allow the regeneration of the filter at temperatures attainable in the exhaust.

Our objective was to search for noble metal free diesel soot oxidation catalyst by established technologies of combinatorial heterogeneous catalysis. According to the literature, the basic oxides CoO_x, CeO_x, and MnO_x show catalytic activity for soot oxidation and were selected as starting point for this investigation. The search strategy adopted here was that of variation, selection, and optimization. Variation was obtained by doping the based oxides given above with 50 different metal ions and composition spread of the binary and ternary mixed oxides. The catalysts were prepared using composition tolerant sol-gel methods to assure identical synthesis procedures for the members of the library. The sol-gel method allows the preparation of polynary mixed metal oxides under mild synthesis conditions with a homogeneous elemental distribution and high surface area. The automated preparation of the mixed oxides was planned with the library design software and performed with the help of a pipetting robot. Selection was through the catalytic activity which was determined through the heat of reaction. The selection process was accomplished through the used of emissivity-corrected IR-thermography which allowed the parallel screening of soot oxidation catalysts. Printex U which is widely believed to possess identical properties as diesel soot was used as model soot in this study.

For the high-throughput screening, two approaches were considered in creating a contact between the catalyst and soot. In method one, catalyst libraries were decorated with a smooth soot film by the used of an air brush. Unfortunately, catalytic combustion was observable be ec-IRT, but the reproducibility was not acceptable. The reason for the failure was due to the difficulties in achieving a uniform soot film on the library and the detection of catalytic activity been made through an unreacted soot film. Method two involved a prior mixing of catalyst and soot before filling in the library well. This method has proven to be quite reliable. All in all about 1400 materials were tested for soot oxidation in 16 libraries in a high-throughput fashion. Among generation one materials, K_3Ce_{97} and Cs_3Co_{97} were found to be very active for the combustion of soot. These samples were capable to decrease the T_{50} values for soot oxidation by 160 °C and 140 °C respectively. The effect of the alkali metal on the activity of the ceria catalyst was successfully verified. The catalysts $Cu_{10}Cs_{20}Co_{70}$, $Cu_3Cs_{20}Co_{70}$, $Ag_{10}Cs_{20}Co_{70}$, and $Pb_{10}La_5Co_{70}$ from the generation 3 samples were found to possess strong soot oxidation activities. These catalysts were able to combust considerable amount of soot below 450 °C. This work has successfully integrated high-throughput methods in the development of soot oxidation catalyst. This success is due to the particular sol-gel synthesis method used and the high sensitivity of the ec-IR-thermography. However, the weighing of the soot and catalyst before introduction in the library wells was time consumptive. Attempts to accelerate this process with the help of a solid dispensing robot were not successful. For future work, in order to explore the true potential of HTE, a precise powder dispensing robot is advisable.

For validation of high-through findings TGA was selected as conventional test equipment. The activities of most of the identified soot oxidation catalysts were successfully reproduced. Our TGA results have shown that the combustion activity of the Zn_3Ce_{97} catalyst depends on the quantity of oxygen present in the reactant gas. It was also observed that the combustion activity of the Cs_3Co_{97} is influenced by the catalyst-soot ratio, whereby the catalytic activity was found to be better at catalyst-soot ratio of 9:1 compared to the ratio at 4:1. A binary composition spread of the KCe and CsCo systems were successfully optimized by a TGA whereby samples with compositions $K_{15}Ce_{85}$ and $Ce_{20}Co_{80}$ were identified as the optimum compositions respectively. One of the most important properties of a good soot combustion catalyst is its ability to maintain its activity over a long period. This condition was successfully verified by performing repeated experiments with the same catalyst. One of the catalysts found to be very stable was the $Cs_{20}Co_{80}$ catalyst. The calcinations temperature is an

important factor that may affect the catalytic properties of a sample. The effect of the calcinations temperature on $Cu_{10}Cs_{20}Co_{70}$ and $Pb_{10}La_5Co_{70}$ were verified at different temperatures. The catalyst $Cu_{10}Cs_{20}Co_{70}$ and $Pb_{10}La_5Co_{70}$ were observed to maintain their high activity even after calcination at 700 °C. In order to accelerate the characterisation of potential soot oxidation catalyst using TGA in future, it would be advisable to use an auto sampling TGA equipment.

The activity of the two catalysts $Cu_{10}Cs_{20}Co_{70}$ and $Pb_{10}La_5Co_{70}$ were further examined in a flow reactor. Interestingly, the strong activities observed during the HTE and TGA experiments were confirmed here also. Experiments conducted in the presence of NO have shown that the $Cu_{10}Cs_{20}Co_{70}$ catalyst soot combustion activity was not affected by nitrogen monoxide presence. On the other hand, the presence of NO was found to have a strong positive effect on catalytic soot combustion. Under this condition $Pb_{10}La_5Co_{70}$ was capable to combust most of the soot at 380 °C which is quiet remarkable. This work has successfully achieved new catalysts formulations that are capable to oxidize soot at a remarkably reduced temperature compared to non catalytic soot combustion. Some of these catalysts were reproduced by our project partner and the activities reported here were confirmed.

Through a rational design of experiments, we were able to achieve improved catalytic activity from one generation to another especially in the case of the Co-based samples. Of crucial importance was the measurement of catalytic activity through the loose catalyst-soot mixture. To the best of my knowledge, no successful application of the high-throughput methodology in the development of soot oxidation catalyst has been reported in the literature so far although the development of diesel soot oxidation catalysts is a hot topic with global dimension. Therefore, the high-throughput technique reported here is a powerful tool specially suited at an early stage of the discovery of low temperature soot oxidation catalysts to narrow down the number of candidate catalysts.

Zusammenfassung und Ausblick

Das Hauptziel dieser Arbeit war die Entdeckung und Verbesserung neuer Katalysatoren für die Verbrennung von Ruß, vorzugsweise mit niedrigem oder keinem Edelmetallgehalt. Dieselruß ist einer der Hauptumweltschadstoffe, besonders in ökonomisch weit entwickelten Ländern, da dort die Zahl der Automobile mit Dieselmotor in den letzten Jahren ungemein zunimmt. Zwar waren Motorenveränderungen ausreichend um vorherige Verordnungen wie Euro 3 zu erfüllen, allerdings ist vorhersehbar, dass solche Veränderungen nicht ausreichend sein werden, um Zulassungen zukünftiger Dieselautos zu erlauben. Die Autoindustrie konzentriert ihre Anstrengungen nun auf die Entwicklung von Nachbehandlungssystemen. Der vielversprechendste Ansatz zur Entfernung von Dieselruß aus Dieselabgasen ist die Verwendung von Partikelfiltern zum Einfangen von Ruß aus Abgasen. Obwohl die Partikelfilter einen Durchbruch in Dieselrußentfernung mit sich brachten, musste dies mit einem Preis bezahlt werden, da der aufgefangene Ruß zur Erhöhung des Filterrückdruckes führt und als begleitender Nebeneffekt zu einem erhöhten Treibstoffverbrauch nachsichzieht.

Ein raffinierter Weg um Filterverstopfung zu verhindern ist die Anwendung von Oxidationskatalysatoren im Filtersystem, die es erlauben werden den Filter zu regenerieren, bei im Abgas erreichbaren Temperaturen.

Unser Ziel war die Suche nach edelmetallfreien Dieselruß-Oxidationskatalysatoren mit etablierten Methoden der kombinatorischen heterogenen Katalyse. Der Literatur nach zeigen die einfachen Oxide CoO_x, CeO_x und MnO_x katalytische Aktivität hinsichtlich der Rußoxidation und wurden als Ausgangspunkt für diese Untersuchung ausgewählt. Die hier übernommene Suchstrategie war die der Variation, Selektion und Optimierung. Variation wurde durch Dotierung der oben genannten Basisoxide mit 50 verschiedenen Metallionen und Kompositionsspreads von binären und ternären Mischoxiden erreicht. Die Katalysatoren wurden durch die Verwendung hinsichtlich der Zusammensetzung toleranten Sol-Gel Methoden dargestellt, um identische Syntheseverfahren für die Bibliothekssubstanzen sicherzustellen. Das Sol-Gel Verfahren erlaubt die Darstellung polynärer gemischter Metalloxide unter milden Synthesebedingungen mit einer homogenen Elementverteilung und großen Oberflächen. Die automatisierte Darstellung der Mischoxide wurde mit einer Bibliothekendesignsoftware geplant und unter zu Hilfenahme eines Pipettierroboters durchgeführt. Selektion erfolgte durch katalytische Aktivität, die durch Bestimmung der Reaktionswärme erfolgte. Das Selektionsverfahren wurde bewältigt durch die Verwendung

von Emmisivitäts korrigierter IR-Thermographie, welche das parallele Screening von Ruß Oxidationskatalysatoren erlaubt. Für das Hochdurchsatz-screening wurden zwei Ansätze betrachtet, um Kontakt zwischen Katalysator und Ruß herzustellen. In Methode Eins wurde eine Airbrushpistole verwendet um die Bibliothek mit einem glatten dünnen Film an Ruß zu überziehen. Unglücklicherweise war zwar die Verbrennung durch ec-IRT beobachtbar, allerdings war die Reproduzierbarkeit nicht akzeptabel. Der Grund für den Misserfolg war auf die Schwierigkeit einen gleichmäßigen Rußfilm auf der Bibliothek zu erhalten und auf die Detektion von Aktivität durch einen nicht reagierten Russfilm hindurch zurückzuführen. Die zweite Methode umfasste das vorherige Mischen von Katalysator und Ruß bevor die in der Bibliothek Wells befüllt wurden. Diese Methode hat sich als recht zuverlässig erwiesen. Insgesamt wurden 1400 Materialien in 16 Bibliotheken auf die Oxidation von Ruß mittels Hochdurchsatz-experimenten untersucht.

Unter den Materialien der ersten Generation stellten sich K_3Ce_{97} und Cs_3Co_{97} als sehr aktiv für die Verbrennung von Ruß heraus. Diese Proben waren in der Lage die T_{50}-Werte bei 160 °C und 140 °C zu verkleinern. Der Effekt des Alkalimetalls auf die Aktivität des auf Cer basierenden Katalysators wurde erfolgreich verifiziert. Die Katalysatoren $Cu_{10}Cs_{20}Co_{70}$, $Cu_3Cs_{20}Co_7$, $Ag_{10}Cs_{20}Co_7$, und $Pb_{10}Cs_{20}Co_7$ der dritten Generation verfügten über große Aktivität bezüglich der Russoxidation. Diese Katalysatoren waren in der Lage beträchtliche Mengen an Ruß unter 450 °C zu verbrennen. Diese Arbeit integrierte erfolgreich Hochdurchsatzsmethoden in die Entwicklung von Katalysatoren zur Rußoxidation. Der Erfolg liegt begründet in der Verwendung der Sol-Gel Methode und der hohen Sensitivität der ec-IR-Thermographie. Allerdings nahm das Wiegen der Katalysatoren und des Rußes sowie Befüllen der Bibliotheken viel Zeit in Anspruch. Versuche diese Prozesse mit Hilfe eines Feststoffdosierungsroboters zu beschleunigen waren nicht erfolgreich. Für zukünftige Arbeiten ist die Verwendung eines präzisen Feststoffdosierroboters ratsam, um das volle Potential von HTE auszuschöpfen.

Zur Validierung der Highthroughput Ergebnisse wurde TGA als konventionelles Testequipment gewählt. Die Aktivitäten der meisten identifizierten Rußoxidationskatalysatoren wurden erfolgreich reproduziert. Unsere TGA Ergebnisse haben gezeigt, dass die Verbrennungsaktivität des Zn_3Ce_{97} Katalysators abhängig von der Menge des im Reaktionsgas befindlichen Sauerstoffes ist. Es wurde ebenfalls beobachtet, dass die Verbrennungsaktivität von dem Ruß : Katalysator Verhältnis beeinflusst wird, wonach sich eine bessere katalytische Aktivität bei einem Katalysator : Ruß Verhältnis von 9:1 feststellen

ließ im Vergleich zu einem Verhältnis von 4:1. Ein binärer Kompositionspread der Systeme KCe und CsCo wurde erfolgreich mittels TGA optimiert, wonach Proben mit den Zusammensetzungen $K_{15}Ce_{85}$ und $Ce_{20}Co_{80}$ als die optimalen Zusammensetzungen in genannter Reihenfolge identifiziert wurden. Eine der wichtigsten Eigenschaften eines Katalysators zur Rußoxidation ist die Beibehaltung seiner katalytischen Aktivität über eine lange Periode hinweg. Diese Auflage wurde durch wiederholte Experimente mit demselben Katalysator bestätigt. Eine der Katalysatoren der sich als besonders stabil erwies war der $Cs_{20}Co_{80}$ Katalysator. Die Kalzinierungstemperatur ist ein wichtiger Faktor, der die katalytischen Eigenschaften einer Probe beeinflussen kann. Der Effekt der Kalzinierungstemperatur auf $Cu_{10}Cs_{20}Co_{70}$ und $Pb_{10}La_5Co_{70}$ wurden bei verschiedenen Temperaturen verifiziert. Die Katalysatoren $Cu_{10}Cs_{20}Co_{70}$ und $Pb_{10}La_5Co_{70}$ behielten ihre hohe Aktivität sogar nach Kalzinierung bei 700 °C bei. Zur Beschleunigung der Charakterisierung potentieller Katalysatoren zur Russoxidation wäre es empfehlenswert automatisierte TGA-Apparaturen zu verwenden.

Die Aktivität der zwei Katalysatoren $Cu_{10}Cs_{20}Co_{70}$ und $Pb_{10}La_5Co_{70}$ wurden weiter in einem Strömungsreaktor untersucht. Interessanterweise wurden die hohen Aktivitäten, die während der HTE und TGA-Experimenten beobachtet wurden, auch hier bestätigt. Experimente, die in der Anwesenheit von Stickstoffmonoxid durchgeführt wurden, zeigten, dass die Aktivität der Rußoxidation des $Cu_{10}Cs_{20}Co_{70}$ Katalysators nicht durch die Gegenwart von Stickstoffmonoxid beeinflusst wurde. Andererseits zeigte sich das die Gegenwart zu einem starken positiven Effekt auf die Verbrennung von Ruß führte. Unter diesen Bedingungen war $Pb_{10}La_5Co_{70}$ in der Lage den größten Teil an Ruß bei 380 °C zu verbrennen, was ein sehr beachtliches Ergebnis ist. Diese Arbeit hat erfolgreich zu neuen Katalysatorformulierungen geführt, die in der Lage sind Ruß bei beträchtlich reduzierten Temperaturen zu oxidieren, verglichen mit der nicht-katalytischen Rußverbrennung.

Durch ein rationales Design of Experiment waren wir in der Lage die Aktivitäten von einer Generation zur Nächsten zu verbessern, vor allem im Fall der Co basierten Katalysatoren. Von entscheidender Bedeutung war die Messung von Aktivität in loser Schüttung des Katalysator-Ruß Gemisches. Nach meinem besten Wissen wurde bisher von keiner erfolgreichen Anwendung der Highthroughput Methode zur Entwicklung von Katalysatoren zur Rußoxidation in der Literatur berichtet, obwohl die Entwicklung von Katalysatoren zur Oxidation von Dieselruß ein weltweit bedeutendes Forschungsgebiet ist. Daher ist die hier berichtete Highthroughput Technik ein leistungsfähiges Werkzeug, das besonders geeignet ist

im Anfangsstadium der Entdeckung von Niedrigtemperaturkatalysatoren zur Rußoxidation die Anzahl der in Frage kommenden Katalysatorkandidaten einzuschränken.

5 References

[1] www.Dieselnet.com, accessed in November 2006.

[2] Panorama 2005 Road transport fuels in Europe: the explosion of demand for diesel fuel

[3] G. Oberdörster, Z. Sharp, V. Atudorei, A. Elder, R. Gelein, W. Kreyling, C. Cox Inhal. Toxicol. 16 (2004) 437

[4] B. A. A. Van Setten, M. Makkee, J. A. Moulijn, Catal. Rev. 43 (4) (2001) 489

[5] S. K. Kabin, L. R. Muncrief, M. P. Harold, Catal. Today 96 (2004) 79

[6] E. V. Genc, E. F. Altay, D. Uner, Catal. Today 105 (2005) 537

[7] D. Fino, E. Cauda, G. Saracco, Catal. Today 114 (2006) 31

[8] M. Iwamoto, T. Zengyo, M. A. Hernandez, H. Araki, Appl. Catal. B 17 (1998) 259

[9] A. O. Anunzita, R. A. Beltramone, Z. Juri, Appl. Catal. A. (2004) 1

[10] A. Ueda , M. Haruta, Appl. Catal. B 18 (1998) 115

[11] D. Fino, N. Russo, G. Saracco, J. V. Specchia, J. Catal. 242 (2006) 38

[12] W. F. Maier, Angew. Chem. Int. Ed. 38 (1999) 1216

[13] M. S. P. Kahandawala, J. L. Graham, S. S. Sidhu, Fuel, (2004) 1829

[14] J. Zhu, K. O. Lee, M. Y. Choi, Proc. Com. Inst. (2005) 2781

[15] S. Tosaka, Y. Fujiwara, JSAE Review, 21 (2000) 463

[16] D. B. Kittelson, J. Aerosol. Sci. 29 (1998) 575

[17] J. H. Johnson, S. T. Bagley, L. D. Gratz, D. G. Leddy, SAE Techn. Papers (1994) 940233

[18] M. Masoudi, SAE Techn. Papers (2005) 2005-01-0971

[19] C. A. Querini, L. M. Cornaglia, M. A. Ulla, E. E. Miro, Appl. Catal. B 20 (1999) 165

[20] G. Neri, G. Rizzo, S. Galvagno, A. Donato, M. G. Musolino, R. Pietropaolo Appl. Catal. B 42 (2003) 381

[21] J. Oi-Uchisawa, A. Obuchi, S. Wang, T. Nanba, A. Ohi Appl. Catal. B 42 (2003) 117

[22] M. R. Kim, D. H. Kim, S. I. Woo, Appl. Catal. B 45 (2003) 269

[23] N. F. Galdeano, A. L. Carrascull, M. I. Ponzi, I. D. Lick, E. N. Ponzi, Thermochimica Acta 421 (2004) 117

[24] C. Badini, G. Saracco, V. Specchia, Catal. Lett. 55 (1998) 201

[25] B. A. A. van Setten, J. M. Schouten, M. Makkee, J. A. Moulijn 28 (2000) 253

[26] S. Kureti, K. Hizbullah, W. Weisweiler Chem. Eng. Technol. 26 (2003) 9

[27] I. C. L. Leocadio, S. Braun, M. Schmal, J. Catal. 223 (2004) 114

[28] J. P. A. Neeft, M. Makkee, J. A. Moulijn Appl. Catal. B 8 (1996) 57

[29] A. Setiadudi, M. Makkee, J. A. Moulijn, Appl. Catal. B 42 (2003) 35

[30] M. V. Twigg, Appl. Earth Sci. 114 (2005) 159

[31] K. Tikhomirov, O. Kröcher, M. Elsener, A. Wokaum, Appl. Catal. B 64 (2006) 72

[32] K. Villani, C. E. E. Kirschhock, D. Liang, G. van Tendeloo, J. A. Martens, Angew. Chem. Int. Ed. 45 (2006) 3106

[33] J. P. A. Neeft, O. P. van Pruissen, M. Makkee, Appl. Catal. B 12 (1997) 21

[34] J. P. A. Neeft, M. Makkee, J. M. Moulijn, Fuel 77 (3) (1998)111

[35] P. G. Harrison, I. K. Ball, W. Daniell, P. Lukinskas, M. Cespedes, E. Miro, M. A. Ulla, Chem. Eng. J. 95 (2003)

[36] D. Fino, V. Specchia, Chem. Eng. Sci. 59 (2004) 4825

[37] H. An, C. Kilroy, P. J. McGinn, Catal. Today 98 (2004) 423

[38] H. An, P. J. McGinn, Appl. Catal. B 62 (2006) 46

[39] V. G. Milt, M. L. Pissarello, E. E. Miro, C. A. Querini, Appl. Catal. B 41 (2003) 397

[40] G. Neri, G. Rizzo, S. Galvagno, A. Donato, M. G. Mugolino, R. Pietropaolo, Thermochim Acta 381 (2002) 165

[41] www.jmcatalysts.com

[42] R. Allansson, C. Görrsmann, M. Lavenius, P. R. Phillips, A. J. Uusimaki, A. P. Walker, SAE Technical Paper, (2004) 2004-01-0072

[43] A. Shoji, S. Kamoshita, T. Watanabe, T. Tanaka, M. Yabe, SAE Techn. Papers (2004) 2004-01-0579

[44] H. Toorisaka, H. Narita, J. Minamikawa, T. Muramatsu, T. Kominami, T. Sone, SAE Technical Papers (2004) 2004-01-0824

[45] O. Salvat, P. Marez, G. Belot, SAE Paper (2000) 2000-01-0473

[46] N. Jeuland, J. B. Dementhon, J. C. Momique, G. Belot, D. Bruchet SAE Techn. Papers (2004) 2004-01-0073

[47] M. Astarita, F.E. Corcione, B. M. Vaglieco, Experimental Thermal and Fluid Sci. 21 (2000) 142

[48] A. Yezerets, N. W. Currier, H. A. Eadler, SAE Techn. Papers (2003) 2003-01-0833

[49] C. Setzer, W. Schütz, F. Schüth, In. Proceedings 10th International Congress on Catal. Budapest, Hungary, Amsterdam, Elsevier, (1993) 2629

[50] C. A. Querini, L. M. Cornaglia, M. A. Ulla, E. E. Miro, Catal. Today 53 (1999) 631

[51] C. A. Querini, L. M. Cornaglia, M. A. Ulla, E. E. Miro, Stud. Surf. Sci. Catal. 130 (2000) 731

[52] E. Baumgarten, A. Schuck, Appl. Catal. 37 (1988) 247

[53] B. J. Cooper, J. E. Thoss, SAE Techn. Papers (1989) 890404

[54] G. Mul, F. Kapteijn, C. Doornkamp, J. A. Moulijn

[55] P. Denton, H. Praliaud, M. Primet, J. Catal. 189 (2000) 410

[56] K. Hirata, N. Masaki, H. Ueno, H. Akagawa SAE Techn. Papers (2005) 2005-01-1860

[57] A. Solla; SAE Techn. Papers (2005) 2005-01-1856

[58] N. Takahashi, H. Shinjoh, T. Suzuki, K. Yamazaki, K. Yokota, N. Miyoshi, Catal. Today 27 (1996) 63.

[59] S. S. Mulla, N. Chen, L. Cumaranatung, G. E. Blau, D. Y. Zemlyanov, W. N. Delgass W. S. Epling, F. H. Ribeiro 241 (2006) 389

[60] A. P Walzer, R. Allansson, P.G. Blakeman, M. Lavenius, S. Erkfeld, H. Landalv, B. Ball, P. Harrod, D. Manning SAE Techn. Papers (2003) 2003-01-0778

[61] A. Hinz, T. Jarvis, L. Andersson, B. Otterholm, R. Allansson, A. P. Walker, J. W. Geyer, K. Narasaki, K J. Wiemers SAE Techn. Paper (2006) 2006-01-0421

[62] W.F. Shangguan, Y. Teraoka, S. Kagawa, Appl. Catal. B 12 (1997)237

[63] Y. Teraoka, K. Kanada, S. Kagawa, Appl. Catal. B 34 (2001) 73

[64] S. Kureti, W. Weisweiler, K. Hizbullah, Chem. Eng. Technol. 25 (2002) 140

[65] R. Domesle, H. Klein, T. Kreuzer, E. Lox,US Patent 6685900 (2004)

[66] M. Heruichi, T. Mokomizo, US Patent 5911961 (1999)

[67] I. Hachisuka, US Patent 7056859 (2006)

[68] M. Shinzawa, Y. Murofushi, US Patent 5855854 (1999)

[69] C.-B. Lim, C.-H. Pak, J.-H. Cho, US Patent 6265342 (2001)

[70] T. Takemoto, K. Okamoto, H. Yamada, H. Murakami, T. Shimizu, US 6090744 (2000)

[71] M. V. Twigg, A. J. J. Wilkins, N. S. Will US Patent 6294141 (2001)

[72] W. Zhang, US Patent 6764664 (2004)

[73] M. M. Hartwig, US Patent 4510265 (1985)

[74] Z. Dang, Y. Huang, A. Bar-llan, US Patent 6613299 (2003)

[75] R. P. Ziebarth, R. T. Nilsson, US Patent Appl. 20060018806

[76] H. Tanada, O. Nakayama, K. Iwachido, T. Watanabe, US Patent 6825145 (2003)

[77] I. Manson, US Patent 6248689 (2001)

[78] S. J. Golden, US Patent 6352955 (2002)

[79] R. Domesle, V. Herbert, K. Edgar, P. Hans-Dieter, US Patent 4477417 (1992)

[80] R. Schlögl, Angew. Chem. Int. Ed. 37 (1996) 2333

[81] S. Senkan Angew. Chem. Int. Ed. 40 (2001) 312

[82] J. J. Hanak, J. Mater. Sci. 5 (1970) 964

[83] G. Lowe, Chem. Soc. Rev. 24 (1995) 309

[84] F. Balkenhohl, C. von dem Bussche-Hünnefeldt, A. Lansky, C. Zechel, Angew. Chem. 108 (1996) 2436

[85] X. D. Xiang, X. D. Sun, G. Briceno, Y. Lou, K. A. Wang, H. Chang, W. G. Wallace Freedman, S. W. Chen, P. G. Schultz, Sci. 268 (1995) 1738

[86] E. Danielson, J. H. Golden, E. W. McFarland, C. M. Reaves, W. H. Weinberg, X. D. Wu, Nature 389 (1997) 944

[87] E. Danielson, J. H. Golden, M. Devenney, D. M. Giaquinta, E.W. McFarland, C. M. Reaves, W. H. Weinberg, X. D. Wu, Sci. 279 (1998) 837

[88] N. Katada, M. Niwa, Chem. Vap. Dep. 2 (1996) 125

[89] T. Miyao, I. Shishikura, M. Matsuoka, M. Nagai, Chem. Lett. 121 (1996) 561

[90] R. C. Smith, N. Chien, Chem. Mater. 15 (2003) 292

[91] Q. Wang, Thin solid films 430 (2003) 78

[92] Y. Matsumoto, M. Murakami, Appl. Surf. Sci. 189 (2002) 344

[93] T. Ohnishi, D. Komiyama, T. Koida, Appl. Phys. Lett. 79 (2001) 536

[94] A. A. Gorbunov, W. Pompe, A. Sewing, S. V. Gapanov, A. D. Akhsakhalyan, R. Dietsch, S. Vollmar et al., Appl. Surf. Sci. 96 (1996) 649

[95] R. E. Russo, X. L. Mao, D. L. Perry, Chemtech. 12 (1994) 14

[96] S. M. Senkan, S. Ozturk, Angew. Chem. Int. Ed. 38 (1999) 791

[97] C. Hoffmann, A. Wolf, F. Schüth 38 (1999) 2800

[98] H. M. Reichenbach, P. J. McGinn, J. Mater. Res. 16 (2001) 967

[99] J. Klein, C. W. Lehmann, H–W. Schmidt, W. F. Maier Angew. Chem. Int. Ed. 37 (1998) 3369

[100] D. E. Akporiaye, I. M. Dahl, A. Karlsson, R. Wendelbo, Angew. Chem. Int. Ed. 37 (1998) 609

[101] A. Holzwarth, H-W. Schmidt, W. F. Maier, Angew. Chem. Int. Ed. 37 (1998) 2644

[102] J. Saalfrank, W. F. Maier Angew. Chem. Ed. 43 (2004) 2028

[103] J. N. Cawse, Acc. Chem. Res. 34 (2001) 213

[104] S. Senkan, Nature 394 (1998) 350

[105] F. C. Moates, M. Somani, J. Annamalai, J. T. Richardson, D. Luss, R. C. Willson, Ind. Eng. Chem. Res. 35 (1996) 4801

[106] A. Holzwarth, W. F. Maier, Platinum Metals Rev. 44 (2000) 16

[107] H. Su, E. S. Yeung, J. Am. Chem. Soc. 122 (2000) 7422

[108] P. Cong, A. Dehestani, R. Doolen, D. M. Giaquinta, S. Guan, V. Markov, D. Poojary,

K. Self, H. W. Turner, W. H. Weinberg, Proc. Natl. Acad. Sci. USA 96 (1999) 11077

[109] R. Vijay, R. J. Hendershot, W. B. Rogers, B. J. Feist, C. M. Snively, J. Lauterbach Cat. Comm. 6 (2005) 167

[110] R. Vijay, C. M. Snively, J. Lauterbach, J. Catal. 243 (2006) 368

[111] Y. Yamada, T. Kobayashi, J. Japan Petroleum Instut. 49 (2006) 157

[112] A. C. Cooper, L. H. McAlexander, D-H. Lee, M. T. Torres, R. H. Crabtree, J. Am. Chem. Soc. 120 (1998) 9971

[113] J-H. Park, M. S. Han, S. J. Park, D. H. Kim, I.-S. Nam, G. K. Yeo, J. K. Kil, Y. Youn, J. Catal. 241 (2006) 470

[114] M. Orschel, J. Klein, H-W. Schmidt, W. F. Maier Angew. Chem. Int. Ed. 38 (1999) 2791

[115] S. Senkan, K. Krantz, S. Ozturk, V. Zengin, I. Onal, Angew. Chem. Int. Ed. 38 (1999) 2794

[116] P. Cong, R. D. Doolen, Q. Fan, D. M. Giaquinta, S. Guan, E. W. McFarland, D. M. Poohary, K. Self, H. W. Turner, W. H. Weinberg, Angew. Chem. Int. Ed. 111 (1999) 508

[117] P. Cong, R. D. Doolen, Q. Fan, D. M. Giaquinta, S. Guan, E. W. McFarland, D. M. Poohary, K. Self, H. W. Turner, W. H. Weinberg, Angew. Chem. Int. Ed. 38 (1999) 484

[118] H. An, C. Kilroy, P. J. McGinn, Catal. Today 98 (2004) 423

[119] C. Mirodatos, Y. Schuurman, C. Hayaud, A. Holzwarth, D. Farusseng, T. Richter, EP 1,293,772 A2 (2003)

[120] C. Hoffmann, H. W. Schmidt, F. Schüth, J. Catal. 198 (2001) 348

[121] O. Lavastre, I. Illitchev, G. Jegou, P. H. Dixneuf, J. Am. Chem. Soc. 124 (19) (2002) 5278

[122] A. Corma, J. M. Serra, P. Serna, E. Argente, S. Valero, V. Botti, J. Catal. 229 (2005) 513

[123] A. Corna, J. M. Serra, Catal. Today 107-108 (2005) 3

[124] Y. Yamada, A. Ueda, Z. Zhao, T. Maekawa, K. Suzuki, T Takada, T. Kobayashi, Catal. Today, 67 (2001) 379

[125] P. C. Pawlicki, R. A. Schmitz, Chem. Eng. Prog. 2 (1987) 40

[126] G. Georgiades, V. A. Self, P. A. Sermon, Angew. Chem. Int. Ed. 26 (1987) 1042

[127] L. Vegvari, A. Tomposb, S. Gobölös, J. Margitfalvi, Catal. Today 81 (2003) 517

[128] J. Klein, T. Zech, J. N. Newsam, S. A. Schunk, Appl. Catal. A 254 (2003) 121

[129] D. Wolf, O. V. Buyevska, M. Baerns, Appl. Catal. A 200 (2000) 63

[130] M. Serra, A. Corma, S. Valero, E. Argente, V. Botti, QSAR & Combi. Sci. 26 (2007) 11

[131] G. Kirsten, W. F. Maier, Appl. Surf. Sci. 233 (2004) 87

[132] G. Grubert, S. Kolf, M. Baerns, I. Vauthey, D. Farrusseng, A. C. van Veen, C. Mirodatos, E. R. Stobbe, P. D. Cobden Appli. Catal. A 306 (2006) 17

[133] S. Linic, J. Jankowiak, M. A. Barteau, 224 (2004) 489

[134] J. Klein, C. Lettman, W. F. Maier, J. Non-Cryst. Sol. 282 (2001) 203

[135] S. Klein, W. F. Maier, Angew. Chem. Int. Ed. 35 (1996) 2230

[136] L. L. Hench, J. K. West, Chem. Rev. 90 (1990) 33

[137] C. J. Brinker, G. W. Scherer, Sol-Gel Science: The physics and Chemistry of Sol-Gel Processing, Academic Press, New York, (1990)

[138] G. Frenzer, W. F. Maier, Annu. Rev. Mater. Res. 36 (2006) 281

[139] J. Mendez-Vivar, R. Mendoza-Serna, L. Valdes-Castro J. Non-Cryst. Sol. 288 (2001) 200

[140] H. M. Reichenbach, H. An, P. J. McGinn, Appl. Catal. B 44 (2003) 347

[141] I. E. Marko, P. R. Giles, M. Tsukazaki, S. M. Brown, C. J. Urch, Sci. 274 (1996) 2044

[142] G.-Z. Wang, U. Andeasson, J.-E. Backvall, J. Chem. Soc., Chem. Commun. 1 (1994) 1037

[143] A. Hanyu, E. Takewaza, S. Sakaguchi, Y. Ishii, Tetrahedron Lett. 39 (1998) 5557

[144] T. Nishimura, T. Onoue, K. Ohe, S. Uemura, Tetrahedron Lett. 39 (1998) 6011

[145] S. B. Kumar, S. P. Mirajkar, G. C. G. Paris, P. Kumar, R. Kumar J. Catal. 156 (1995) 163

[146] F. Maspero, U. Romano, J. Catal. 146 (1994) 476

[147] Q. Tang, Y. Wang, J. Liang, P. Wang, Q. Zhang, H. Wan, Chem. Commun, (2004) 440

[148] M. L. Kantam, B. P. C. Rao, R. S. Reddy, N. S. Sekhar, B. Sreedhar, B. M. Choudary, J. Mol. Catal. A. Chem. 272 (2007) 1

[149] X. Meng, K. Lin, X. Yang, Z. Sun, D. Jiang, F.-S. Xiao, J. Catal. 218 (2003) 460

[150] P. Desrosiers, A. Guram, A. Hagermeyer, B. Jandeleit, D. M. Poojary, H. Turner, H. Weinberg, Catal. Today 67 (2001) 397

[151] K. Yamaguchi, N. Mizuno, Ang. Chem. Int. Ed. 41 (2002) 4539

[152] K. Yamaguchi, N. Mizuno, Chem. Eur. J. 9 (2003) 4353

[153] C. Klanner, D. Farrusseng, L. Baumes, C. Mirodatos, F. Schüth, QSAR Comb. Sci. 22

(2003) 729

[154] J. Scheidtman, Dissertation, Universität des Saarlandes, 2003

[155] J. P. A Neeft, M. Makkee, J. A. Moulijn, Chem. Eng. J. 64 (1996) 295

[156] D. Uner, M. K. Demirkol, B. Dernaika Apl. Catal. B 61 (2005) 334

[157] M. I. Khan, C. H. T Wang, B. E. Langridge, Combustion and Flame 17 (1971) 409

[158] K. Otto, M. H. Sieg, M. Zinbo, SAE Paper (1980) 800336

[159] N. Miyamoto, H. Ogawa, N. Goto, H. Sasaki SAE Paper (1990) 900640

[160] K. Pattas, Z. Samaras, D. Sherwood, K. Umehara, C. Cantiani, O. Aguerre, P. Barthe, J. Lemaire, SAE Paper (1992) 920363

[161] J. Lemaire, D. Petta, O. Touret, EP 599,717 (1994)

[162] M. L Pisarello, C. A. Querini, and E. E Miro, Catal. Today, 75 (2000) 465.

[163] A. Trovatelli, Catal. Rev. Sci. Eng. 38 (1996) 439

[164] M. A. Peralta, V. G. Milt, L. M. Cornaglia, C. A. Querini, J. Catal. 242 (2006) 118.

[165] J. V. Craenenbroeck, D. Andreeva, T. Tabakova, K. V. Werde, J. Mullens, F. Verpoort, J. Catal. 209 (2002) 515

[166] S. Sieg, PhD thesis, Universität des Saarlandes, 2007

[167] R. Allanson, B. J. Cooper, J. E. Thoss, A. Uusimaki, A. P. Walker, J. P. Warren, SAE Paper (2000) 2000-01-0480

[168] D. Rende, PhD thesis, Universität des Saarlandes, 2007

[169] K. Yamaguchi, K. Mori, T. Mizugaki, K. Ebitani, K. Kaneda, J. Am. Chem. Soc. 122 (2000) 7144

[170] TOPAS, Version 2.1, Bruker AXS, Karlsruhe

[171] R.W. Cheary, A. A. Coelho, J. Appl. Cryst. 25 (1992) 109

[172] J. Van Doorn, J. Varloud, P. Meriaudeau, V. Perrichon, Appl. Catal. B 1 (1992) 117

[173] A. Bueno-Lopez, K. Krishna, M. Makkee, J. A. Moulijn, J. Catal. 230 (2005) 237

[174] G. Fierro, M. L. Jacono, M. Inversi, R. Gragone, P. Porta, Topics Catal. 10 (2000) 39

[175] T. Wolter, PhD thesis, Universität des Saarlandes, 2002

[176] J. Saalfrank, PhD thesis, Universität des Saarlandes, 2003

[177] T. Schmidt, PhD thesis, Universität des Saarlandes, 2005

6 Attachment

6.1 Symbols and abbreviations

EDX	Energy dispesive x-ray analysis
A/F	Air to fuel ratio
Ø	Diameter
Θ	Theta
Å	Angstroms
c	Concentration
DOC	Diesel oxidation catalyst
µl	Microliter
µm	Micrometer
°C	Degrees Centigrade
h	Hour
min	Minute
mg	Milligram
m	Meter
µmol	Micromole
B.E.T	Brunauer, Emmet and Teller method
B.J.H	Barret, Joyner and Halenda method
CRT	Continuous regenerating trap
GC	Gaschromatography
IR	Infrared
MFC	Mass flow controller
MS	Mass spectrometer
NO_x	Nitrogen oxides
Pa	Pascal
PM	Particulate matter
T	Temperature
TEM	Transmission electron microscope
TGA	Thermogravimetric analysis
XRD	X-ray diffractometry
SCR	Selective catalytic reduction
MSC	Multiple Sample Concept
REMPI	Resonance-enhanced multiphoton ionization
PTD	Photothermal deflection
WGSR	Water gas shift reaction
NSR	NO_x storage reduction
DPNR	Diesel particulate NO_x reduction

6.2 Used chemicals

Chemical	Supplier	Chemical	Supplier
$AgNO_3$	ABCR	$Mo[OCH(CH_3)_2]_5$	Alfa Aesar
$Al[C_2H_5CH(CH_3)O]_3$	Aldrich	$NaNO_3$	Merck
$B(OH)_3$	Fluka	$Nd(NO_3)_3 \cdot 6\ H_2O$	Aldrich
$Ba(NO_3)_2$	Fluka	$Pb(CH_3CO_2)_2$	Merck
$Bi[C_4H_9CH(C_2H_5)COO]_3$	Alfa Aesar	$Pr(NO_3)_3 \cdot 5\ H_2O$	Aldrich
$Ca(NO_3)_2 \cdot 4\ H_2O$	Fluka	$PtBr_4$	Alfa Aesar
$Cd(NO_3)_2 \cdot 4\ H_2O$	Fluka	$Rb[CH_3COCHCOCH_3]$	Aldrich
$Ce(NO_3)_2 \cdot 6\ H_2O$	Fluka	$RuCl_3$	Johnson Matthey
$Co(NO_3)_2 \cdot 6\ H_2O$	Fluka	$SbCl_3$	Aldrich
$CoCO_3$	Alfa Aesar	$Sc(NO_3)_3 \cdot 5\ H_2O$	Strem Chemicals
$Cr(NO_3)_3 \cdot 9\ H_2O$	Aldrich	SeO_2	Aldrich
CsCl	Merck	$Si(OC_2H_5)_4$	Acros
$Cu(NO_3)_2 \cdot 3\ H_2O$	Fluka	$Sm(NO_3)_3 \cdot 6\ H_2O$	Riedel
$Dy(NO_3)_3 \cdot 5\ H_2O$	Aldrich	$Sn[OCH(CH_3)_2]_4$	Merck
$Er(NO_3)_3 \cdot 5\ H_2O$	Aldrich	$Sr(NO_3)_2$	Merck
$Eu(NO_3)_3 \cdot 6\ H_2O$	Strem	$Ta(OC_2H_5)_5$	Alfa Aesar
$Fe(NO_3)_3 \cdot 9\ H_2O$	Riedel	$Tb(NO_3)_3 \cdot x\ H_2O$	Alfa
$Ga(NO_3)_3 \cdot xH_2O$	Aldrich	$TeCl_4$	Aldrich
$Gd(NO_3)_3 \cdot 6H_2O$	Aldrich	$Ti[OCH(CH_3)_2]_4$	Adrich
$Ge[OCH(CH_3)_2]_4$	Aldrich	$Tm(NO_3)_3 \cdot 6\ H_2O$	Strem
$HfCl_4$	Aldrich	$V[CH_3COCHCOCH_3]_3$	Strem
$Ho(NO_3)_3 \cdot 5\ H_2O$	Strem	$W[OCH(CH_3)_2]_6$	
$In(NO_3)_3 \cdot 5\ H_2O$	Aldrich	$Y(NO_3)_3 \cdot 6\ H_2O$	Fluka
KNO_3		$Yb(NO_3)_3 \cdot x\ H_2O$	Chempur
$La(NO_3)_3$	Fluka	$Zn(NO_3)_2 \cdot 4\ H_2O$	Merck
$Lu(NO_3)_3 \cdot xH_2O$	Aldrich	$ZrO(NO_3)_2 \cdot x\ H_2O$	Alfa Aesar
$Mg(NO_3)_2 \cdot 6H_2O$	Merck	4-Hydroxy-4-methyl-2-pentanone	Aldrcih
$Mn(NO_3)_2 \cdot 4H_2O$	Merck		

6.3 Used software and equipment

Description	Classification	Manufacturer
Pepitting robot	Lissy	Zinsser Analytic
Orbital stirrer	Titramax 100	Heidolph Instrument
Muffle furnace	Program Controller S27	Nabertherm
Muffle furnace		Carbolite
Muffle furnace		Carbolite
Physisorption equipment	Carlo Erba Sorptomatic 1990	Fision Instrument
TEM measurement	JEM-2011	JEOL JEM-2011
EDX measurement		Oxford Instrument
X-ray measurement	G670	Huber Guinier
Infrared camera	PtSi 640x480, PtSi-FPA detector	Thermosensorik
Infrared reactor		Uni. des Saarlandes
Mass flow controller	Mass-Flo	MKS Instruments
Temperature controller	dTron 16.1, dicon-401	Jumo
CO_2 gas transmitter	IR24	GfG
CO gas transmitter	IR24	GfG
MS-GC		Thermo electron Corp.
TGA	T50	Schimadzu
Software	Plattenbau	J. Scheidtmann
Robot-software	Zinsser REDI	Zinsser Analytic
IR-camera control software	Testrig	J. Scheidtmann
Reflux cooler	Kryoflex KF 40	Mgw Lauda
2-neck round bottom glass		Uni. des Saarlandes

6.4 Library filling plan

The filling plan of libraries 1, 2, 3 and 4

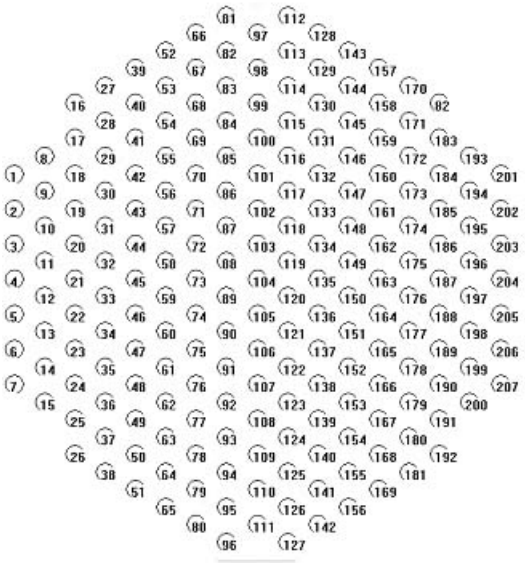

Position	Catalyst composition	Position	Catalyst composition
1	Pr_3Mn_{97}	57	In_3Co_{97}
2	La_3Mn_{97}	58	Gd_3Co_{97}
3	Mo_3Mn_{97}	59	Ti_3Co_{97}
4	Li_3Mn_{97}	60	Zr_3Co_{97}
5	Sr_3Mn_{97}	61	Mg_3Co_{97}
6	Ca_3Mn_{97}	62	Sr_3Co_{97}
7	Rb_3Mn_{97}	63	Ca_3Co_{97}
8	Ti_3Mn_{97}	64	Ce_3Co_{97}
9	Na_3Mn_{97}	65	Ge_3Co_{97}
10	In_3Mn_{97}	66	Al_3Co_{97}
11	Gd_3Mn_{97}	67	Er_3Co_{97}
12	Mg_3Mn_{97}	68	Tm_3Co_{97}
13	Sm_3Mn_{97}	69	B_3Co_{97}
14	V_3Mn_{97}	70	Se_3Co_{97}
15	Ce_3Mn_{97}	71	Tb_3Co_{97}
16	Ge_3Mn_{97}	72	Dy_3Co_{97}
17	Al_3Mn_{97}	73	Cd_3Co_{97}
18	B_3Mn_{97}	74	Zn_3Co_{97}
19	Se_3Mn_{97}	75	Ga_3Co_{97}
20	Tb_3Mn_{97}	76	Ba_3Co_{97}

21	Dy_3Mn_{97}	77	Na_3Co_{97}
22	Zn_3Mn_{97}	78	Te_3Co_{97}
23	Er_3Mn_{97}	79	W_3Co_{97}
24	Ru_3Mn_{97}	80	Cd_3Co_{97}
25	Tm_3Mn_{97}	81	Fe_3Co_{97}
26	Cd_3Mn_{97}	82	Hf_3Co_{97}
27	W_3Mn_{97}	83	Lu_3Co_{97}
28	Bi_3Mn_{97}	84	Cs_3Co_{97}
29	Fe_3Mn_{97}	85	Ho_3Co_{97}
30	Hf_3Mn_{97}	86	Y_3Co_{97}
31	Lu_3Mn_{97}	87	Sb_3Co_{97}
32	Cs_3Mn_{97}	88	Sm_3Co_{97}
33	Co_3Mn_{97}	89	Sn_3Co_{97}
34	Eu_3Mn_{97}	90	Nd_3Co_{97}
35	Cr_3Mn_{97}	91	Rb_3Co_{97}
36	Ho_3Mn_{97}	92	Cr_3Co_{97}
37	Ag_3Mn_{97}	93	Ag_3Co_{97}
38	Zr_3Mn_{97}	94	Sc_3Co_{97}
39	Ga_3Mn_{97}	95	Ta_3Co_{97}
40	Ba_3Mn_{97}	96	Si_3Co_{97}
41	Te_3Mn_{97}	97	Bi_3Co_{97}
42	Cu_3Mn_{97}	98	Cu_3Co_{97}
43	Sc_3Mn_{97}	99	Yb_3Co_{97}
44	Ta_3Mn_{97}	100	Mn_3Co_{97}
45	Si_3Mn_{97}	101	Eu_3Co_{97}
46	Nd_3Mn_{97}	102	V_3Co_{97}
47	Sn_3Mn_{97}	103	$Cs_2V_1Fe_2/Al_2O_3$
48	Y_3Mn_{97}	104	Sr_3Ce_{97}
49	Yb_3Mn_{97}	105	Ni_3Ce_{97}
50	Sb_3Mn_{97}	106	Tm_3Ce_{97}
51	$Pt/Rh/ZrO_2$	107	Ba_3Ce_{97}
52	Pt/ZrO_2	108	Fe_3Ce_{97}
53	Pr_3Co_{97}	109	Sc_3Ce_{97}
54	La_3Co_{97}	110	W_3Ce_{97}
55	Mo_3Co_{97}	111	Ti_3Ce_{97}
56	Li_3Co_{97}	112	Te_3Ce_{97}
113	Cu_3Ce_{97}	147	Al_3Ce_{97}
114	Na_3Ce_{97}	148	B_3Ce_{97}
115	Si_3Ce_{97}	149	Cd_3Ce_{97}

116	Tb_3Ce_{97}	150	Cr_3Ce_{97}
117	Yb_3Ce_{97}	151	Rh_3Ce_{97}
118	Zr_3Ce_{97}	152	Ta_3Ce_{97}
119	Sn_3Ce_{97}	153	Dy_3Ce_{97}
120	Eu_3Ce_{97}	154	Pd/Al_2O_3
121	Sb_3Ce_{97}	155	$Cu_{20}Mn_{80}$
122	Ga_3Ce_{97}	156	$Cu_{50}Mn_{50}$
123	Ge_3Ce_{97}	157	$Cu_{56}Mn_{44}$
124	V_3Ce_{97}	158	$Cu_{67}Mn_{33}$
125	In_3Ce_{97}	159	$Cu_{80}Mn_{20}$
126	Hf_3Ce_{97}	160	$Ce_{30}Co_{40}Mn_{30}$
127	Ag_3Ce_{97}	161	$Co_{50}Cu_{50}$
128	Se_3Ce_{97}	162	$Co_{70}Ni_{30}$
129	Y_3Ce_{97}	163	$Co_{70}Cu_{10}Ni_{20}$
130	Bi_3Ce_{97}	164	$Co_{20}Cu_{50}Mn_{30}$
131	Mo_3Ce_{97}	165	$Mn_{70}Ni_{30}$
132	Nb_3Ce_{97}	166	$Cu_{10}Mn_{90}$
133	Zn_3Ce_{97}	167	$Fe_6Zr_{20}Al_{74}$
134	Er_3Ce_{97}	168	$Se_{20}Ti_{80}$
135	Gd_3Ce_{97}	169	Mn_5Co_{95}
136	Ho_3Ce_{97}	170	$Cd_{15}Co_{85}$
137	Ca_3Ce_{97}	171	$Al_1Mn_{6.7}Co_{92.4}$
138	Co_3Ce_{97}	172	$Co_{10}Ni_{90}$
139	La_3Ce_{97}	173	$Sb_{20}Ti_{80}$
140	K_3Ce_{97}	174	$Ba_{20}Ce_{40}Fe_{40}$
141	Lu_3Ce_{97}	175	$Cu_{15}Mn_{85}$
142	Mg_3Ce_{97}	176	$Co_3Si_{45}Al_{42}$
143	Mn_3Ce_{97}	177	$Cu_{40}Ce_{20}Ni_{40}$
144	Nd_3Ce_{97}	178	$Na_2Mn_{4.2}Co_{93.8}$
145	Pr_3Ce_{97}	179	$Zr_{20}Al_{80}$
146	Sm_3Ce_{97}	180	$Ag_8Mo_5Fe_{87}$

Library 2

Position	Catalyst composition	Position	Catalyst composition
66	Al_3Ce_{97}	97	Pd/Al_2O_3
67	Na_3Ce_{97}	98	Nd_3Ce_{97}
68	Si_3Ce_{97}	99	Ga_3Ce_{97}
69	Tb_3Ce_{97}	100	Sm_3Ce_{97}
70	Yb_3Ce_{97}	101	In_3Ce_{97}
71	Zr_3Ce_{97}	102	B_3Ce_{97}
72	Sn_3Ce_{97}	103	Ag_3Ce_{97}
73	$Pt/Rh/ZrO_2$	104	K_3Ce_{97}
74		105	Rh_3Ce_{97}
75		106	Ta_3Ce_{97}
76		107	$Cs_2V_1Fe_2/Al_2O_3$
77		108	Sr_3Ce_{97}
78		109	Ni_3Ce_{97}
79		110	Cr_3Ce_{97}
80		111	Pt/ZrO_2
81	Se_3Ce_{97}	112	Co_3Ce_{97}
82	Y_3Ce_{97}	113	Te_3Ce_{97}
83	Bi_3Ce_{97}	114	V_3Ce_{97}
84	Mo_3Ce_{97}	115	W_3Ce_{97}
85	Sc_3Ce_{97}	116	Hf_3Ce_{97}
86	Ba_3Ce_{97}	117	Lu_3Ce_{97}
87	Er_3Ce_{97}	118	Dy_3Ce_{97}
88	Gd_3Ce_{97}	119	Cu_3Ce_{97}
89	Ho_3Ce_{97}	120	Cd_3Ce_{97}
90	Nb_3Ce_{97}	121	Ca_3Ce_{97}
91	Pd/ZrO_2	122	Fe_3Ce_{97}
92	Eu_3Ce_{97}	123	Pr_3Ce_{97}
93	Sb_3Ce_{97}	124	Ge_3Ce_{97}
94	La_3Ce_{97}	125	Ti_3Ce_{97}
95	Mg_3Ce_{97}	126	Tm_3Ce_{97}
96	Mn_3Ce_{97}	127	Zn_3Ce_{97}

Library 3

Position	Catalyst composition	Position	Catalyst composition
1	Pr_3Co_{97}	41	W_3Co_{97}
2		42	Bi_3Co_{97}
3	La_3Co_{97}	43	Fe_3Co_{97}
4		44	Hf_3Co_{97}
5	Mo_3Co_{97}	45	Lu_3Co_{97}
6		46	Cs_3Co_{97}
7	Li_3Co_{97}	47	Mn_3Co_{97}
8	Sr_3Co_{97}	48	Eu_3Co_{97}
9		49	Cr_3Co_{97}
10	Ca_3Co_{97}	50	Ho_3Co_{97}
11		51	Ag_3Co_{97}
12	Rb_3Co_{97}	52	
13		53	
14	Ti_3Co_{97}	54	
15		55	
16	Na_3Co_{97}	56	
17		57	
18	In_3Co_{97}	58	
19		59	
20	Gd_3Co_{97}	60	
21		61	
22	Mg_3Co_{97}	62	
23		63	
24	Sm_3Co_{97}	64	
25		65	
26	V_3Co_{97}	66	Zr_3Co_{97}
27		67	Ga_3Co_{97}
28	Ce_3Co_{97}	68	Ba_3Co_{97}
29		69	Te_3Co_{97}
30	Ge_3Co_{97}	70	Cu_3Co_{97}
31	Al_3Co_{97}	71	Sc_3Co_{97}
32	B_3Co_{97}	72	Ta_3Co_{97}
33	Se_3Co_{97}	73	Si_3Co_{97}
34	Tb_3Co_{97}	74	Nd_3Co_{97}
35	Dy_3Co_{97}	75	Sn_3Co_{97}
36	Zn_3Co_{97}	76	Y_3Co_{97}
37	Er_3Co_{97}	77	Yb_3Co_{97}
38	Ru_3Co_{97}	78	Sb_3Co_{97}
39	Tm_3Co_{97}	79	
40	Cd_3Co_{97}	80	

Library 4

Position	Catalyst composition	Position	Catalyst composition
1	Pr_3Mn_{97}	41	W_3Mn_{97}
2		42	Bi_3Mn_{97}
3	La_3Mn_{97}	43	Fe_3Mn_{97}
4		44	Hf_3Mn_{97}
5	Mo_3Mn_{97}	45	Lu_3Mn_{97}
6		46	Cs_3Mn_{97}
7	Li_3Mn_{97}	47	Co_3Mn_{97}
8	Sr_3Mn_{97}	48	Eu_3Mn_{97}
9		49	Cr_3Mn_{97}
10	Ca_3Mn_{97}	50	Ho_3Mn_{97}
11		51	Ag_3Mn_{97}
12	Rb_3Mn_{97}	52	
13		53	
14	Ti_3Mn_{97}	54	
15		55	
16	Na_3Mn_{97}	56	
17		57	
18	In_3Mn_{97}	58	
19		59	
20	Gd_3Mn_{97}	60	
21		61	
22	Mg_3Mn_{97}	62	
23		63	
24	Sm_3Mn_{97}	64	
25		65	
26	V_3Mn_{97}	66	Zr_3Mn_{97}
27		67	Ga_3Mn_{97}
28	Ce_3Mn_{97}	68	Ba_3Mn_{97}
29		69	Te_3Mn_{97}
30	Ge_3Mn_{97}	70	Cu_3Mn_{97}
31	Al_3Mn_{97}	71	Sc_3Mn_{97}
32	B_3Mn_{97}	72	Ta_3Mn_{97}
33	Se_3Mn_{97}	73	Si_3Mn_{97}
34	Tb_3Mn_{97}	74	Nd_3Mn_{97}
35	Dy_3Mn_{97}	75	Sn_3Mn_{97}
36	Zn_3Mn_{97}	76	Y_3Mn_{97}
37	Er_3Mn_{97}	77	Yb_3Mn_{97}
38	Ru_3Mn_{97}	78	Sb_3Mn_{97}
39	Tm_3Mn_{97}	79	
40	Cd_3Mn_{97}	80	

All other libraries were filled with the plan given below.

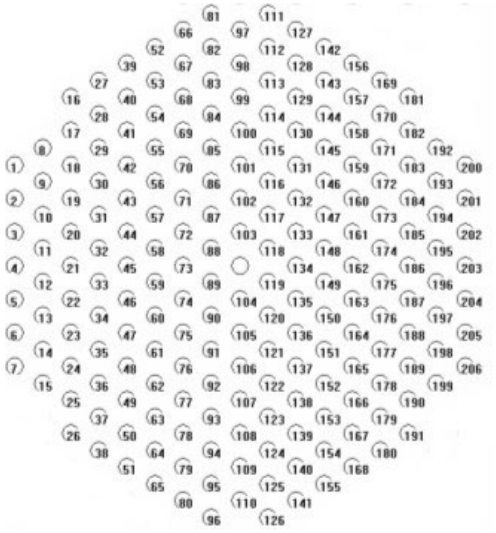

Library 6

Position	Catalyst composition	Position	Catalyst composition
1	$Al_3Cs_{20}Co_{77}$	108	$Tm_{10}Cs_{20}Co_{70}$
3	$B_3Cs_{20}Co_{77}$	110	$Ta_{10}Cs_{20}Co_{70}$
5	$Cd_3Cs_{20}Co_{77}$	111	$Sr_{10}Cs_{20}Co_{70}$
7	$Cr_3Cs_{20}Co_{77}$	113	$Sc_{10}Cs_{20}Co_{70}$
8	$Dy_3Cs_{20}Co_{77}$	115	$W_{10}Cs_{20}Co_{70}$
10	$Er_3Cs_{20}Co_{77}$	122	$Ti_{10}Cs_{20}Co_{70}$
12	$Gd_3Cs_{20}Co_{77}$	123	$Te_{10}Cs_{20}Co_{70}$
14	$Ho_3Cs_{20}Co_{77}$	125	$Ni_{10}Cs_{20}Co_{70}$
15	$Ca_3Cs_{20}Co_{77}$	126	$Ba_{10}Cs_{20}Co_{70}$
16	$Ru_3Cs_{20}Co_{77}$	127	$Tb_{10}Cs_{20}Co_{70}$
18	$La_3Cs_{20}Co_{77}$	128	$Yb_{10}Cs_{20}Co_{70}$
20	$Mn_3Cs_{20}Co_{77}$	130	$Se_{10}Cs_{20}Co_{70}$
22	$Lu_3Cs_{20}Co_{77}$	137	$Zr_{10}Cs_{20}Co_{70}$
24	$Mg_3Cs_{20}Co_{77}$	139	$Mo_{10}Cs_{20}Co_{70}$
26	$Ce_3Cs_{20}Co_{77}$	141	$Nb_{10}Cs_{20}Co_{70}$
27	$Nd_3Cs_{20}Co_{77}$	142	$Ga_{10}Cs_{20}Co_{70}$
29	$Pr_3Cs_{20}Co_{77}$	144	$Ge_{10}Cs_{20}Co_{70}$
31	$Sm_3Cs_{20}Co_{77}$	146	$Hf_{10}Cs_{20}Co_{70}$
33	$Se_3Cs_{20}Co_{77}$	148	$Na_{10}Cs_{20}Co_{70}$
35	$Y_3Cs_{20}Co_{77}$	150	$Bi_{10}Cs_{20}Co_{70}$
37	$Zn_3Cs_{20}Co_{77}$	152	$Cu_{10}Cs_{20}Co_{70}$
38	$Sn_3Cs_{20}Co_{77}$	154	$In_{10}Cs_{20}Co_{70}$
39	$Eu_3Cs_{20}Co_{77}$	155	$Si_{10}Cs_{20}Co_{70}$
41	$Sb_3Cs_{20}Co_{77}$	156	$Zn_{10}Cs_{20}Co_{70}$
43	$Pt_3Cs_{20}Co_{77}$	158	$Sn_{10}Cs_{20}Co_{70}$
45	$Fe_3Cs_{20}Co_{77}$	160	$Eu_{10}Cs_{20}Co_{70}$
47	$Ga_3Cs_{20}Co_{77}$	162	$Sb_{10}Cs_{20}Co_{70}$
49	$Ge_3Cs_{20}Co_{77}$	164	$Pt_{10}Cs_{20}Co_{70}$
51	$Hf_3Cs_{20}Co_{77}$	166	$V_{10}Cs_{20}Co_{70}$
52	$In_3Cs_{20}Co_{77}$	168	$Fe_{10}Cs_{20}Co_{70}$
53	$Cu_3Cs_{20}Co_{77}$	169	$Ce_{10}Cs_{20}Co_{70}$
55	$Na_3Cs_{20}Co_{77}$	171	$Nd_{10}Cs_{20}Co_{70}$
57	$Ag_3Cs_{20}Co_{77}$	173	$Pr_{10}Cs_{20}Co_{70}$
59	$Si_3Cs_{20}Co_{77}$	175	$Sm_{10}Cs_{20}Co_{70}$
61	$Tb_3Cs_{20}Co_{77}$	177	$Ag_{10}Cs_{20}Co_{70}$
63	$Yb_3Cs_{20}Co_{77}$	179	$Y_{10}Cs_{20}Co_{70}$
65	$Zr_3Cs_{20}Co_{77}$	181	$Ca_{10}Cs_{20}Co_{70}$
66	$Bi_3Cs_{20}Co_{77}$	183	$Ru_{10}Cs_{20}Co_{70}$
68	$Mo_3Cs_{20}Co_{77}$	185	$La_{10}Cs_{20}Co_{70}$
70	$Nb_3Cs_{20}Co_{77}$	187	$Mn_{10}Cs_{20}Co_{70}$
76	$Sr_3Cs_{20}Co_{77}$	189	$Lu_{10}Cs_{20}Co_{70}$
78	$Sc_3Cs_{20}Co_{77}$	190	$Mg_{10}Cs_{20}Co_{70}$
80	$W_3Cs_{20}Co_{77}$	192	$Dy_{10}Cs_{20}Co_{70}$
81	$V_3Cs_{20}Co_{77}$	194	$Er_{10}Cs_{20}Co_{70}$
83	$Ti_3Cs_{20}Co_{77}$	196	$Gd_{10}Cs_{20}Co_{70}$
85	$Te_3Cs_{20}Co_{77}$	198	$Ho_{10}Cs_{20}Co_{70}$
92	$Ni_3Cs_{20}Co_{77}$	200	$Al_{10}Cs_{20}Co_{70}$
94	$Ba_3Cs_{20}Co_{77}$	202	$B_{10}Cs_{20}Co_{70}$
96	$Tm_3Cs_{20}Co_{77}$	204	$Cd_{10}Cs_{20}Co_{70}$
97	$Ta_3Cs_{20}Co_{77}$	206	$Cr_{10}Cs_{20}Co_{70}$

Library 7

Position	Catalyst composition	Position	Catalyst composition
1	$Al_3K_{15}Ce_{82}$	106	$Ba_{10}K_{15}Ce_{75}$
3	$B_3K_{15}Ce_{82}$	108	$Tm_{10}K_{15}Ce_{75}$
5	$Cd_3K_{15}Ce_{82}$	110	$Ta_{10}K_{15}Ce_{75}$
7	$Cr_3K_{15}Ce_{82}$	111	$Sc_{10}K_{15}Ce_{75}$
8	$Dy_3K_{15}Ce_{82}$	113	$W_{10}K_{15}Ce_{75}$
10	$Er_3K_{15}Ce_{82}$	115	$V_{10}K_{15}Ce_{75}$
12	$Gd_3K_{15}Ce_{82}$	121	$Ti_{10}K_{15}Ce_{75}$
14	$Ho_3K_{15}Ce_{82}$	123	$Te_{10}K_{15}Ce_{75}$
15	$Ca_3K_{15}Ce_{82}$	125	$Ni_{10}K_{15}Ce_{75}$
16	$Ru_3K_{15}Ce_{82}$	127	$Yb_{10}K_{15}Ce_{75}$
18	$La_3K_{15}Ce_{82}$	128	$Zr_{10}K_{15}Ce_{75}$
20	$Mn_3K_{15}Ce_{82}$	130	$Bi_{10}K_{15}Ce_{75}$
22	$Lu_3K_{15}Ce_{82}$	137	$Mo_{10}K_{15}Ce_{75}$
24	$Mg_3K_{15}Ce_{82}$	139	$Nb_{10}K_{15}Ce_{75}$
26	$Ce_3K_{15}Ce_{82}$	141	$Sr_{10}K_{15}Ce_{75}$
27	$Nd_3K_{15}Ce_{82}$	142	$Ge_{10}K_{15}Ce_{75}$
29	$Pr_3K_{15}Ce_{82}$	144	$Hf_{10}K_{15}Ce_{75}$
31	$Sm_3K_{15}Ce_{82}$	146	$In_{10}K_{15}Ce_{75}$
33	$Se_3K_{15}Ce_{82}$	148	$Cu_{10}K_{15}Ce_{75}$
35	$Y_3K_{15}Ce_{82}$	150	$Na_{10}K_{15}Ce_{75}$
37	$Zn_3K_{15}Ce_{82}$	152	$Ag_{10}K_{15}Ce_{75}$
38	$Sn_3K_{15}Ce_{82}$	154	$Si_{10}K_{15}Ce_{75}$
39	$Eu_3K_{15}Ce_{82}$	155	$Tb_{10}K_{15}Ce_{75}$
41	$Sb_3K_{15}Ce_{82}$	156	$Zn_{10}K_{15}Ce_{75}$
43	$Pt_3K_{15}Ce_{82}$	158	$Sn_{10}K_{15}Ce_{75}$
45	$Fe_3K_{15}Ce_{82}$	160	$Eu_{10}K_{15}Ce_{75}$
47	$Ga_3K_{15}Ce_{82}$	162	$Sb_{10}K_{15}Ce_{75}$
49	$Ge_3K_{15}Ce_{82}$	164	$Pt_{10}K_{15}Ce_{75}$
51	$Hf_3K_{15}Ce_{82}$	166	$Fe_{10}K_{15}Ce_{75}$
52	$In_3K_{15}Ce_{82}$	168	$Ga_{10}K_{15}Ce_{75}$
53	$Cu_3K_{15}Ce_{82}$	169	$Co_{10}K_{15}Ce_{75}$
55	$Na_3K_{15}Ce_{82}$	171	$Nd_{10}K_{15}Ce_{75}$
57	$Ag_3K_{15}Ce_{82}$	173	$Pr_{10}K_{15}Ce_{75}$
59	$Si_3K_{15}Ce_{82}$	175	$Sm_{10}K_{15}Ce_{75}$
61	$Tb_3K_{15}Ce_{82}$	177	$Se_{10}K_{15}Ce_{75}$
63	$Yb_3K_{15}Ce_{82}$	179	$Y_{10}K_{15}Ce_{75}$
65	$Zr_3K_{15}Ce_{82}$	181	$Ru_{10}K_{15}Ce_{75}$
66	$Bi_3K_{15}Ce_{82}$	185	$La_{10}K_{15}Ce_{75}$
68	$Mo_3K_{15}Ce_{82}$	187	$Mn_{10}K_{15}Ce_{75}$
70	$Nb_3K_{15}Ce_{82}$	189	$Lu_{10}K_{15}Ce_{75}$
76	$Sr_3K_{15}Ce_{82}$	191	$Mg_{10}K_{15}Ce_{75}$
78	$Sc_3K_{15}Ce_{82}$	192	$Dy_{10}K_{15}Ce_{75}$
80	$W_3K_{15}Ce_{82}$	194	$Er_{10}K_{15}Ce_{75}$
81	$V_3K_{15}Ce_{82}$	196	$Gd_{10}K_{15}Ce_{75}$
83	$Ti_3K_{15}Ce_{82}$	198	$Ho_{10}K_{15}Ce_{75}$
85	$Te_3K_{15}Ce_{82}$	199	$Ca_{10}K_{15}Ce_{75}$
92	$Ni_3K_{15}Ce_{82}$	200	$Al_{10}K_{15}Ce_{75}$
94	$Ba_3K_{15}Ce_{82}$	202	$B_{10}K_{15}Ce_{75}$
96	$Tm_3K_{15}Ce_{82}$	204	$Cd_{10}K_{15}Ce_{75}$
97	$Ta_3K_{15}Ce_{82}$	206	$Cr_{10}K_{15}Ce_{75}$

Library 8

Position	Catalyst composition	Position	Catalyst composition
1	$Ag_3La_5Co_{92}$	111	$Ag_{10}La_5Co_{85}$
3	$Al_3La_5Co_{92}$	113	$Al_{10}La_5Co_{85}$
5	$B_3La_5Co_{92}$	115	$B_{10}La_5Co_{85}$
7	$Ba_3La_5Co_{92}$	117	$Ba_{10}La_5Co_{85}$
8	$Bi_3La_5Co_{92}$	119	$Bi_{10}La_5Co_{85}$
10	$Ca_3La_5Co_{92}$	121	$Ca_{10}La_5Co_{85}$
12	$Cd_3La_5Co_{92}$	123	$Cd_{10}La_5Co_{85}$
14	$Ce_3La_5Co_{92}$	125	$Pt_{10}La_5Co_{85}$
16	$Cr_3La_5Co_{92}$	127	$Cr_{10}La_5Co_{85}$
18	$Cu_3La_5Co_{92}$	129	$Cu_{10}La_5Co_{85}$
20	$Dy_3La_5Co_{92}$	131	$Dy_{10}La_5Co_{85}$
22	$Er_3La_5Co_{92}$	133	$Er_{10}La_5Co_{85}$
24	$Eu_3La_5Co_{92}$	135	$Eu_{10}La_5Co_{85}$
26	$Fe_3La_5Co_{92}$	137	$Fe_{10}La_5Co_{85}$
27	$Ga_3La_5Co_{92}$	139	$Ga_{10}La_5Co_{85}$
29	$Gd_3La_5Co_{92}$	141	$Gd_{10}La_5Co_{85}$
31	$Ge_3La_5Co_{92}$	142	$Ge_{10}La_5Co_{85}$
33	$Hf_3La_5Co_{92}$	144	$Hf_{10}La_5Co_{85}$
35	$Ho_3La_5Co_{92}$	146	$Ho_{10}La_5Co_{85}$
37	$In_3La_5Co_{92}$	148	$In_{10}La_5Co_{85}$
39	$Lu_3La_5Co_{92}$	150	$Lu_{10}La_5Co_{85}$
41	$Mg_3La_5Co_{92}$	152	$Mg_{10}La_5Co_{85}$
43	$Mn_3La_5Co_{92}$	154	$Mn_{10}La_5Co_{85}$
45	$Mo_3La_5Co_{92}$	156	$Mo_{10}La_5Co_{85}$
47	$Na_3La_5Co_{92}$	158	$Sn_{10}La_5Co_{85}$
49	$Nb_3La_5Co_{92}$	160	$Nb_{10}La_5Co_{85}$
51	$Nd_3La_5Co_{92}$	162	$Nd_{10}La_5Co_{85}$
52	$Ni_3La_5Co_{92}$	164	$Ni_{10}La_5Co_{85}$
54	$Pb_3La_5Co_{92}$	166	$Pb_{10}La_5Co_{85}$
56	$Pr_3La_5Co_{92}$	168	$Pr_{10}La_5Co_{85}$
58	$Pt_3La_5Co_{92}$	169	$Ce_{10}La_5Co_{85}$
60	$Ru_3La_5Co_{92}$	171	$Ru_{10}La_5Co_{85}$
62	$Sb_3La_5Co_{92}$	173	$Sb_{10}La_5Co_{85}$
64	$Sc_3La_5Co_{92}$	175	$Sc_{10}La_5Co_{85}$
66	$Se_3La_5Co_{92}$	177	$Se_{10}La_5Co_{85}$
68	$Si_3La_5Co_{92}$	179	$Si_{10}La_5Co_{85}$
70	$Sm_3La_5Co_{92}$	181	$Sm_{10}La_5Co_{85}$
72	$Sn_3La_5Co_{92}$	183	$Na_{10}La_5Co_{85}$
74	$Sr_3La_5Co_{92}$	185	$Sr_{10}La_5Co_{85}$
76	$Ta_3La_5Co_{92}$	187	$Ta_{10}La_5Co_{85}$
78	$Tb_3La_5Co_{92}$	189	$Tb_{10}La_5Co_{85}$
80	$Te_3La_5Co_{92}$	191	$Te_{10}La_5Co_{85}$
81	$Ti_3La_5Co_{92}$	192	$Ti_{10}La_5Co_{85}$
83	$Tm_3La_5Co_{92}$	194	$Tm_{10}La_5Co_{85}$
85	$V_3La_5Co_{92}$	196	$V_{10}La_5Co_{85}$
87	$W_3La_5Co_{92}$	198	$W_{10}La_5Co_{85}$
89	$Y_3La_5Co_{92}$	200	$Y_{10}La_5Co_{85}$
91	$Yb_3La_5Co_{92}$	202	$Yb_{10}La_5Co_{85}$
93	$Zn_3La_5Co_{92}$	204	$Zn_{10}La_5Co_{85}$
95	$Zr_3La_5Co_{92}$	206	$Zr_{10}La_5Co_{85}$

Library 10

Position	Catalyst composition	Position	Catalyst composition
1	$Ag_{10}Co_{15}Cs_{75}$	57	$Ag_{55}Co_{5}Cs_{40}$
2	$Ag_{5}Co_{20}Cs_{75}$	58	$Ag_{50}Co_{10}Cs_{40}$
3	$Ag_{25}Co_{5}Cs_{70}$	59	$Ag_{45}Co_{15}Cs_{40}$
4	$Ag_{20}Co_{10}Cs_{70}$	60	$Ag_{40}Co_{20}Cs_{40}$
5	$Ag_{15}Co_{15}Cs_{70}$	61	$Ag_{35}Co_{25}Cs_{40}$
6	$Ag_{10}Co_{20}Cs_{70}$	62	$Ag_{30}Co_{30}Cs_{40}$
7	$Ag_{5}Co_{25}Cs_{70}$	63	$Ag_{25}Co_{35}Cs_{40}$
8	$Ag_{30}Co_{5}Cs_{65}$	64	$Ag_{20}Co_{40}Cs_{40}$
9	$Ag_{25}Co_{10}Cs_{65}$	65	$Ag_{15}Co_{45}Cs_{40}$
10	$Ag_{20}Co_{15}Cs_{65}$	66	$Ag_{10}Co_{50}Cs_{40}$
11	$Ag_{15}Co_{20}Cs_{65}$	67	$Ag_{5}Co_{55}Cs_{40}$
12	$Ag_{10}Co_{25}Cs_{65}$	68	$Co_{60}Cs_{40}$
13	$Ag_{5}Co_{30}Cs_{65}$	69	$Ag_{65}Cs_{35}$
14	$Co_{35}Cs_{65}$	70	$Ag_{60}Co_{5}Cs_{35}$
15	$Ag_{40}Cs_{60}$	71	$Ag_{55}Co_{10}Cs_{35}$
16	$Ag_{35}Co_{5}Cs_{60}$	72	$Ag_{50}Co_{15}Cs_{35}$
17	$Ag_{30}Co_{10}Cs_{60}$	73	$Ag_{45}Co_{20}Cs_{35}$
18	$Ag_{25}Co_{15}Cs_{60}$	74	$Ag_{40}Co_{25}Cs_{35}$
19	$Ag_{20}Co_{20}Cs_{60}$	75	$Ag_{35}Co_{30}Cs_{35}$
20	$Ag_{15}Co_{25}Cs_{60}$	76	$Ag_{30}Co_{35}Cs_{35}$
21	$Ag_{10}Co_{30}Cs_{60}$	77	$Ag_{25}Co_{40}Cs_{35}$
22	$Ag_{5}Co_{35}Cs_{60}$	78	$Ag_{20}Co_{45}Cs_{35}$
23	$Ag_{45}Cs_{55}$	79	$Ag_{15}Co_{50}Cs_{35}$
24	$Ag_{40}Co_{5}Cs_{55}$	80	$Ag_{10}Co_{55}Cs_{35}$
25	$Ag_{35}Co_{10}Cs_{55}$	81	$Ag_{10}Co_{60}Cs_{35}$
26	$Ag_{30}Co_{15}Cs_{55}$	82	$Co_{65}Cs_{35}$
27	$Ag_{25}Co_{20}Cs_{55}$	83	$Ag_{70}Cs_{30}$
28	$Ag_{20}Co_{25}Cs_{55}$	84	$Ag_{65}Co_{5}Cs_{30}$
29	$Ag_{15}Co_{30}Cs_{55}$	85	$Ag_{60}Co_{10}Cs_{30}$
30	$Ag_{10}Co_{35}Cs_{55}$	86	$Ag_{55}Co_{15}Cs_{30}$
31	$Ag_{5}Co_{40}Cs_{55}$	87	$Ag_{50}Co_{20}Cs_{30}$
32	$Co_{45}Cs_{55}$	88	$Ag_{45}Co_{25}Cs_{30}$
33	$Ag_{50}Cs_{50}$	89	$Ag_{40}Co_{30}Cs_{30}$
34	$Ag_{45}Co_{5}Cs_{50}$	90	$Ag_{35}Co_{35}Cs_{30}$
35	$Ag_{40}Co_{10}Cs_{50}$	91	$Ag_{30}Co_{40}Cs_{30}$
36	$Ag_{35}Co_{15}Cs_{50}$	92	$Ag_{25}Co_{45}Cs_{30}$
37	$Ag_{30}Co_{20}Cs_{50}$	93	$Ag_{20}Co_{50}Cs_{30}$
38	$Ag_{25}Co_{25}Cs_{50}$	94	$Ag_{15}Co_{55}Cs_{30}$
39	$Ag_{20}Co_{30}Cs_{50}$	95	$Ag_{10}Co_{60}Cs_{30}$
40	$Ag_{15}Co_{35}Cs_{50}$	96	$Ag_{5}Co_{65}Cs_{30}$
41	$Ag_{10}Co_{40}Cs_{50}$	97	$Co_{70}Cs_{30}$
42	$Ag_{5}Co_{45}Cs_{50}$	98	$Ag_{75}Cs_{25}$
43	$Co_{50}Cs_{50}$	99	$Ag_{70}Co_{5}Cs_{25}$
44	$Ag_{55}Cs_{45}$	100	$Ag_{65}Co_{10}Cs_{25}$
45	$Ag_{50}Co_{5}Cs_{45}$	101	$Ag_{60}Co_{15}Cs_{25}$
46	$Ag_{45}Co_{10}Cs_{45}$	102	$Ag_{55}Co_{20}Cs_{25}$
47	$Ag_{40}Co_{15}Cs_{45}$	103	$Ag_{50}Co_{25}Cs_{25}$
48	$Ag_{35}Co_{20}Cs_{45}$	104	$Ag_{45}Co_{30}Cs_{25}$
49	$Ag_{30}Co_{25}Cs_{45}$	105	$Ag_{40}Co_{35}Cs_{25}$
50	$Ag_{25}Co_{30}Cs_{45}$	106	$Ag_{35}Co_{40}Cs_{25}$
51	$Ag_{20}Co_{35}Cs_{45}$	107	$Ag_{30}Co_{45}Cs_{25}$
52	$Ag_{15}Co_{40}Cs_{45}$	108	$Ag_{25}Co_{50}Cs_{25}$
53	$Ag_{10}Co_{45}Cs_{45}$	109	$Ag_{20}Co_{55}Cs_{25}$
54	$Ag_{5}Co_{50}Cs_{45}$	110	$Ag_{15}Co_{60}Cs_{25}$
55	$Co_{55}Cs_{45}$	111	$Ag_{10}Co_{65}Cs_{25}$
56	$Ag_{60}Cs_{40}$	112	$Ag_{5}Co_{70}Cs_{25}$

Position	Catalyst composition	Position	Catalyst composition
113	$Co_{75}Cs_{25}$	160	$Ag_{30}Co_{60}Cs_{10}$
114	$Ag_{80}Cs_{20}$	161	$Ag_{25}Co_{65}Cs_{10}$
115	$Ag_{75}Co_{5}Cs_{20}$	162	$Ag_{20}Co_{70}Cs_{10}$
116	$Ag_{70}Co_{10}Cs_{20}$	163	$Ag_{15}Co_{75}Cs_{10}$
117	$Ag_{65}Co_{15}Cs_{20}$	164	$Ag_{10}Co_{80}Cs_{10}$
118	$Ag_{60}Co_{20}Cs_{20}$	165	$Ag_{5}Co_{85}Cs_{10}$
119	$Ag_{55}Co_{25}Cs_{20}$	166	$Co_{90}Cs_{10}$
120	$Ag_{50}Co_{30}Cs_{20}$	167	$Ag_{95}Cs_{5}$
121	$Ag_{45}Co_{35}Cs_{20}$	168	$Ag_{90}Co_{5}Cs_{5}$
122	$Ag_{40}Co_{40}Cs_{20}$	169	$Ag_{85}Co_{10}Cs_{5}$
123	$Ag_{35}Co_{45}Cs_{20}$	170	$Ag_{80}Co_{15}Cs_{5}$
124	$Ag_{30}Co_{50}Cs_{20}$	171	$Ag_{75}Co_{20}Cs_{5}$
125	$Ag_{25}Co_{55}Cs_{20}$	172	$Ag_{70}Co_{25}Cs_{5}$
126	$Ag_{20}Co_{60}Cs_{20}$	173	$Ag_{65}Co_{30}Cs_{5}$
127	$Ag_{15}Co_{65}Cs_{20}$	174	$Ag_{60}Co_{35}Cs_{5}$
128	$Ag_{10}Co_{70}Cs_{20}$	175	$Ag_{55}Co_{40}Cs_{5}$
129	$Ag_{5}Co_{75}Cs_{20}$	176	$Ag_{50}Co_{45}Cs_{5}$
130	$Co_{80}Cs_{20}$	177	$Ag_{45}Co_{50}Cs_{5}$
131	$Ag_{80}Co_{5}Cs_{15}$	178	$Ag_{40}Co_{55}Cs_{5}$
132	$Ag_{75}Co_{10}Cs_{15}$	179	$Ag_{35}Co_{60}Cs_{5}$
133	$Ag_{70}Co_{15}Cs_{15}$	180	$Ag_{30}Co_{65}Cs_{5}$
134	$Ag_{65}Co_{20}Cs_{15}$	181	$Ag_{25}Co_{70}Cs_{5}$
135	$Ag_{60}Co_{25}Cs_{15}$	182	$Ag_{20}Co_{75}Cs_{5}$
136	$Ag_{55}Co_{30}Cs_{15}$	183	$Ag_{15}Co_{80}Cs_{5}$
137	$Ag_{50}Co_{35}Cs_{15}$	184	$Ag_{10}Co_{85}Cs_{5}$
138	$Ag_{45}Co_{40}Cs_{15}$	185	$Ag_{5}Co_{90}Cs_{5}$
139	$Ag_{40}Co_{45}Cs_{15}$	186	$Co_{95}Cs_{5}$
140	$Ag_{35}Co_{50}Cs_{15}$	187	$Ag_{95}Co_{5}$
141	$Ag_{30}Co_{55}Cs_{15}$	188	$Ag_{90}Co_{10}$
142	$Ag_{25}Co_{60}Cs_{15}$	189	$Ag_{85}Co_{15}$
143	$Ag_{20}Co_{65}Cs_{15}$	190	$Ag_{80}Co_{20}$
144	$Ag_{15}Co_{70}Cs_{15}$	191	$Ag_{75}Co_{25}$
145	$Ag_{10}Co_{75}Cs_{15}$	192	$Ag_{70}Co_{30}$
146	$Ag_{5}Co_{80}Cs_{15}$	193	$Ag_{65}Co_{35}$
147	$Co_{85}Cs_{15}$	194	$Ag_{60}Co_{40}$
148	$Ag_{90}Cs_{10}$	195	$Ag_{55}Co_{45}Cs_{5}$
149	$Ag_{85}Co_{5}Cs_{10}$	196	$Ag_{50}Co_{50}$
150	$Ag_{80}Co_{10}Cs_{10}$	197	$Ag_{45}Co_{55}$
151	$Ag_{75}Co_{15}Cs_{10}$	198	$Ag_{40}Co_{60}$
152	$Ag_{70}Co_{20}Cs_{10}$	199	$Ag_{35}Co_{75}$
153	$Ag_{65}Co_{25}Cs_{10}$	200	$Ag_{30}Cs_{70}$
154	$Ag_{60}Co_{30}Cs_{10}$	201	$Ag_{25}Co_{75}$
155	$Ag_{55}Co_{35}Cs_{10}$	202	$Ag_{20}Co_{80}$
156	$Ag_{50}Co_{40}Cs_{10}$	203	$Ag_{15}Co_{85}$
157	$Ag_{45}Co_{45}Cs_{10}$	204	$Ag_{10}Co_{90}$
158	$Ag_{40}Co_{50}Cs_{10}$	205	$Ag_{5}Co_{95}$
159	$Ag_{35}Co_{55}Cs_{10}$	206	

Library 11

Position	Catalyst composition	Position	Catalyst composition
1	Fe_{100}	58	$Ce_{20}Cu_{20}Fe_{60}$
2	$Cu_{20}Fe_{80}$	59	$Ce_{20}Cu_{40}Fe_{40}$
3	$Cu_{40}Fe_{60}$	60	$Ce_{20}Cu_{60}Fe_{20}$
4	$Cu_{60}Fe_{40}$	61	$Ce_{20}Cu_{80}$
5	$Cu_{60}Fe_{40}$	62	$Ce_{20}Cr_{20}Fe_{60}$
6	Cu_{100}	63	$Ce_{20}Cr_{20}Cu_{20}Fe_{40}$
7	$Cr_{20}Fe_{80}$	64	$Ce_{20}Cr_{20}Cu_{40}Fe_{20}$
8	$Cr_{20}Cu_{20}Fe_{60}$	65	$Ce_{20}Cr_{20}Cu_{60}$
9	$Cr_{20}Cu_{40}Fe_{40}$	66	$Ce_{20}Cr_{40}Fe_{40}$
10	$Cr_{20}Cu_{60}Fe_{20}$	67	$Ce_{20}Cr_{40}Cu_{20}Fe_{20}$
11	$Cr_{20}Cu_{80}$	68	$Ce_{20}Cr_{40}Cu_{40}$
12	$Cr_{40}Fe_{60}$	69	$Ce_{20}Cr_{60}Fe_{20}$
13	$Cr_{40}Cu_{20}Fe_{40}$	70	$Ce_{20}Cr_{60}Cu_{20}$
14	$Cr_{40}Cu_{40}Fe_{20}$	71	$Ce_{20}Cr_{80}$
15	$Cr_{40}Cu_{60}$	72	$Ce_{20}Co_{20}Fe_{60}$
16	$Cr_{40}Cu_{60}$	73	$Ce_{20}Co_{20}Cu_{20}Fe_{40}$
17	$Cr_{60}Cu_{20}Fe_{20}$	74	$Ce_{20}Co_{20}Cu_{40}Fe_{20}$
18	$Cr_{60}Cu_{40}$	75	$Ce_{20}Co_{20}Cr_{20}Fe_{40}$
19	$Cr_{80}Fe_{20}$	76	$Ce_{20}Co_{20}Cr_{20}Fe_{40}$
20	$Ce_{40}V_{40}La_{20}$	77	$Ce_{20}Co_{20}Cr_{20}Fe_{20}$
21	Cr_{100}	78	$Ce_{20}Co_{20}Cr_{20}Cu_{40}$
22	$Co_{20}Fe_{80}$	79	$Ce_{20}Co_{20}Cr_{40}Fe_{20}$
23	$Co_{20}Cu_{20}Fe_{60}$	80	$Ce_{20}Co_{20}Cr_{40}Cu_{20}$
24	$Co_{20}Cu_{40}Fe_{20}$	81	$Ce_{20}Co_{20}Cr_{60}$
25	$Co_{20}Cu_{60}Fe_{20}$	82	$Ce_{20}Co_{40}Fe_{40}$
26	$Co_{20}Cu_{80}$	83	$Ce_{20}Co_{40}Fe_{20}$
27	$Co_{20}Cr_{20}Fe_{60}$	84	$Ce_{20}Co_{40}Cu_{40}$
28	$Co_{20}Cr_{20}Cu_{20}Fe_{40}$	85	$Ce_{20}Co_{40}Cr_{20}Fe_{20}$
29	$Co_{20}Cr_{20}Cu_{40}Fe_{20}$	86	$Ce_{20}Co_{40}Cr_{20}Cu_{20}$
30	$Co_{20}Cr_{20}Cu_{60}$	87	$Ce_{20}Co_{40}Cr_{20}$
31	$Co_{20}Cr_{40}Fe_{40}$	88	$Ce_{20}Co_{60}Fe_{20}$
32	$Co_{20}Cr_{40}Cu_{20}Fe_{20}$	89	$Ce_{20}Co_{60}Cu_{20}$
33	$Co_{20}Cr_{40}Cu_{40}$	90	$Ce_{20}Co_{60}Cr_{20}$
34	$Co_{20}Cr_{60}Fe_{20}$	91	$Ce_{20}Co_{80}$
35	$Co_{20}Cr_{60}Cu_{20}$	92	$Ce_{40}Fe_{60}$
36	$Co_{20}Cr_{80}$	93	$Ce_{20}Cu_{20}Fe_{40}$
37	$Co_{40}Fe_{60}$	94	$Ce_{40}Cu_{40}Fe_{20}$
38	$Co_{40}Fe_{60}$	95	$Ce_{40}Cu_{60}$
39	$Co_{40}Cu_{40}Fe_{20}$	96	$Ce_{40}Cr_{20}Fe_{40}$
40	$Co_{40}Cu_{60}$	97	$Ce_{40}Cr_{20}Cu_{20}Fe_{20}$
41	$Co_{40}Cr_{20}Fe_{40}$	98	$Ce_{40}Cr_{20}Cu_{40}$
42	$Co_{40}Cr_{20}Cu_{20}Fe_{20}$	99	$Ce_{40}Cr_{40}Fe_{20}$
43	$Co_{40}Cr_{20}Cu_{40}$	100	$Ce_{40}Cr_{40}Cu_{20}$
44	$Co_{40}Cr_{40}Fe_{20}$	101	$Ce_{40}Cr_{60}$
45	$Co_{40}Cr_{40}Cu_{20}$	102	$Ce_{40}Co_{20}Fe_{40}$
46	$Co_{40}Cr_{60}$	103	$Ce_{40}Co_{20}Cu_{20}Fe_{20}$
47	$Co_{60}Fe_{40}$	104	$Ce_{40}Co_{20}Cu_{40}$
48	$Co_{60}Cu_{20}Fe_{20}$	105	$Ce_{40}Co_{20}Cr_{20}Fe_{20}$
49	$Co_{60}Cu_{40}$	106	$Ce_{40}Co_{20}Cr_{20}Cu_{20}$
50	$Co_{60}Cr_{20}Fe_{20}$	107	$Ce_{40}Co_{20}Cr_{40}$
51	$Co_{60}Cr_{20}Cu_{20}$	108	$Ce_{40}Co_{40}Fe_{20}$
52	$Co_{60}Cr_{40}$	109	$Ce_{40}Co_{40}Cu_{20}$
53	$Co_{80}Fe_{20}$	110	$Ce_{40}Co_{40}Cr_{20}$
54	$Co_{80}Cu_{20}$	111	$Ce_{40}Co_{40}$
55	$Co_{80}Cr_{20}$	112	$Ce_{60}Fe_{40}$
56	Co_{100}	113	$Ce_{60}Cu_{20}Fe_{20}$
57	$Ce_{20}Fe_{80}$	114	$Ce_{60}Cu_{40}$

Position	Catalyst composition	Position	Catalyst composition
115	$Ce_{60}Cr_{20}Fe_{20}$	121	$Ce_{60}Co_{40}$
116	$Ce_{60}Cr_{20}Cu_{20}$	122	$Ce_{80}Fe_{20}$
117	$Ce_{60}Cr_{40}$	123	$Ce_{80}Cu_{20}$
118	$Ce_{60}Co_{20}Fe_{20}$	124	$Ce_{80}Cr_{20}$
119	$Ce_{60}Co_{20}Cr_{20}$	125	$Ce_{80}Co_{20}$
120	$Ce_{60}Co_{20}Cr_{20}$	126	Ce_{100}

Library 12

Position	Catalyst composition	Position	Catalyst composition
1	$Ce_{40}Co_{20}V_{40}$	58	$Co_{20}V_{20}La_{60}$
2	$Co_{20}Mo_{80}$	59	$Co_{40}Mo_{20}La_{40}$
3	$Ce_{20}V_{20}La_{60}$	60	$Ce_{20}Co_{80}$
4	V_{100}	61	$Ce_{40}Co_{20}Mo_{20}La_{20}$
5	$Co_{60}Mo_{40}$	62	$Ce_{20}V_{40}La_{40}$
6	$Ce_{60}V_{40}$	63	$Ce_{20}V_{80}$
7	$Ce_{20}Mo_{80}$	64	$Ce_{80}Co_{20}$
8	$Mo_{60}La_{40}$	65	$Ce_{60}Mo_{20}La_{20}$
9	$V_{20}Mo_{60}La_{20}$	66	$Co_{80}V_{20}$
10	$V_{40}La_{60}$	67	$V_{80}La_{20}$
11	$Ce_{20}Co_{40}Mo_{40}$	68	$V_{60}Mo_{40}$
12	$V_{60}La_{40}$	69	$Ce_{40}Mo_{40}$
13	$Co_{60}V_{40}$	70	$Co_{20}V_{60}La_{20}$
14	$Ce_{40}Co_{20}La_{40}$	71	$Mo_{40}La_{60}$
15	$Ce_{60}V_{20}La_{20}$	72	$Ce_{60}Co_{20}Mo_{20}$
16	$Ce_{20}Co_{60}La_{20}$	73	$Co_{80}La_{20}$
17	$Ce_{20}Co_{20}V_{20}Mo_{20}La_{20}$	74	$Ce_{20}V_{20}Mo_{40}$
18	$Ce_{80}V_{20}$	75	$Co_{20}V_{80}$
19	$Mo_{80}La_{20}$	76	$Co_{20}V_{40}Mo_{40}$
20	$Ce_{40}V_{40}La_{20}$	77	$Ce_{20}Co_{40}La_{40}$
21	$Ce_{40}Co_{20}Mo_{40}$	78	$Ce_{20}Co_{20}Mo_{40}La_{20}$
22	$Ce_{20}La_{80}$	79	$V_{20}Mo_{40}La_{40}$
23	$V_{80}Mo_{20}$	80	$Co_{80}Mo_{20}$
24	$Ce_{20}Co_{60}Mo_{20}$	81	La_{100}
25	$Ce_{40}Co_{40}Mo_{20}$	82	$Ce_{60}Mo_{40}$
26	$Ce_{40}V_{20}Mo_{20}La_{20}$	83	$Co_{40}Mo_{60}$
27	$Ce_{20}Co_{20}V_{60}$	84	$Ce_{20}Co_{40}Mo_{20}La_{20}$
28	$Ce_{40}V_{20}Mo_{20}$	85	$Ce_{20}V_{40}Mo_{40}$
29	$Co_{20}V_{60}Mo_{20}$	86	$Co_{20}Mo_{60}La_{20}$
30	$Ce_{20}V_{60}Mo_{20}$	87	$V_{40}Mo_{60}$
31	$Ce_{20}Mo_{40}La_{40}$	88	$Co_{20}V_{20}Mo_{20}La_{40}$
32	$Co_{40}V_{20}Mo_{40}$	89	$Ce_{40}Co_{20}V_{20}La_{20}$
33	$Ce_{20}V_{20}Mo_{60}$	90	$Ce_{20}Co_{40}V_{20}Mo_{20}$
34	$Ce_{20}Co_{40}V_{40}$	91	$Mo_{20}La_{80}$
35	$V_{40}Mo_{40}La_{20}$	92	$Co_{20}Mo_{20}La_{60}$
36	$Ce_{60}La_{40}$	93	$Co_{40}V_{40}Mo_{20}$
37	$Ce_{40}Co_{40}La_{20}$	94	$Ce_{40}V_{40}Mo_{20}$
38	$Ce_{20}V_{20}Mo_{20}La_{40}$	95	$Ce_{40}V_{20}La_{40}$
39	$Co_{40}V_{60}$	96	$Ce_{20}Mo_{20}La_{60}$
40	$Ce_{20}Co_{20}V_{40}La_{20}$	97	$Ce_{60}Co_{20}V_{20}$
41	$Co_{60}V_{20}La_{20}$	98	$Ce_{20}Mo_{60}La_{20}$
42	$Ce_{40}Co_{60}$	99	$Co_{40}V_{40}La_{20}$
43	$Ce_{40}La_{60}$	100	$Co_{40}V_{20}Mo_{20}La_{20}$
44	$Ce_{40}Mo_{20}La_{40}$	101	$Co_{40}Mo_{40}La_{20}$
45	$Co_{20}V_{20}Mo_{40}La_{20}$	102	$V_{40}Mo_{20}La_{40}$
46	$Ce_{20}Co_{20}Mo_{20}La_{40}$	103	$Ce_{80}Mo_{20}$
47	$Ce_{20}Co_{20}V_{20}La_{40}$	104	$Ce_{80}La_{20}$
48	$Ce_{20}Co_{20}Mo_{60}$	105	$Co_{20}V_{40}Mo_{20}La_{20}$
49	$Ce_{20}Co_{20}V_{20}Mo_{40}$	106	$Ce_{60}Co_{20}La_{20}$
50	$V_{20}Mo_{20}La_{60}$	107	$Ce_{40}V_{60}$
51	$V_{20}La_{80}$	108	$V_{20}Mo_{80}$
52	$Ce_{20}Co_{40}V_{20}La_{20}$	109	$Ce_{20}V_{60}La_{20}$
53	$Co_{20}La_{80}$	110	$Ce_{20}Co_{20}La_{60}$
54	Ce_{100}	111	$Co_{60}V_{20}Mo_{20}$
55	$Ce_{40}Co_{20}V_{20}Mo_{20}$	112	$V_{60}Mo_{20}La_{20}$
56	$Co_{20}V_{20}Mo_{60}$	113	Co_{100}
57	$Co_{20}Mo_{40}La_{40}$	114	$Ce_{40}Mo_{60}$

Position	Catalyst composition	Position	Catalyst composition
115	$Ce_{40}Co_{40}V_{20}$	121	Co_{60} $Mo_{20}La_{20}$
116	$Ce_{60}Co_{40}$	122	$Ce_{20}Co_{20}V_{40}Mo_{20}$
117	$Ce_{60}V_{20}Mo_{20}$	123	Mo_{100}
118	$Co_{60}La_{40}$	124	$Ce_{20}V_{40}Mo_{20}La_{20}$
119	$Co_{40}La_{60}$	125	$Co_{20}V_{40}La_{40}$
120	$Co_{40}V_{20}La_{40}$	126	$Ce_{20}Co_{60}V_{20}$

Library 13

Position	Catalyst composition	Position	Catalyst composition
1	$Cr_{80}Mn_{20}$	58	$Cr_{20}Fe_{40}Mo_{40}$
2	$Fe_{40}Mn_{20}Mo_{40}$	59	$Cr_{20}Fe_{20}Mo_{60}$
3	$Cr_{20}Cu_{40}Fe_{20}Mn_{20}$	60	$Cr_{20}Cu_{20}Fe_{60}$
4	$Cr_{20}Fe_{20}Mn_{40}Mo_{20}$	61	$Cr_{20}Cu_{40}Fe_{20}Mo_{20}$
5	$Cr_{60}Cu_{20}Fe_{20}$	62	$Cr_{60}Cu_{20}Mn_{20}$
6	$Fe_{40}Mn_{60}$	63	$Cr_{40}Cu_{20}Mn_{40}$
7	$Cr_{60}Fe_{20}Mo_{20}$	64	$Cr_{80}Mo_{20}$
8	$Fe_{20}Mn_{80}$	65	$Cr_{40}Cu_{20}Mo_{40}$
9	Fe_{100}	66	$Cu_{60}Fe_{20}Mn_{20}$
10	$Cr_{20}Cu_{40}Mo_{40}$	67	$Cu_{80}Fe_{20}$
11	$Cr_{20}Cu_{80}$	68	$Cr_{40}Cu_{20}Fe_{20}Mn_{20}$
12	$Cu_{40}Fe_{40}Mo_{20}$	69	$Cr_{60}Fe_{40}$
13	$Mn_{60}Mo_{40}$	70	$Cu_{20}Fe_{40}Mo_{40}$
14	$Cr_{20}Cu_{20}Mn_{60}$	71	$Cu_{20}Mn_{20}Mo_{60}$
15	$Cu_{20}Mn_{80}$	72	$Cr_{20}Cu_{60}Mo_{20}$
16	$Cr_{40}Mn_{60}$	73	$Cr_{20}Cu_{20}Fe_{40}Mn_{20}$
17	$Mn_{20}Mo_{80}$	74	$Cu_{60}Fe_{40}$
18	$Cr_{40}Fe_{40}Mn_{20}$	75	$Cr_{40}Mn_{20}Mo_{40}$
19	$Fe_{60}Mo_{40}$	76	$Cr_{20}Cu_{20}Mo_{60}$
20	$Cu_{20}Fe_{60}Mo_{20}$	77	$Cr_{40}Fe_{20}Mo_{40}$
21	$Cu_{80}Mn_{20}$	78	$Cr_{20}Cu_{20}Mn_{40}Mo_{20}$
22	$Cr_{20}Cu_{20}Fe_{20}Mo_{40}$	79	$Cu_{40}Mo_{60}$
23	$Cr_{80}Cu_{20}$	80	$Cr_{40}Cu_{20}Fe_{40}$
24	$Cu_{40}Fe_{20}Mn_{40}$	81	$Cr_{40}Cu_{20}Mn_{40}$
25	$Cr_{60}Cu_{40}$	82	$Cr_{80}Fe_{20}$
26	$Cu_{40}Fe_{60}$	83	$Cr_{60}Cu_{20}Mo_{20}$
27	$Mn_{80}Mo_{20}$	84	$Cu_{20}Mn_{60}Mo_{20}$
28	$Cu_{20}Mn_{40}Mo_{40}$	85	$Fe_{60}Mn_{20}Mo_{20}$
29	$Fe_{60}Mn_{40}$	86	$Cr_{40}Cu_{40}Mo_{20}$
30	$Cr_{20}Mn_{60}Mo_{20}$	87	$Cr_{20}Cu_{20}Fe_{20}Mn_{40}$
31	$Fe_{80}Mo_{20}$	88	$Cr_{20}Cu_{40}Fe_{40}$
32	$Cu_{40}Fe_{20}Mo_{40}$	89	$Cr_{40}Fe_{60}$
33	$Cu_{60}Mo_{40}$	90	$Cr_{60}Fe_{20}Mn_{20}$
34	$Cr_{20}Fe_{20}Mn_{60}$	91	$Cr_{40}Fe_{20}Mn_{20}Mo_{20}$
35	$Cr_{20}Fe_{60}Mn_{20}$	92	$Cr_{20}Mo_{80}$
36	$Cu_{40}Fe_{20}Mn_{20}Mo_{20}$	93	$Cr_{40}Cu_{20}Fe_{20}Mo_{20}$
37	$Mn_{40}Mo_{60}$	94	$Cu_{80}Mo_{20}$
38	Mo_{100}	95	Cr_{100}
39	$Cr_{40}Cu_{60}$	96	$Cr_{20}Fe_{20}Mn_{20}Mo_{40}$
40	$Fe_{20}Mo_{80}$	97	$Cu_{60}Mn_{40}$
41	$Cr_{40}Mn_{40}Mo_{20}$	98	$Cu_{40}Mn_{40}Mo_{20}$
42	$Cu_{40}Fe_{40}Mn_{20}$	99	$Cr_{20}Cu_{40}Mn_{40}$
43	$Cr_{20}Fe_{80}$	100	$Cu_{20}Fe_{20}Mn_{60}$
44	$Cu_{40}Mn_{20}Mo_{40}$	101	$Cr_{20}Cu_{20}Mn_{20}Mo_{40}$
45	$Cu_{20}Fe_{40}Mn_{40}$	102	$Cr_{20}Fe_{40}Mn_{40}$
46	$Cr_{60}Mo_{40}$	103	$Cr_{20}Cu_{60}Mn_{20}$
47	$Cr_{20}Cu_{40}Mn_{20}Mo_{20}$	104	$Cr_{20}Fe_{40}Mn_{20}Mo_{20}$
48	$Cr_{20}Mn_{80}$	105	Mn_{100}
49	$Cr_{40}Mo_{60}$	106	$Cr_{40}Cu_{40}Fe_{20}$
50	$Cr_{20}Cu_{20}Fe_{40}Mo_{20}$	107	$Cu_{40}Mn_{60}$
51	$Cu_{60}Mn_{20}Mo_{20}$	108	$Fe_{20}Mn_{60}$
52	$Cr_{20}Cu_{20}Fe_{20}Mn_{20}Mo_{20}$	109	$Cu_{20}Mo_{80}$
53	$Fe_{40}Mo_{60}$	110	$Cr_{20}Fe_{60}Mo_{20}$
54	$Fe_{80}Mn_{20}$	111	$Cr_{40}Fe_{40}Mo_{20}$
55	$Cu_{20}Fe_{40}Mn_{20}Mo_{20}$	112	$Cr_{40}Cu_{20}Mn_{20}Mo_{20}$
56	$Cu_{20}Fe_{20}Mn_{20}Mo_{40}$	113	$Fe_{20}Mn_{40}Mo_{40}$
57	$Cu_{60}Fe_{20}Mo_{20}$	114	$Cr_{20}Cu_{60}Fe_{20}$

Position	Catalyst composition	Position	Catalyst composition
115	Cu_{100}	161	$Ce_{40}La_{20}Fe_{40}$
116	$Cu_{20}Fe_{20}Mo_{60}$	162	$Ce_{40}Cu_{60}$
117	$Cu_{20}Fe_{20}Mn_{40}Mo_{20}$	163	$Ce_{20}La_{80}$
118	$Cu_{20}Fe_{20}Mn_{40}Mo_{20}$	164	$Cu_{60}K_{20}La_{20}$
119	$Cr_{40}Fe_{20}Mn_{40}$	165	$Ce_{20}La_{60}Fe_{20}$
120	$Cr_{20}Mn_{20}Mo_{60}$	166	$Ce_{20}Cu_{20}K_{20}Fe_{40}$
121	$Cr_{60}Mn_{40}$	167	$Ce_{20}Fe_{80}$
122	$Cr_{60}Mn_{20}Mo_{20}$	168	$Ce_{40}K_{40}Fe_{20}$
123	$Cu_{20}Fe_{60}Mn_{20}$	169	$Ce_{40}Cu_{40}Fe_{20}$
124	$Cr_{20}Mn_{40}Mo_{40}$	170	$Ce_{20}K_{20}La_{20}Fe_{40}$
125	$Cu_{20}Fe_{80}$	171	$Cu_{20}La_{20}Fe_{60}$
126	$Fe_{40}Mn_{40}Mo_{20}$	172	$K_{40}La_{60}$
127	$Cu_{40}Fe_{60}$	173	$K_{20}La_{40}Fe_{40}$
128	$Ce_{40}Cu_{20}K_{20}Fe_{20}$	174	$Ce_{20}K_{80}$
129	$Ce_{20}K_{40}La_{20}Fe_{20}$	175	$Cu_{40}La_{60}$
130	$Ce_{60}Fe_{40}$	176	$Ce_{60}Cu_{20}La_{20}$
131	$Cu_{20}K_{20}La_{40}Fe_{20}$	177	$Ce_{40}Cu_{20}K_{40}$
132	$Cu_{20}K_{40}La_{20}Fe_{20}$	178	$Ce_{60}Cu_{20}Fe_{20}$
133	$Cu_{20}K_{40}La_{40}$	179	$Ce_{20}K_{40}La_{40}$
134	$Cu_{20}K_{20}Fe_{60}$	180	$K_{40}Fe_{60}$
135	$Ce_{20}Cu_{40}La_{20}Fe_{20}$	181	$K_{80}Fe_{20}$
136	$Ce_{20}Cu_{20}K_{60}$	182	$Ce_{60}K_{40}$
137	$Ce_{20}Cu_{40}Fe_{40}$	183	$Ce_{60}Cu_{40}$
138	$Ce_{20}Cu_{20}K_{40}Fe_{20}$	184	$Cu_{20}K_{40}Fe_{40}$
139	$Ce_{20}K_{40}Fe_{40}$	185	$Ce_{20}K_{20}La_{60}$
140	$Ce_{20}Cu_{40}K_{20}$	186	$Ce_{40}Cu_{20}Fe_{40}$
141	$Ce_{60}Cu_{20}K_{20}$	187	$Cu_{40}La_{40}Fe_{20}$
142	$Ce_{20}Cu_{80}$	188	$Ce_{40}K_{20}La_{40}$
143	$Cu_{40}K_{20}La_{20}Fe_{20}$	189	$Cu_{20}La_{40}Fe_{40}$
144	$K_{20}La_{60}Fe_{20}$	190	$Cu_{20}K_{80}$
145	$Ce_{80}Fe_{20}$	191	$Ce_{40}Cu_{20}K_{20}La_{20}$
146	$Ce_{20}Cu_{40}K_{20}La_{20}$	192	$Ce_{20}Cu_{20}La_{40}Fe_{20}$
147	$Ce_{20}K_{60}La_{20}$	193	$Ce_{80}Cu_{20}$
148	$Cu_{60}La_{20}Fe_{20}$	194	$Ce_{80}La_{20}$
149	$Ce_{20}K_{20}La_{40}Fe_{20}$	195	$Cu_{20}K_{20}La_{60}$
150	$Ce_{20}Cu_{20}Fe_{60}$	196	$Ce_{20}Cu_{20}La_{20}Fe_{40}$
151	$Ce_{60}La_{40}$	197	$Cu_{60}La_{40}$
152	$Ce_{20}K_{20}Fe_{60}$	198	$Cu_{20}La_{60}Fe_{20}$
153	$Ce_{60}K_{20}La_{20}$	199	$La_{20}Fe_{80}$
154	Ce_{100}	200	$Ce_{60}K_{20}Fe_{20}$
155	$Cu_{80}La_{20}$	201	$Ce_{40}La_{40}Fe_{20}$
156	$Cu_{40}La_{20}Fe_{40}$	202	$Ce_{80}K_{20}$
157	$Ce_{40}La_{60}$	203	
158	$Cu_{80}K_{20}$	204	
159	$Ce_{20}Cu_{60}K_{20}$	205	
160	$Cu_{20}La_{80}$	206	

Library 14

Position	Catalyst composition	Position	Catalyst composition
1	$Ce_{10}Co_{40}Mo_{50}$	57	$Ce_{80}Co_{10}Mo_{10}$
2	$Ce_{5}Co_{35}Mo_{60}$	58	$Ce_{35}Mo_{65}$
3	$Ce_{5}Co_{70}Mo_{25}$	59	$Ce_{75}Mo_{25}$
4	$Ce_{20}Co_{70}Mo_{10}$	60	$Ce_{25}Co_{15}Mo_{60}$
5	$Ce_{5}Co_{55}Mo_{40}$	61	$Ce_{20}Co_{35}Mo_{45}$
6	$Ce_{40}Co_{60}$	62	$Ce_{25}Co_{5}Mo_{70}$
7	$Ce_{10}Co_{85}Mo_{5}$	63	$Ce_{50}Co_{40}Mo_{10}$
8	$Ce_{15}Co_{85}$	64	$Ce_{10}Co_{65}Mo_{25}$
9	$Co_{10}Mo_{90}$	65	$Ce_{35}Co_{60}Mo_{5}$
10	$Ce_{15}Co_{40}Mo_{45}$	66	$Ce_{15}Co_{70}Mo_{15}$
11	$Ce_{20}Co_{65}Mo_{15}$	67	$Ce_{40}Co_{20}Mo_{40}$
12	$Ce_{20}Co_{25}Mo_{55}$	68	$Co_{35}Mo_{65}$
13	$Ce_{20}Co_{60}Mo_{20}$	69	$Ce_{60}Co_{25}Mo_{15}$
14	$Ce_{10}Co_{25}Mo_{65}$	70	$Co_{80}Mo_{20}$
15	$Ce_{20}Co_{15}Mo_{65}$	71	$Ce_{40}Co_{5}Mo_{55}$
16	$Ce_{75}Co_{10}Mo_{15}$	72	$Ce_{55}Co_{35}Mo_{10}$
17	$Ce_{35}Co_{5}Mo_{60}$	73	$Ce_{90}Co_{5}Mo_{5}$
18	$Ce_{50}Co_{15}Mo_{35}$	74	$Ce_{30}Co_{25}Mo_{45}$
19	$Ce_{25}Co_{70}Mo_{5}$	75	$Ce_{30}Co_{65}Mo_{5}$
20	$Ce_{65}Co_{30}Mo_{5}$	76	$Ce_{10}Co_{30}Mo_{60}$
21	$Ce_{10}Co_{45}Mo_{45}$	77	$Ce_{30}Co_{50}Mo_{20}$
22	$Ce_{15}Co_{55}Mo_{30}$	78	$Ce_{15}Co_{60}Mo_{25}$
23	$Ce_{25}Co_{65}Mo_{10}$	79	$Ce_{20}Co_{75}Mo_{5}$
24	$Ce_{70}Co_{5}Mo_{25}$	80	$Ce_{50}Co_{30}Mo_{20}$
25	$Ce_{50}Co_{35}Mo_{15}$	81	$Ce_{30}Co_{70}$
26	$Ce_{10}Co_{20}Mo_{70}$	82	$Ce_{80}Mo_{20}$
27	$Ce_{60}Mo_{40}$	83	$Ce_{45}Co_{55}$
28	$Ce_{65}Co_{10}Mo_{25}$	84	$Ce_{70}Mo_{30}$
29	$Ce_{5}Co_{60}Mo_{35}$	85	$Ce_{35}Co_{65}$
30	$Ce_{10}Co_{80}Mo_{10}$	86	$Ce_{85}Co_{10}Mo_{5}$
31	$Ce_{10}Co_{60}Mo_{30}$	87	$Ce_{5}Co_{80}Mo_{15}$
32	$Ce_{5}Co_{75}Mo_{20}$	88	$Ce_{30}Co_{15}Mo_{55}$
33	$Ce_{55}Co_{30}Mo_{15}$	89	$Co_{40}Mo_{60}$
34	$Ce_{20}Co_{40}Mo_{40}$	90	$Ce_{35}Co_{35}Mo_{30}$
35	$Ce_{20}Co_{55}Mo_{25}$	91	$Ce_{20}Co_{20}Mo_{60}$
36	$Ce_{5}Co_{40}Mo_{55}$	92	$Ce_{50}Co_{25}Mo_{25}$
37	$Co_{50}Mo_{50}$	93	$Ce_{70}Co_{10}Mo_{20}$
38	$Ce_{55}Co_{45}$	94	$Ce_{95}Mo_{5}$
39	$Ce_{20}Co_{10}Mo_{70}$	95	$Ce_{55}Co_{40}Mo_{5}$
40	$Ce_{30}Co_{35}Mo_{35}$	96	$Ce_{5}Co_{25}Mo_{70}$
41	Ce_{100}	97	$Ce_{15}Co_{20}Mo_{65}$
42	$Ce_{20}Mo_{80}$	98	$Ce_{75}Co_{15}Mo_{10}$
43	$Ce_{55}Co_{15}Mo_{30}$	99	$Ce_{15}Co_{30}Mo_{55}$
44	$Ce_{45}Co_{40}Mo_{15}$	100	$Ce_{30}Co_{20}Mo_{50}$
45	$Ce_{65}Co_{5}Mo_{30}$	101	$Ce_{55}Co_{5}Mo_{40}$
46	$Ce_{70}Co_{15}Mo_{15}$	102	$Ce_{40}Co_{45}Mo_{15}$
47	$Ce_{45}Co_{30}Mo_{25}$	103	$Ce_{45}Co_{10}Mo_{45}$
48	$Ce_{5}Co_{5}Mo_{90}$	104	Ce80Co5Mo$_{15}$
49	$Ce_{30}Co_{30}Mo_{40}$	105	$Ce_{40}Co_{25}Mo_{35}$
50	$Ce_{60}Co_{10}Mo_{30}$	106	$Ce_{5}Co_{15}Mo_{80}$
51	$Ce_{80}Co_{15}Mo_{5}$	107	$Ce_{50}Mo_{50}$
52	$Ce_{50}Co_{10}Mo_{40}$	108	$Ce_{30}Co_{5}Mo_{65}$
53	$Ce_{15}Co_{80}Mo_{5}$	109	$Ce_{35}Co_{50}Mo_{15}$
54	$Ce_{5}Co_{85}Mo_{10}$	110	$Ce_{20}Co_{30}Mo_{50}$
55	$Ce_{45}Co_{45}Mo_{10}$	111	$Ce_{40}Co_{10}Mo_{50}$
56	$Ce_{55}Co_{25}Mo_{20}$	112	$Ce_{15}Co_{25}Mo_{60}$

Position	Catalyst composition	Position	Catalyst composition
113	$Co_{75}Mo_{25}$	155	$Ce_{65}Co_{35}$
114	$Co_{90}Mo_{10}$	156	$Ce_{35}Co_{25}Mo_{40}$
115	$Ce_5Co_{45}Mo_{50}$	157	$Ce_{20}Co_{45}Mo_{35}$
116	$Ce_{40}Co_{35}Mo_{25}$	158	$Co_{45}Mo_{55}$
117	$Ce_{15}Co_5Mo_{80}$	159	$Ce_{75}Co_{25}$
118	$Ce_5Co_{90}Mo_5$	160	$Ce_{10}Co_{75}Mo_{15}$
119	$Ce_{75}Co_5Mo_{20}$	161	$Ce_{40}Co_{50}Mo_{10}$
120	$Co_{45}Mo_5Mo_{50}$	162	$Ce_{10}Co_{50}Mo_{40}$
121	$Ce_{15}Co_{50}Mo_{35}$	163	$Ce_{25}Co_{10}Mo_{65}$
122	$Ce_{30}Co_{60}Mo_{10}$	164	$Ce_{70}Co_{20}Mo_{10}$
123	$Ce_{35}Co_{45}Mo_{20}$	165	$Ce_{30}Co_{55}Mo_{15}$
124	$Ce_{25}Co_{25}Mo_{50}$	166	$Ce_5Co_{30}Mo_{65}$
125	$Ce_{45}Mo_{55}$	167	$Ce_{50}Co_{20}Mo_{30}$
126	$Ce_{35}Co_{20}Mo_{45}$	168	$Ce_{25}Co_{75}$
127	$Ce_{65}Co_{20}Mo_{15}$	169	$Ce_{30}Co_{45}Mo_{25}$
128	$Ce_{75}Co_{20}Mo_5$	170	$Ce_{20}Co_{80}$
129	$Ce_{10}Co_{70}Mo_{20}$	171	$Ce_{55}Co_{20}Mo_{25}$
130	$Ce_{85}Co_5Mo_{10}$	172	$Ce_{70}Co_{30}$
131	$Ce_{70}Co_{25}Mo_5$	173	$Ce_5Co_{50}Mo_{45}$
132	$Ce_{60}Co_{30}Mo_{10}$	174	$Ce_{40}Co_{15}Mo_{45}$
133	$Ce_{25}Co_{35}Mo_{40}$	175	$Ce_{50}Co_5Mo_{45}$
134	$Ce_{15}Co_{65}Mo_{20}$	176	$Ce_{45}Co_{15}Mo_{40}$
135	$Ce_{10}Co_{55}Mo_{35}$	177	$Ce_{60}Co_{35}Mo_5$
136	$Co_{85}Mo_{15}$	178	$Ce_{60}Co_{15}Mo_{25}$
137	$Ce_{60}Co_{20}Mo_{20}$	179	$Ce_{60}Mo_{40}$
138	$Ce_{35}Mo_{30}$ Mo_{35}	180	
139	$Ce_{35}Co_{15}Mo_{50}$	181	$Ce_{25}Co_{20}Mo_{55}$
140	$Ce_{60}Co_5Mo_{35}$	182	$Ce_{25}Co_{30}Mo_{45}$
141	$Ce_{25}Co_{45}Mo_{30}$	183	$Ce_{25}Co_{40}Mo_{35}$
142	$Ce_{25}Co_{50}Mo_{25}$	184	$Ce_{45}Co_{35}Mo_{20}$
143	$Ce_{40}Co_{40}Mo_{20}$	185	$Ce_{50}Co_{50}$
144	$Ce_{65}Co_{15}Mo_{20}$	186	$Ce_{15}Co_{45}Mo_{40}$
145	$Ce_{25}Co_{60}Mo_{15}$	187	$Ce_{20}Co_{50}Mo_{30}$
146	$Ce_{25}Co_{55}Mo_{20}$	188	$Ce_{15}Co_{35}Mo_{50}$
147	$Ce_{45}Co_{20}Mo_{35}$	189	$Ce_{15}Co_{75}Mo_{10}$
148	$Ce_{55}Co_{10}Mo_{35}$	190	$Ce_{35}Co_{55}Mo_{10}$
149	$Ce_{40}Co_{55}Mo_5$	191	$Ce_{10}Co_{35}Mo_{55}$
150	$Ce_{50}Co_{45}Mo_5$	192	$Ce_{10}Co_{90}$
151	$Ce_{20}Co_{20}Mo_{75}$	193	$Co_{95}Mo_5$
152	$Ce_{30}Mo_{70}$	194	$Ce_{65}Mo_{35}$
153	$Ce_{45}Co_{50}Mo_5$	195	$Ce_5Co_{65}Mo_{30}$
154	$Ce_{35}Co_{40}Mo_{25}$	196	$Ce_5Co_{65}Mo_{30}$

Library 15

Position	Catalyst composition	Position	Catalyst composition
1	$Pr_2V_1Fe_2/AlO_x$	45	$Cs_2V_1Fe_2/AlO_x$
2		46	$Lu_2V_1Fe_2/AlO_x$
3	$La_2V_1Fe_2/AlO_x$	47	$Mn_2V_1Fe_2/AlO_x$
4		48	$Yb_2V_1Fe_2/AlO_x$
5	$Mo_2V_1Fe_2/AlO_x$	49	$Cr_2V_1Fe_2/AlO_x$
6		50	$Ho_2V_1Fe_2/AlO_x$
7	$Li_2V_1Fe_2/AlO_x$	51	$Ag_2V_1Fe_2/AlO_x$
8		52	
9		53	
10	$Ca_2V_1Fe_2/AlO_x$	54	
11		55	
12	$Rb_2V_1Fe_2/AlO_x$	56	
13		57	
14	$Ti_2V_1Fe_2/AlO_x$	58	
15		59	
16	$Na_2V_1Fe_2/AlO_x$	60	
17		61	
18	$In_2V_1Fe_2/AlO_x$	62	
19		63	
20	$Gd_2V_1Fe_2/AlO_x$	64	
21		65	
22	$Mg_2V_1Fe_2/AlO_x$	66	$Zr_2V_1Fe_2/AlO_x$
23		67	$Ga_2V_1Fe_2/AlO_x$
24	$Sm_2V_1Fe_2/AlO_x$	68	$Ba_2V_1Fe_2/AlO_x$
25		69	$Te_2V_1Fe_2/AlO_x$
26	$_2V_1Fe_2/AlO_x$	70	$Cu_2V_1Fe_2/AlO_x$
27		71	$Sc_2V_1Fe_2/AlO_x$
28	$Ce_2V_1Fe_2/AlO_x$	72	$Ta_2V_1Fe_2/AlO_x$
29		73	$Si_2V_1Fe_2/AlO_x$
30	$Ge_2V_1Fe_2/AlO_x$	74	$Nd_2V_1Fe_2/AlO_x$
31		75	$Sn_2V_1Fe_2/AlO_x$
32	$B_2V_1Fe_2/AlO_x$	76	$Y_2V_1Fe_2/AlO_x$
33	$Se_2V_1Fe_2/AlO_x$	77	$Eu_2V_1Fe_2/AlO_x$
34	$Tb_2V_1Fe_2/AlO_x$	78	$Sb_2V_1Fe_2/AlO_x$
35	$Dy_2V_1Fe_2/AlO_x$	79	$K_2V_1Fe_2/AlO_x$
36	$Zn_2V_1Fe_2/AlO_x$	80	
37	$Er_2V_1Fe_2/AlO_x$	81	$Ni_2V_1Fe_2/AlO_x$
38	$Nb_2V_1Fe_2/AlO_x$	82	$Ru_2V_1Fe_2/AlO_x$
39	$Tm_2V_1Fe_2/AlO_x$	83	$Ir_2V_1Fe_2/AlO_x$
40	$Cd_2V_1Fe_2/AlO_x$	84	$Rh_2V_1Fe_2/AlO_x$
41	$W_2V_1Fe_2/AlO_x$		
42			
43			
44	$Hf_2V_1Fe_2/AlO_x$		

Library 16

Position	Catalyst composition	Position	Catalyst composition
111	$Gd_2V_1Cs_2/AlO_x$	159	
112	$Ba_2V_1Cs_2/AlO_x$	160	
113	$Tm_2V_1Cs_2/AlO_x$	161	
114	$Tb_2V_1Cs_2/AlO_x$	162	
115		163	
116	$Cu_2V_1Cs_2/AlO_x$	164	
117		165	
118	$Zn_2V_1Cs_2/AlO_x$	166	
119	$W_2V_1Cs_2/AlO_x$	167	
120	$B_2V_1Cs_2/AlO_x$	168	
121		169	$Yb_2V_1Cs_2/AlO_x$
122	$Ir_2V_1Cs_2/AlO_x$	170	$Te_2V_1Cs_2/AlO_x$
123		171	$Mn_2V_1Cs_2/AlO_x$
124		172	$Ce_2V_1Cs_2/AlO_x$
125		173	$Fe_2V_1Cs_2/AlO_x$
126	$Rb_2V_1Cs_2/AlO_x$	174	$Ca_2V_1Cs_2/AlO_x$
127		175	$Se_2V_1Cs_2/AlO_x$
128		176	$Ln_2V_1Cs_2/AlO_x$
129		177	$Dy_2V_1Cs_2/AlO_x$
130		178	$Cr_2V_1Cs_2/AlO_x$
131		179	$Hf_2V_1Cs_2/AlO_x$
132		180	$Li_2V_1Cs_2/AlO_x$
133		181	$Eu_2V_1Cs_2/AlO_x$
134		182	
135		183	$Ge_2V_1Cs_2/AlO_x$
136		184	$Pr_2V_1Cs_2/AlO_x$
137		185	$Mg_2V_1Cs_2/AlO_x$
138		186	
139		187	
140		188	$La_2V_1Cs_2/AlO_x$
141		189	$Sb_2V_1Cs_2/AlO_x$
142	$Mo_2V_1Cs_2/AlO_x$	190	
143		191	$Nb_2V_1Cs_2/AlO_x$
144	$K_2V_1Cs_2/AlO_x$	192	$Ta_2V_1Cs_2/AlO_x$
145	$Cd_2V_1Cs_2/AlO_x$	193	$Ti_2V_1Cs_2/AlO_x$
146	$Ga_2V_1Cs_2/AlO_x$	194	
147	$Sm_2V_1Cs_2/AlO_x$	195	$Sn_2V_1Cs_2/AlO_x$
148	$Ho_2V_1Cs_2/AlO_x$	196	$Na_2V_1Cs_2/AlO_x$
149	$Y_2V_1Cs_2/AlO_x$	197	
150	$Ni_2V_1Cs_2/AlO_x$	198	$Zr_2V_1Cs_2/AlO_x$
151	$Er_2V_1Cs_2/AlO_x$	199	
152	$Lu_2V_1Cs_2/AlO_x$	200	$Ag_2V_1Cs_2/AlO_x$
153	$Si_2V_1Cs_2/AlO_x$	201	
154		202	$Nd_2V_1Cs_2/AlO_x$
155	$Rh_2V_1Cs_2/AlO_x$	203	
156	$Rh_2V_1Cs_2/AlO_x$	204	$Sc_2V_1Cs_2/AlO_x$
157		205	
158		206	$Ru_2V_1Cs_2/AlO_x$

Erklärung

Hiermit versichere ich an Eides statt, dass ich die vorliegende Arbeit selbständig und ohne Benutzung anderer als der angegebenen Hilfsmittel angefertigt habe. Die aus anderen Quellen oder indirekt übernommenen Daten und Konzepte sind unter Angabe der Quelle gekennzeichnet.

Die Arbeit wurde bisher weder im in- noch im Ausland in gleicher oder ähnlicher Form in einem Verfahren zur Erlangung eines akademischen Grades vorgelegt.

……

Nelson Ewane Olong